

The role of astrocytes in neurological phenotypes associated with deficiency of the *m*-AAA protease

Inaugural-Dissertation

zur

Erlangung des Doktorgrades

der Mathematisch-Naturwissenschaftlichen Fakultät

der Universität zu Köln



vorgelegt von

Sara Murru

aus Carbonia, Italien

Köln, 2018

Berichtersteller:

Prof. Dr. Elena I. Rugarli

Prof. Dr. Matteo Bergami

Tag der Mündlichen Prüfung:

19.11.2018

For my beloved ones, for those who believe in me...

Table of content

Abbreviations.....	i
Abstract.....	i
Zusammenfassung.....	2
1 Introduction.....	4
1.1 Astrocytes.....	4
1.1.1 Astrocytic functions.....	5
1.1.1.1 Synaptic function.....	5
1.1.1.2 Regulation of blood flow and fluid homeostasis.....	6
1.1.1.3 Energy support.....	6
1.1.1.4 Reactive astrogliosis.....	8
1.1.2 Astrocytes involvement in neurodegeneration.....	9
1.2 Mitochondria.....	12
1.2.1 Mitochondrial functions.....	13
1.2.2 Mitochondrial quality control.....	15
1.3 The <i>m</i> -AAA protease.....	19
1.3.1 <i>m</i> -AAA protease structure.....	19
1.3.2 The <i>m</i> -AAA protease functions.....	21
1.3.3 Neurodegeneration caused by <i>m</i> -AAA protease dysfunction.....	24
1.3.3.1 Paraplegin-associated neurodegenerative disease.....	24
1.3.3.2 AFG3L2 associated neurodegenerative diseases.....	25
1.4 Mitochondrial function in astrocytes.....	30
1.4.1 Mitochondrial dysfunction in astrocytes and diseases.....	32
2 Aim.....	35
3 Material and methods.....	37
3.1 Mouse models.....	37
3.1.1 Astrocyte-specific Afg3l2 knock-out line (astro-L2 KO).....	37
3.1.2 Astrocyte specific <i>m</i> -AAA protease ablation mouse model (astro-DKO).....	37
3.2 Tamoxifen injection procedure.....	38
3.3 Behavioral analysis.....	38
3.3.1 Rotarod assay (performed by Steffen Hermans).....	38
3.3.2 Ataxic score evaluation.....	38
3.4 Tissue collection.....	39
3.4.1 Transcardial perfusion.....	39
3.4.2 Cervical dislocation.....	40
3.5 Histological analyses.....	40

3.5.1	Immunofluorescence stainings on free floating sections	40
3.5.2	Electron microscopy (performed by Esther Barth).....	42
3.5.3	Immunohistochemistry on paraffin sections	43
3.5.4	COX-SDH histochemistry	43
3.6	Molecular Biology.....	44
3.6.1	Genotyping and recombination assessment	44
3.6.2	RNA extraction and quantitative real time PCR	47
3.7	Biochemistry	50
3.7.1	Amino acid extraction (performed by Dr Susanne Brodesser)	50
3.7.2	Liquid Chromatography -Electrospray Ionization Tandem Mass Spectrometry (performed by Dr Susanne Brodesser)	50
3.7.3	Protein extraction for western blot	51
3.7.4	Western Blot.....	52
3.8	Electrophysiological recordings (performed by Dr Simon Hess)	53
3.9	Statistical analysis.....	54
4	Results.....	56
4.1	Specific targeting of Bergmann glia in the mouse cerebellum with an inducible GFAP-driven Cre-LoxP system	56
4.2	Generation of two mouse models of <i>m</i> -AAA dysfunction in astrocytes	60
4.3	Phenotypical evaluation of astro-L2 KO and astro-DKO mice	62
4.4	<i>m</i> -AAA protease depletion induces mitochondrial fragmentation, aberrant cristae morphology and loss of targeted cells.....	66
4.5	<i>m</i> -AAA protease function is necessary for BG survival.....	69
4.6	The GFAP promoter does not target NG2 precursor cells.....	72
4.7	Regulation of mitochondrial functions in astrocyte-specific <i>m</i> -AAA protease deficient mouse models	74
4.7.1	<i>m</i> -AAA protease deficiency does not alter respiratory efficiency in targeted BG ...	74
4.7.2	<i>m</i> -AAA protease ablation induces metabolic stress response.....	77
4.8	Glutamate transport is affected in <i>m</i> -AAA protease deficient astrocytes.....	78
4.9	<i>m</i> -AAA protease deficiency causes cell autonomous reactive astrogliosis	80
4.10	<i>m</i> -AAA protease depletion causes neuroinflammation	83
4.11	Astrocyte-specific <i>m</i> -AAA protease ablation causes morphological and electrophysiological abnormalities in PCs	86
4.12	<i>m</i> -AAA protease ablation in astrocytes causes upregulation of necroptotic markers, but not apoptosis	90
5	Discussion	93
5.1	Conditional KO mouse models as a tool for understanding the contribution of glial cells to neurodegeneration.....	93
5.2	Gender-specific phenotype delay	95

5.3	Mitochondrial morphology, phenotype development and cell death	96
5.4	Mitochondrial dysfunction and BG response.....	99
5.5	Neuroinflammation upon <i>m</i> -AAA protease dysfunction in astrocytes.....	101
5.6	Glutamate dysregulation and secondary neuronal phenotype development.....	103
6	Conclusions	105
7	Bibliography.....	109
8	Appendix.....	140
9	Acknowledgements.....	145
10	Eidesstattliche Erklärung.....	149
11	Curriculum Vitae.....	150

Abbreviations

AAA	ATPase associated with diverse cellular activities proteases
ADCA	Autosomal dominant cerebellar ataxia
AFG3L1/2	ATPase family gene 3-like1/ 2
ANLS	Astrocyte-neuron lactate shuttle
AQP4	Aquaporin 4 water channels
ATP	Adenosine triphosphate
BAK	Bcl-2 homologous antagonist/killer
BG	Bergmann glia cell bodies
CB	Cerebellum
CCL2 and CCL4	C-C motif ligand 2 and 4
Ccp	cytochrome c peroxidase
CLPP	Clp protease
CNS	Central nervous system
COX	Cytochrome c oxidase
dNTP	deoxynucleoside triphosphate
DRP1	dynammin-related protein 1
EAAT1 and 2	Excitatory amino acids transporters 1 and 2
ER	Endoplasmic reticulum
FADD	Fas-associated protein with death domain
Fis1	fission protein 1
fl	floxed
GCL	Granule cell layer
GFP	green fluorescent protein
Hsp	Heat-shock proteins
HSP	hereditary spastic paraplegia
IL-1 β	Interleukin-1 β
IMM	inner mitochondrial membrane
IMS	Intermembrane space
KO	knockout
L1	AFG3L1
L2	AFG3L2
LC3	Protein 1A/1B light chain 3

MCL1	myeloid cell leukemia 1 protein
MCU	mitochondrial calcium uniporter
Mff	mitochondrial fission factor
Mfn	Mitofusin
MICOS	Mitochondrial contact site and cristae organizing system
MICU	mitochondrial calcium uniporter protein
MiD	mitochondrial dynamics proteins
ML	Molecular layer
MLKL	mixed lineage kinase domain-like
MPTP	Mitochondrial permeability transition pore
MRPL32	Mitochondrial ribosomal protein L32
MTC1 and 2	Monocarboxylate transporter 1 and 2
mtDNA	Mitochondrial DNA
mtHsp	Mitochondrial chaperons
MTS	Mitochondrial-targeting sequence
mtUPR	Mitochondrial unfolded protein response
NCLX	Na ⁺ /Ca ²⁺ /Li ⁺ exchanger
NRFs	Nuclear respiratory factors
OMA1	overlapping activity with <i>m</i> -AAA protease 1
OMM	Outer mitochondrial membrane
OPA1	Optic atrophy protein 1
PC	Purkinje neurons
PCL	Purkinje cell layer
PGC-1 α	Peroxisome proliferator-activated receptor- γ coactivator-1 alpha
PHB1 and 2	prohibitin proteins 1 and 2
PPAR	Peroxisome proliferator-activated receptors
PUMA	p53 upregulated modulator of apoptosis
RIPK	Receptor-interacting protein family of serine/threonine protein kinases
RIPK1 and 3	receptor-interacting serine/threonine protein kinases 1/3
SCA	Spinocerebellar ataxia
SCA28	SCA type 28
SDH	succinate dehydrogenase
SPG7	Spastic paraplegia gene 7
TCA	tricarboxylic acid cycle

TFAM	Mitochondrial transcription factor A
tg	transgenic
TIM	Translocase of the IMM
TNF- α	Tumor necrosis factor α
TOM	Translocase of the OMM
VWM	vanishing white matter
wt	wild-type
YFP	yellow fluorescent protein
ZBP1	Z-DNA binding protein 1

Abstract

Ongoing research is unveiling the role of glial cells in the development of neurological diseases. However, it is yet unclear whether mitochondrial dysfunction or altered mitochondrial dynamics can trigger astrocytic death or secondarily affect neuronal function. The mitochondrial *m*-AAA protease is essential for neuronal survival. Mutations in its subunits AFG3L2 and paraplegin lead to the development of different neurodegenerative diseases, spinocerebellar ataxia 28 (SCA28) and hereditary spastic paraplegia (HSP) respectively, which strongly affect patients' motility. Glutamate excitotoxicity may be a contributor to the neurodegeneration, and increasing glutamate uptake by astrocytes ameliorates the phenotype caused by *m*-AAA protease dysfunction in a *Afg3l2*-deficient mouse model of SCA28. In order to dissect the contribution of astrocytes to the development of the neuronal death, I used two different murine models of *m*-AAA dysfunction. In my thesis, I show that deletion of *Afg3l2* in astrocytes (astro-L2 KO) leads to the demise of the highly targeted Bergmann glia, radial cells in the cerebellar cortex, accompanied with a mild, late-onset motor impairment. When I ablated the *m*-AAA protease in astrocytes by eliminating both *Afg3l2* and its murine-expressed homologue *Afg3l1* (astro-DKO), the animals show a very strong and early-onset ataxic phenotype, characterized by induction of mitochondrial stress response, Bergmann glia loss, reactive astrogliosis and inflammation. EAAT1 and EAAT2 glutamate transporters are strongly reduced in cerebella of astro-DKO, and glutamate levels are also reduced. Furthermore, necroptotic markers are upregulated and Purkinje neurons, the biggest neurons in the cerebellum that are strongly affected in SCA28, show morphological and electrophysiological alterations, revealing a secondary neuronal dysfunction. I propose that the *m*-AAA protease dysfunction in astrocytes leads to glutamate excitotoxicity and inflammation that worsen the already dysfunctional neurons in patients carrying mutations in AFG3L2.

Zusammenfassung

Die Rolle von Gliazellen bei der Entwicklung von neurologischen Erkrankungen ist der Fokus vieler laufender Studien. Es ist jedoch noch unklar, ob mitochondriale Dysfunktion oder veränderte mitochondriale Dynamik den Tod der Astrozyten auslösen oder sekundär die neuronale Funktion beeinflussen können. Die mitochondriale *m*-AAA-Protease ist essentiell für das neuronale Überleben. Mutationen in den Untereinheiten AFG3L2 oder Paraplegin führen zur Entwicklung verschiedener neurodegenerativer Erkrankungen, der spinocerebellären Ataxie 28 (SCA28) und der hereditären spastischen Paraplegie (HSP), die die Beweglichkeit der Patienten stark beeinflussen. Glutamat-Exzitotoxizität kann zur Neurodegeneration beitragen und eine erhöhte Glutamataufnahme durch Astrozyten verbessert den durch *m*-AAA-Proteasedysfunktion in einem *Afg3l2*-defizienten Mausmodell von SCA28 verursachten Phänotyp. Um den Beitrag von Astrozyten zur Entwicklung des neuronalen Todes zu analysieren, verwendete ich zwei verschiedene murine Modelle der *m*-AAA-Dysfunktion. In meiner Dissertation zeige ich, dass die Deletion von *Afg3l2* in Astrozyten (Astro-L2 KO) zum Absterben der hochgradig zielgerichteten Bergmann-Gliazellen im Kleinhirnkortex führt, begleitet von einer milden, spät einsetzenden Motorschädigung. Wenn ich die *m*-AAA-Protease in Astrozyten eliminiere, indem ich sowohl *Afg3l2* als auch sein nur in der Maus exprimiertes Homolog *Afg3l1* (Astro-DKO) ausknocke, zeigten die Tiere einen sehr starken und früh einsetzenden ataxischen Phänotyp, gekennzeichnet durch Induktion der mitochondrialen Stressreaktion, dem Verlust von Bergmann Glia, Zellen, reaktiver Astroglia und Entzündung. EAAT1 und EAAT2 Glutamat-Transporter sind im Kleinhirn von Astro-DKO-Mäusen stark reduziert, und der Glutamat-Spiegel ist ebenfalls reduziert. Darüber hinaus sind nekrotische Marker hochreguliert und Purkinje Neuronen, die größten Neuronen im Kleinhirn, die in SCA28 stark betroffen sind, zeigen morphologische und elektrophysiologische Veränderungen, die eine sekundäre neuronale Dysfunktion zeigen. Ich postuliere, dass die *m*-

AAA-Protease-Dysfunktion in Astrozyten zu Glutamat-Exzitotoxizität und Entzündung führt, die die bereits dysfunktionalen Neuronen bei Patienten, die Mutationen in AFG3L2 tragen, zusätzlich verschlechtern.

1 INTRODUCTION

1.1 Astrocytes

The central nervous system (CNS) includes several cell types, beside neurons. These other cells are commonly called glia or glial cells, and consist of astrocytes, oligodendrocytes, microglia and ependymal cells [1]. Astrocytes are considered the most abundant glial type, and are in charge of different functions within the CNS, such as maintaining brain homeostasis, providing metabolic support to neurons, supporting synapse formation and plasticity, regulating ion balance, uptaking and recycling neurotransmitters [2]. Collectively known as astroglia, astrocytes are quite heterogeneous: they have been classified depending on the morphology, developmental features, proliferative capability and factors controlling their proliferation, ion channels, electrophysiological properties, gap junctions, specific proteins and RNA, activation after injury [3].

Astrocytes are usually categorized morphologically and localization-wise in protoplasmic and fibrous. Protoplasmic astrocytes are located in the gray matter, have ovoid somata that give rise to several branches, whereas fibrous astrocytes are found in the white matter and have several fiber-like processes. While processes of protoplasmic astrocytes envelop synaptic buttons, fibrous astrocytes are in intimate contact with the nodes of Ranvier. Many more types of astroglial cells have been described, such as Bergman glia, Müller cells of the retina, perivascular astrocytes and radial astrocytes [4]. Astrocytes are organized in domains, which are distinct and non-overlapping. The first evidence came from a study on hippocampal astrocytes [5, 6], but other studies confirmed the same organization in rodents cortex [7-9]. The functional role of the domains is not clear yet, but these domains are quite extensive: one single astrocyte can enwrap 140,000 synapses in the hippocampus, as well as regulating the blood flow in the area by being in contact with the blood vessels [5].

Astrocytes are histochemically identified using antibodies against the glial fibrillary acidic protein (GFAP), which is a protein of the intermediate filaments, highly expressed in this cell type [10, 11]. However, GFAP is not always histochemically detectable in astrocytes in healthy conditions. In fact, studies with several markers for astrocytes demonstrated that many astrocytes show variability in the GFAP expression level, which is regulated by intracellular and extracellular stimuli [2]. Nevertheless, GFAP is a reliable marker for reactive astrocytes. In fact, in case of tissue injury, infection and neurodegenerative diseases, the extracellular space is flooded with chemokines, cytokines and debris. When triggered by these stimuli, astrocytes increase in size, upregulate GFAP and induce molecular, cellular and functional changes aimed to limit the tissue damage, or provide aid for tissue repair [2, 12].

1.1.1 Astrocytic functions

Glial cells were considered to be the glue connecting the neurons in the CNS, but it has become clear that this definition does not reflect the reality of the complexity, or the functional properties of glial cells [13]. Indeed, astrocytes are pleiotropic cells, which exert different functions aimed to maintain CNS homeostatic equilibrium and sustain neuronal function.

1.1.1.1 Synaptic function

As they enwrap the synapses, astrocytes have a stringent contact with pre and postsynaptic entities. The environmental control of the synaptic cleft must be tightly regulated to avoid hyper-stimulation of the postsynaptic neuron. Astrocytes express on their surface both GABA transporters (GATs) [14] and excitatory amino acids transporters (EAATs) [15], and are involved in their recycling to replenish neuronal pools [16]. As for their role in synaptic regulation, the former bipartite synapse is now accepted as a tripartite synapse [17-19]. They have potassium and sodium channels, and calcium fluctuations that can elicit inward currents, but differently from neurons, as astrocytes do not propagate action potentials [20, 21]. Despite

that, the astrocytic inward currents can induce release of neuroactive substances such as purines and neurotransmitters (GABA and glutamate), therefore affecting neuronal activity [18-20, 22]. Moreover, astrocytes influence the synapses by releasing also neuroactive steroids (estradiol and progesterone) and metabolites that influence the postsynaptic button [23]. In addition, synapse formation is highly regulated by astrocytes during development: they guide axons during their elongation phase by releasing thrombospondin and other signaling molecules [24-26].

1.1.1.2 Regulation of blood flow and fluid homeostasis

Astrocytes physically contact blood vessels with their processes, and can regulate the blood flow in the CNS *via* the release of prostaglandins, nitric oxide and arachidonic acid. These mediators are known to regulate vessel diameter and blood flow [27]. Considering that astrocytes are tightly communicating with neurons, they could be able to regulate blood flow depending on neuronal activity. In fact, it was shown that blood flow changes in response to visual stimuli in the visual cortex, and the changes are mediated by astrocytic activity [28]. Moreover, astrocytic processes express clustered aquaporin 4 water channels (AQP4), which are involved in regulation of water influx. It was shown, in fact, that AQP4 knockout animals have an increased extracellular space volume (+25%) and increased water content compared to control animals [29-31]. AQP4 function is critical in the first postnatal days, when water volume in the brain is reduced up to 80%. Furthermore, several studies tried to understand the role of AQP4 in management of edema and stroke, but conflicting results, mainly obtained using transgenic animals, did not allow to uncover fully the implication of AQP4 in brain trauma [32].

1.1.1.3 Energy support

Astrocytes are considered glycolytic cells and even if oxidative phosphorylation (OXPHOS) is still used for adenosine triphosphate (ATP) production, it is not the main energy production pathway for the cells [33, 34]. In fact, glycolytic genes expression is increased in these cells

[33, 35] and especially they highly express the 6-phosphofructo-2-kinase/fructose-2,6-bisphosphatase isoform 3 (PFKFB3), a glycolysis inducer enzyme. This enzyme is subjected to continuous degradation *via* the proteasome in neurons [36], imposing their requirement for ATP production *via* OXPHOS. Several studies proposed that astrocytes support neuronal function by performing aerobic glycolysis and providing neurons with lactate. When glutamate is released as neurotransmitter from the presynaptic entity, it activates glutamate receptors in neurons. To avoid excitotoxicity, astrocytes express the amino acids transporters 1 and 2 (EAAT1 and 2) to uptake glutamate from the synaptic cleft. To this purpose, the electrochemical gradient of Na^+ , which is maintained by Na^+/K^+ ATPase is used as driving force [37]. Once in astrocytes, glutamate is converted to glutamine by the glutamine synthase and shuttled back to the neurons to be converted to glutamate and replenish the vesicles. Both glutamate signaling in neurons and glutamate uptake in astrocytes are energy-requiring processes. Therefore, the energetic status has to be high. To provide both astrocytes and neurons with enough ATP, glucose coming from the bloodstream is converted to pyruvate *via* glycolysis in astrocytes. To maintain the flux, NADH is oxidized to NAD^+ through the conversion of pyruvate in lactate. This is then released in the extracellular space *via* the monocarboxylate transporter 1 (MCT1). Once in the extracellular space, lactate is transported into neurons *via* the MCT2, where it is converted to pyruvate by the lactate dehydrogenase 1 and used as oxidative substrate for ATP production. This process is known as astrocyte-neuron lactate shuttle (ANLS) [38-45]. Despite being widely accepted, ANLS concept was formulated following experiments developed in cell cultures. *In vivo* experiments have given conflicting results. In fact two independent studies have shown increased glucose uptake following neuronal stimulation in astrocytes [46] or neurons [47]. Moreover, Diaz-Garcia et al., show that, using metabolic biosensors, in both acute hippocampal slices and in brains of awaken mice, synaptically stimulated cytosolic NADH transients appear in neurons rather than in astrocytes. This was independent from astrocytes stimulation *via* glutamate and lactate import in neurons,

whereas NADH transients in neurons reflect increased neuronal glycolysis. In fact, by using the irreversible glycolysis blocker, iodoacetic acid, no transients were observed. The authors propose that ANLS can occur in resting phase, but not during neuronal stimulation [48].

1.1.1.4 Reactive astrogliosis

Astrocytes monitor neuronal activity and function. Following stroke, CNS trauma or neurodegenerative diseases, they are in charge of limiting the damage and restore CNS functionality. To fulfill their duty upon damage, astrocytes enter a state called reactive astrogliosis. Mild reactive astrogliosis consists of cell body hypertrophy and changes in gene expression, but cells maintain their domain distinction. A mild reactive state occurs in case of not severe trauma, viral and bacterial infections that activate the immune system, and is also observed in areas surrounding a lesion in the CNS [2, 4, 49]. Severe reactive astrogliosis is characterized additionally by loss of domain organization and proliferation. It manifests in case of ischemia, severe trauma and neurodegeneration [2, 4]. Reactive astrogliosis leads to the formation of the so called “astroglial scar”, which consists of newly proliferated astrocytes closely packed, with their processes intimately entangled creating a compact border for the affected area [50, 51]. The lesion core contains several types of cells, including astrocytes, fibroblasts, fibrocytes, pericytes and microglial cells. Moreover, the core collagenous extracellular matrix is enriched with astroglia derived proteoglycans that inhibit axonal growth [52].

Reactive astrocytes function does not end with the formation of the glial scar though. In fact, they are responsible for secretion of neurotrophins, clearance of dead cells and debris as well as phagocytosis of synapses and repair of the brain-blood-barrier [12, 53-56]. Another important feature of reactive astrocytes is their interaction and interplay with the resident immune cells of the CNS, called microglia. In fact, microglia and reactive astrocytes can recruit each other to the damaged area and actively interact to limit the tissue damage and promote

repair [57, 58]. It was indeed shown that in case of traumatic brain injury, ischemia, neuropathic pain and more, microglia is the first responder in the core of the injury, and release cytokines, such as interleukin-1 β (IL-1 β), tumor necrosis factor α (TNF- α), and interferon γ . They recruit reactive astrocytes, and downregulate the purinergic receptor P2Y₁ on astrocytes surface, promoting neuroprotection [58]. Moreover, it was also shown that in a model of chronic experimental autoimmune encephalomyelitis (a model of multiple sclerosis) activated astrocytes increase the release the chemokine C-C motif ligand 2 and 4 (CCL2 and CCL4), which induce activation of microglia [59-62].

It should be noted that astrocytes have at least two different activation states. Neuroinflammation produces A1 reactive astrocytes, while ischemia induces A2 reactive astrocytes [4, 12, 63]. A1 astrocytes are considered harmful for the neurons, as they promote release of soluble toxins that kill different types of neurons, as well as mature oligodendrocytes, and upregulate the nuclear factor kappa light chain reaction (NF κ B) [55, 63]. A2 astrocytes are instead considered helpful in case of ischemia, as they promote STAT3-mediated proliferation and scar formation, and in absence of STA3 in astrocytes, there is extensive axonal degeneration following spinal cord injury.[12, 55, 63]. Therefore, reactive astrogliosis is not a unique and uniform state that activated astrocytes undergo in case of injury, but a complex remodeling of astrocyte gene expression and pathway activation aimed to overcome injuries in a selective way, limiting tissue damage or destroying the cause.

1.1.2 Astrocytes involvement in neurodegeneration

Due to their pleiotropic functions during development and maintenance of the CNS, it is not surprising that astrocytes play a key role in neurodegeneration. One of the questions that researchers in the field are trying to answer to is whether during neurodegeneration astrocytes

become unable to support neurons (loss-of-function) or if they upregulate pathways that make them toxic (gain-of-function) [64].

As astrocytes are necessary for neuronal survival [65], loss of their function could be a trigger of neurodegeneration. For example, Alexander disease is an autosomal dominant disease caused by mutations in *GFAP*. It is a leukodystrophy triggered by accumulation of mutated GFAP, heat shock protein 27, and $\alpha\beta$ -crystalline aggregates called Rosenthal fibers. With time, the aggregates become bigger and cause morphological changes such as reduction of fine processes number, enlarged body and nucleus, which could be due to misalignment of chromosomes during mitosis caused by the Rosenthal fibers [66, 67]. The disease progression causes abnormal myelination, maybe because oligodendrocytes precursors express GFAP [68], and glia-induced nitric oxide release, which causes neurodegeneration [69]. Another neurodegenerative disease caused by astrocytes dysfunction is the hepatic encephalopathy. It occurs in cases of cirrhosis and it is a consequence of toxic metabolites coming from impaired liver activity. Particularly ammonia, once reaches the brain through the bloodstream, is detoxified by astrocytes. It results in the excessive production of glutamine, which causes osmotic swelling of the cells. As a response, astrocytes alter the expression of key glutamate transporters and water channels in the attempt to compensate for the swelling. However, by doing this, their function of properly monitor neuronal activity is inhibited and their ability to maintain CNS homeostasis is reduced, leading to the development of a neuropsychiatric syndrome [64, 70].

In addition to diseases caused by primarily astrocyte-specific protein mutations or loss of function caused by toxic metabolites, astrocytes relevance was also demonstrated in neuronal-focused diseases. Accumulation of amyloid- β plaques have been found in astrocytes in post-mortem Alzheimer disease brains [71-73]. Wild-type astrocytes internalize amyloid- β when transplanted in Alzheimer disease mouse model brains [74, 75]. It was also shown that

astrocytes connectivity is impaired [76, 77], and the blockade of hemichannels forming gap-junctions between astrocytes ameliorates memory-related phenotypes without affecting plaques inside the cells [78]. Astrocytes expressing mutated huntingtin, which causes the neurodegenerative disorder Huntington disease, have been found to be toxic for wild-type neurons in co-culture [79], and appear to have reduced expression of Kir4.1 channels [80]. This results in reduced potassium-buffering capability. Moreover, astrocyte-specific mutation of huntingtin protein is sufficient to cause neurodegeneration [81, 82]. In Parkinson disease, astrocytes uptake α -synuclein released from axons [83, 84]. These aggregates lead to production of proinflammatory cytokines and chemokines, and when a mutated α -synuclein was specifically expressed in astrocytes, it led to non-cell autonomous neurodegeneration resulting in paralysis [83]. The aggregates have the capability of impairing glutamate uptake by astrocytes, as well as impairing their ability to regulate the blood-brain barrier [85]. In the case of inherited amyotrophic lateral sclerosis, mouse models in which the mutation occurs only in motor neurons do not show the canonical disease [86-88]. Moreover, chimeric mouse models show that mutated glial cells can damage wild-type neurons, whereas healthy wild-type glial cells can delay the phenotype progression in mutated neurons [89]. Evidences of astrocytes involvement in brain tumors, epilepsy, major depressive disorder have also been gathered [90], further sustaining the hypothesis that neurological diseases and neurodegenerative disorders go beyond neuronal dysfunction as more than one player is indeed involved.

1.2 Mitochondria

Mitochondria are essential organelles for eukaryotic cells. According to the endosymbiotic theory postulated by Wallis [91], mitochondria are descendant of α -proteobacteria that were included into a not yet clarified host. Despite the initial resistance to the theory, nowadays it is well accepted, and more studies were conducted to find out which type of bacteria gave rise to mitochondria and which type of cell was the host. Moreover, heated discussion is currently ongoing, as the timing of mitochondria acquisition and development of the eukaryotic cells is controversial: many believe that mitochondrial incorporation inside the cell was the first step towards the eukaryogenesis, others claim that it was the last one [92]. To add another shadow to the endosymbiosis theory and the eukaryotic evolution, Karnokowska et al., [93] describe the oxymonad *Monocernocomonoides* as a microbial eukaryotic organism that has standard eukaryotic features, but lacks mitochondria. The authors do not deny that mitochondria were present during the evolution of this organism, but were lost overtime, implying that mitochondria cannot and should not be considered indispensable components of eukaryotic cells.

The inheritance from mitochondrial bacterial ancestors is the double membrane surrounding the organelle, and its own DNA. The outer and inner mitochondrial membranes (OMM and IMM) are composed of phospholipids; the space between them is called intermembrane space (IMS). The IMM creates invagination, called cristae, protruding in the core of the mitochondrion, called matrix [94]. The cristae morphology is maintained by the mitochondrial contact site and cristae organizing system (MICOS), and the optic atrophy protein 1 (OPA1) [95-97]. Mitochondrial DNA (mtDNA) is circular; double stranded and has a 16 kbp size. In humans, it encodes for 13 proteins, which are part of the OXPHOS complexes, translated by the mitochondrial translational machinery. All the other mitochondrial proteins are encoded by

the nuclear DNA, as most of the genes present in the original α -proteobacterium were transferred to the nuclear genome [98].

1.2.1 Mitochondrial functions

Mitochondria are dynamic organelles in charge of respiration and ATP production, calcium buffering and cell death regulation. In the CNS, these organelles are of high importance, as the brain consumes 20% of the body's energy production [45].

ATP production starts from different energy sources entering the tricarboxylic acid cycle (TCA) as acetyl-coenzyme A: glucose and/or lactate conversion in pyruvate, fatty acids β -oxydation, and amino acids deamination. The result of the TCA cycle, among the rest, is the production of the reduced carriers NADH and FADH₂ that are electron donors for the OXPHOS, operated by the electron transport chain. It consists of four complexes, which remove electrons from the electron donors and create a proton gradient by pumping protons H⁺ in the IMS. The fifth complex, called ATP synthase generates ATP using the proton gradient generated by the electron transport chain. This series of reactions is very profitable in terms of energy production, with an ATP yield of 30-36 molecules per glucose molecule [45].

Ca²⁺ buffering is of relevance for the CNS, as its imbalance can cause hyper-stimulation and death of the cells. Mainly, mitochondrial Ca²⁺ uptake is mediated by the mitochondrial calcium uniporter (MCU) complex. It is located in the IMM and has low Ca²⁺ affinity. Therefore, it requires high concentrations of cytosolic Ca²⁺ to open. The low affinity of the uniporter to Ca²⁺ is guaranteed by its gatekeeper component, the mitochondrial calcium uniporter protein (MICU), which senses the ion concentrations and induces the morphological changes leading to the opening of the MCU complex at high cytosolic Ca²⁺ concentrations [99]. Calcium efflux from mitochondria is operated *via* the Na⁺/Ca²⁺/Li⁺ exchanger (NCLX) and the mitochondrial permeability transition pore (MPTP). Na⁺ concentrations are higher in the cytosol than in the

matrix, and mitochondrial membrane potential is around -150 to -180 mV. These two conditions generate a strong driving force that activates the NCLX, which transports 3 Na⁺ inside mitochondria and release out 1 Ca²⁺. The MPTP on the other end is an IMM channel that opens when mitochondria undergo Ca²⁺ overload. Its prolonged opening causes IMM potential collapse, blockade of ATP production, mitochondrial cristae swelling and rupture that leads to cell death [100].

Mitochondrial calcium has an effect on mitochondrial ATP production, as it activates 3 different mitochondrial dehydrogenases, increasing NADH production, and it also induces the activity of the ATP synthase [101]. In neurodegenerative diseases, different neuronal populations show higher sensitivity to specific mutations. Understanding what determines this higher susceptibility to cell death is crucial. For some diseases it seems that mitochondrial calcium buffering (and generally, calcium homeostasis) makes specific neuronal populations more susceptible to cell damage and death [102]. In fact, calcium homeostasis is primarily modulated in neurons through voltage or ligand-gated ion channels, and secondarily by intracellular signaling. In glial cells, Ca²⁺ is mainly released by the endoplasmic reticulum (ER) *via* inositol-3 phosphate signaling. In neurons, calcium is buffered by mitochondria and induces TCA cycle when stored in the matrix, increases ATP production and the activity of the aspartate carrier [103]. Moreover, mitochondrial buffering activity is strong enough to modulate the propagation of synaptic signal in neurons, as well as modulate intercommunication among astrocytes [102, 104]. Changes in Ca²⁺ concentrations in mitochondria can also induce cell death, by opening the MPTP and resulting release of pro-apoptotic factors [105].

Cell death can occur in case of cellular dysfunction or external insult. It can be modulated/programmed (apoptosis and necroptosis) or disorganized (necrosis). Mitochondria are involved in both cell death pathways in different ways. Apoptosis is triggered by different signals, such as extracellular ligands that induce the formation of the death-inducing signaling

complex (DISC): this complex drives caspase activation cascade that modulates the elimination of the cell. The activation of caspase 8 *via* the DISC complex leads to the release cytochrome c from mitochondria, amplifying the apoptotic response [106]. Other activators of apoptosis are the intrinsic signal of mitochondrial damage, intracellular calcium overload and oxidative stress. These signals induce the opening of the MPTP, which causes the release of pro-apoptotic factors, such as cytochrome c, inducing the caspases activation cascade [105, 107]. Opposite to apoptosis, necrosis is characterized by mitochondrial swelling, impaired ATP production and, despite the release of pro-apoptotic stimuli form mitochondria, blockade of apoptosis due to ATP insufficiency [105]. Necrosis results in the breakage of cell membrane and release of the cell content in the extracellular space [108]. A regulated form of necrosis is the one induced by activation of the receptor-interacting protein family of serine/threonine protein kinases (RIPK), called necroptosis. This death pathway is dependent on mitochondrial production of reactive oxygen species, but not on the opening of the MPTP [109].

1.2.2 Mitochondrial quality control

Mitochondria must be strictly monitored, as their dysfunction can lead to cellular death. Therefore, organelle quality control is essential to guarantee cellular functionality and survival. The *organelle quality control* consists of regulation of mitochondrial dynamics (fusion/fission), *de novo* mitochondrial biogenesis and mitophagy [148].

During mitochondrial fusion, separated mitochondria fuse together the respective OMM and IMM, and the matrix content is mixed. This process is highly regulated by several GTPases: mitofusin (Mfn) 1 and 2 control OMM fusion, while OPA1, a dynamin related GTPase, controls fusion of the IMM [149]. Mitofusins are located in the OMM and induce mitochondrial fusion by homo and heterotypic interactions and consequent trans-association of the OMMs. Moreover, Mfn2 has been reported to be important also for mitochondrial/ ER tethering, even

though the dynamics are still debated [150, 151]. The mechanism underlying IMM fusion is poorly understood. OPA1 is present in the IMM in different isoforms, called short and long OPA1. It has been shown that the IMM bound long OPA1 is required for mitochondrial fusion and elongated morphology. Moreover, it was shown that increased long OPA1 cleavage, resulting in more short OPA1 isoforms, inhibits fusion and causes mitochondrial fission [152].

Despite being activated by OPA1 proteolytic cleavage, mitochondrial fission has its own set of regulatory elements: the dynamin-related protein 1 (DRP1), the mitochondrial fission protein 1 (Fis1), the mitochondrial fission factor (Mff) and the mitochondrial dynamics proteins (MiD) 49 and 51 kDa. Fission occurs at the mitochondria-ER contact sites, where the ER creates constrictions around the separation line. DRP1 is a cytoplasmic protein recruited to the OMM. It forms oligomers in a ring-like structure that constrict the mitochondria using the hydrolysis of GTP at the ER contact site. For this reason, it has been proposed that the ER may have an important role in identifying the fission sites [153]. Increased fission has been associated with the necessity of eliminating dysfunctional mitochondria, meaning that the dysfunctional part is separated and targeted for mitophagy [143]. Increased mitochondrial fragmentation has been reported in several neurodegenerative diseases caused by mitochondrial dysfunction, but also in diseases caused by mutations in genes not involved in mitochondrial function, such as Huntington disease [143].

Fragmentation of dysfunctional mitochondria leads to their elimination *via* mitophagy. It starts with the identification of dysfunctional mitochondria *via* the ubiquitination of mitochondrial surface proteins by E3-ubiquitin ligases. The ubiquitinated substrates recruit adaptors like p62, which have an interaction sequence recognized by the microtubule associated protein 1A/1B light chain 3 (LC3) located on the autophagosomal membrane. Once the autophagosome is formed, it fuses with lysosomes to digest the organelle [154-157].

Finally, as old/dysfunctional mitochondria are eliminated, new ones must be generated *de novo* to maintain a functional and healthy mitochondrial network. As mitochondria rely on both the nuclear and mtDNA for protein synthesis, mitochondrial protein expression must be coordinated within these two components. The peroxisome proliferator-activated receptor- γ coactivator-1 alpha (PGC-1 α) is considered the master regulator of mitochondrial biogenesis, as it is a scaffold of different nuclear receptor families and as transcriptional coactivator of nuclear respiratory factors (NRFs), peroxisome proliferator-activated receptors (PPAR) and more. NRFs are involved in transcription of nuclear-encoded mitochondrial proteins, as well as mitochondrial transcription factor A (TFAM), which is in charge of mtDNA transcription and replication.

Protein quality control in mitochondria consists of mitochondrial protein turn over (i.e. protein translation and degradation). As mitochondrial proteins are derived from both mitochondrial genome and nuclear DNA, the quality control process includes also protein import, proper folding and activation. Most mitochondrial proteins are identified by a mitochondrial-targeting sequence (MTS) in the N-terminus of the protein, which is usually cleaved upon mitochondrial entrance [110, 111]. Before a nuclear-encoded mitochondrial protein enters the organelle, it is maintained unfolded in the cytosol by chaperons such as heat-shock proteins (Hsp) 70 and 90 preventing degradation [112]. To access mitochondria, proteins must be transported through the OMM and, in case they are IMM or matrix proteins, they also need to pass through the IMM. For these purposes, two translocase complexes exist: the translocase of the OMM (TOM) and the translocase of the IMM (TIM). While passing through the TIM complex or once in the matrix, unfolded proteins are protected by mitochondrial chaperons (mtHsp) like mtHsp70 and Hsp60 [113].

Mitochondria possess several proteases located in all their compartments, and the mitochondrial unfolded protein response (mtUPR) for protein degradation. Mitochondrial proteases exert

proteolytic functions and, by cooperating with chaperons, they participate in the import and activation of mitochondrial proteins. For example, there are two different AAA (ATPase associated with diverse cellular activities) proteases inserted in the IMM: the *i*-AAA protease and the *m*-AAA protease [114, 115]. The *i*-AAA protease has its proteolytic site towards the IMS, while the *m*-AAA protease has its own towards the matrix. Together, the mitochondrial AAA proteases are involved in the degradation of OXPHOS subunits and to protein activation *via* proteolytic cleavage of newly imported pre-proteins. The AAA proteases activity determines also mitochondrial fusion/fission balance. In fact, under metabolic stimulation, the *i*-AAA protease cleaves OPA1, leading to changes in short and long isoforms ratio and inducing mitochondrial fission [116, 117]. Furthermore, *m*-AAA protease dysfunction indirectly influences mitochondrial dynamics by inducing the overlapping activity with *m*-AAA protease 1 (OMA1)-mediated cleavage of OPA1 and increasing fission events [118]. The *m*-AAA protease exert also proteolytic activation functions by cleavage of the N-terminus of the mitochondrial ribosomal protein L32 (MRPL32), allowing its proper folding and activation [114, 119]. Other proteases are located in the matrix such as the mitochondrial processing peptidase (MPP) which is in charge of cleaving off the MTS of the pre-proteins freshly imported in mitochondria. Following its activity, other peptidases further process the proteins to either stabilize or degrade them [113]. In addition, proteostatic stress can induce the activation of the mtUPR, to balance mitochondrial protein homeostasis. In mammals, it was shown that it involves upregulation of chaperones and mitochondrial proteases. However, most of the studies on mtUPR are conducted in *C.elegans*. It was shown that a mitochondrial peptidase called Clp protease (CLPP) is upregulated in case of mtUPR induction, and generates small peptides that are exported out of mitochondria *via* the HAF-1 transporter to activate transcription factors in the nucleus [120, 121].

1.3 The *m*-AAA protease

1.3.1 *m*-AAA protease structure

Maintenance of the mitochondrial proteome is essential for eukaryotic cell survival. Mitochondria have a plethora of proteases in charge of protein quality control, located in different compartments. The *m*-AAA protease is a mitochondrial metallopeptidase anchored to the IMM. Highly conserved through evolution, it is a hexamer composed of two different subunits in humans: AFG3L2 and paraplegin. AFG3L2 can create homooligomeric complexes or heterooligomeric complexes together with paraplegin, whereas paraplegin cannot homooligomerize [122, 123]. In rodents, a third subunit, highly homologous to AFG3L2 was identified and called AFG3L1 [122, 124]. In addition, AFG3L1 is capable of forming both homo and heterooligomers (Fig. 1.1). Interestingly, the expression of AFG3L2 and paraplegin is higher in mouse brains compared to AFG3L1 (respectively 10 and 4 folds). Moreover, the knockout of paraplegin does not change the relative abundance of AFG3L2 over AFG3L1 in mouse brains, and AFG3L2 has been shown to be 10 folds more expressed than AFG3L1 also in absence of paraplegin [122].



Figure 1.1: *m*-AAA protease composition in humans and mice. Human *m*-AAA protease is composed of two subunits: AFG3L2 and paraplegin. AFG3L2 can homooligomerize or heterooligomerize with paraplegin, while paraplegin can only heterooligomerize. In mice, there is another subunit, AFG3L1, which can generate homooligomers or heterooligomers.

Analyses of the yeast homologous of the mammal *m*-AAA protease subunits, allowed for a better understanding of the subunits structure: the protein sequence includes two transmembrane domains, an ATPase domain, and a zinc metallopeptidase domain. While the matrix-facing N-terminus function is still poorly understood, the coiled-coil at the C-terminus seems to be involved in the substrate recognition [125]. The assembly of the hexamer of the AAA oligomers is driven by interactions between the ATPase domains, but for the *m*-AAA protease proper assembly, the interaction between the metalloprotease compartments is also required [126, 127]. Once assembled, the *m*-AAA protease comprises a small portion called distal domain facing the IMS (Fig. 1.2). Its function is still debated: it could be a simple anchor for the protease, or it could be involved in the recognition of substrates [128, 129]. Another interesting hypothesis is that the distal domain allows the interaction with *m*-AAA protease regulatory complexes. In all eukaryotic cells, the distal domain of the *m*-AAA protease interacts with the heterodimeric ring formed by prohibitin proteins 1 and 2 (PHB1 and 2) [130]. It has

been shown that the prohibitins are negative regulators of the *m*-AAA protease. In fact, deletion of PHB1 or 2 leads to an increased turnover of the *m*-AAA protease targets, such as the complex IV subunit Cox3p in yeasts. In a murine model of PHB2 knockout, it was shown that proteolytic cleavage of OPA1 is increased [131, 132].

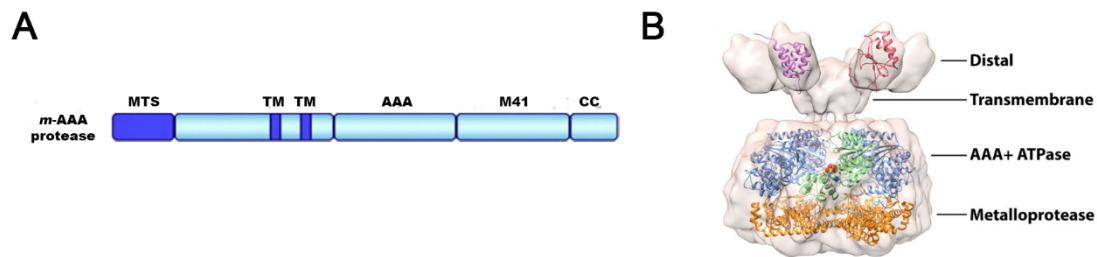


Figure 1.2: *m*-AAA protease structure. (A) Schematic representation of the *m*-AAA protease domains: mitochondrial targeting sequence (MTS), transmembrane domain (TM), AAA domain, metal binding proteolytic domain (M41), coiled coil (CC). Modified from [133]. (B) Structural localization of the *m*-AAA protease domains. Modified from [134].

1.3.2 The *m*-AAA protease functions

The *m*-AAA protease is involved in mitochondrial protein quality control. As protease exerting its *degradation function*, it can completely degrade misassembled, disassembled or damaged proteins. The small peptides resulting from this catalytic activity can be exported out of mitochondria, or further degraded by other peptidases [115]. The elimination of disassembled substrates is extremely important for proper mitochondrial function: accumulation of dysfunctional proteins could lead to aggregates formation, morphological alteration of mitochondrial structure and increased susceptibility to oxidative stress [134, 135]. It was shown that subunits of the respiratory chain and the ATP synthase are targets of the *m*-AAA protease. In fact, Cob subunit of complex III, CoxI and CoxIII of complex IV, and the Su6, 8 and 9 subunits of the ATP synthase are degraded by the *m*-AAA protease [132, 136, 137].

Another important target of the *m*-AAA protease is the essential MCU regulator (EMRE). In fact, in healthy conditions EMRE binds the mitochondrial calcium uniporter protein (MICU). The resulting MICU-EMRE complex creates a cap on the MCU, functioning as gatekeeper for calcium entrance in mitochondria. Excessive EMRE, which does not form the MICU-EMRE complex, is degraded by the *m*-AAA protease. In case of *m*-AAA dysfunction, the excess EMRE is not degraded and competes with the assembled MICU-EMRE complex for the binding to the MCU. The MICU-EMRE-MCU complex (generally referred to as assembled MCU complex) has a low Ca²⁺ affinity and is mostly closed at low cytosolic Ca²⁺ concentration. On the other hand, the EMRE-MCU, lacking the MICU component, is constitutively active and induces Ca²⁺ overloads in mitochondria, inducing then the MPTP opening and a massive release of Ca²⁺ in the cytosol [138, 139]. This specific substrate bestows on the *m*-AAA protease an indirect regulatory effect on Ca²⁺ homeostasis.

Another important function of the *m*-AAA protease is the *proteolytic activation* of some of its targets. MRPL32 is a component of the mitochondrial ribosome. Opposite to the fate of EMRE, MRPL32 is not completely degraded by the *m*-AAA protease. In fact, only the N-terminus, that in yeast is 71 residues, is cleaved. Once the *m*-AAA protease encounters the highly stable zinc-binding domain of the protein, it is unable to process it further and releases it as a mature protein of the ribosomal machinery [140]. Moreover, the nuclear encoded cytochrome c peroxidase (Ccp) is translocated inside mitochondria following translation in the cytosol. The immature form requires two proteolytic processes operated by two different proteases: the *m*-AAA protease processes the premature Ccp between the amino acids in position 36 and 37, whereas the rhomboid peptidase processing of cytochrome c peroxidase (Pcp1) cleaves Ccp between the amino acids 68 and 69 [141, 142]. Furthermore, it was reported that the *m*-AAA protease is important for the localization of Ccp inside mitochondrial cristae, but whether it occurs for diffusion through the cristae opening, or by lateral translocation is not yet clear. It was also

shown that the translocation of Ccp is independent of the *m*-AAA protease proteolytic activity [142, 143]. Another suggested target of the *m*-AAA protease is the long OPA1 [144]. It was shown that AFG3L1 and AFG3L2 homooligomeric complexes are able to cleave more efficiently long isoforms of OPA1 in short isoforms. However, recent findings revealed that OPA1 is cleaved under metabolic stimuli by the *i*-AAA protease and under stress conditions, including *m*-AAA protease dysfunction, by OMA1. Therefore, the *m*-AAA protease is indirectly involved in mitochondrial fusion/fission balance [116, 118]. Moreover, the *m*-AAA protease is also involved in maturation of OMA1: after mitochondrial import, OMA1 undergoes an auto-proteolytic cleavage, but before that it needs to be pre-activated by proteolytic processing by the *m*-AAA protease [117]. Importantly, Koppen et al [145] showed that the *m*-AAA protease undergoes an autocatalytic processing. In fact, AFG3L1 and 2 are nuclear encoded mitochondrial proteins. Following mitochondrial translocation, AFG3L2 is processed by the mitochondrial processing peptidase (MPP), generating an intermediate form of the protein. This intermediate undergoes catalytic processing by pre-existing *m*-AAA protease or autocatalytic processing: *m*-AAA protease depleted cells, in fact, provided with immature AFG3L2 are able to induce maturation of only 40% of the protein, suggesting both the necessity of pre-existing *m*-AAA protease and autocatalytic function. Moreover, the same study revealed that paraplegin undergoes two proteolytic cleavages as well: the first one by the MPP and the second one by pre-existing *m*-AAA protease. However, it has no autocatalytic activity and requires AFG3L2 or AFG3L1 not only for its assembly, but also for its maturation.

Finally, the *m*-AAA protease is indirectly involve in mitochondrial protein translation by processing MRPL32, a component of the mitochondrial translational machinery. It has also been reported that in yeasts that *m*-AAA protease impairment caused by mutations in the proteolytic domain of the protease reduces the transcription of introns-containing mitochondrial RNAs of *COX1* and *Cob* [146].

Overall, the *m*-AAA protease function is not limited to proteolytic degradation of its substrates. It also comprises maturation and activation of its target proteins (including self-activation), translational control of mitochondrial encoded proteins, and translocation of its substrates, calcium mitochondrial entrance and mitochondrial fusion/fission balance.

1.3.3 Neurodegeneration caused by m-AAA protease dysfunction

Due to its pleiotropic functions, *m*-AAA protease proper activity is necessary for cellular survival, particularly for cells which strongly rely on mitochondrial function, such as neurons. In fact, *m*-AAA protease impaired activity causes different neurodegenerative diseases depending on the dysfunctional subunit.

1.3.3.1 Paraplegin-associated neurodegenerative disease

Hereditary spastic paraplegia (HSP) is an autosomal recessive neurodegenerative disease associated with axonal degeneration of the cortico-spinal neurons, which leads to weakness of the lower limbs and proprioceptive problems [147]. It is caused by mutations in several genes involved in mitochondria, ER, lipid droplets or cytoskeleton maintenance and function [148]. Mutations the *SPG7* gene, localized in chromosome 16, which encodes for the *m*-AAA protease subunit paraplegin, are associated with HSP [149]. Several mutations of *SPG7* have been reported [150]. This gene is highly expressed in big pyramidal neuron of the cortex [151]. A *Spg7* knockout mouse model was generated by eliminating, *via* homologous recombination, the first two exons of the gene [152]. Animals develop a progressive motor impairment starting between 4 and 5 months, axonal degeneration of motor neurons of the spinal tract, optic nerve and peripheral nerves, recapitulating the human disease phenotype. Moreover, mitochondrial abnormalities are also prominent in affected axons. An alternative splicing of the murine *Spg7* gene was described to incorporate into the ER, suggesting that the AAA protease could have a function in other cellular compartments [153]. In addition, a recent report suggested that

paraplegin is a conserved and core component of the MPTP, and that its disruption prevented Ca^{2+} imbalance and cell death [154].

1.3.3.2 AFG3L2 associated neurodegenerative diseases

Mutations in *AFG3L2* cause two different neurodegenerative diseases: spinocerebellar ataxia type 28 (SCA28) [155-157] and spastic ataxia neuropathy syndrome (SPAX5) [158, 159]. The disease are caused by missense, deletion, insertion or duplication mutations.

SCA28 was firstly described in 2006 by Cagnoli et al., [160], as a novel form of autosomal dominant cerebellar ataxia (ADCA). It was observed in a 4-generation Italian family, where affected persons developed a slowly progressive cerebellar ataxia around 19-20 years of age. The condition always started with gaze-evoked nystagmus, difficulties in keeping balance while standing and gait incoordination. Cerebellar atrophy was also observed in affected individuals (Fig. 1.3). Through a genome-wide analysis, researchers were able to identify linkage with chromosome 18 markers. In 2010, Di Bella et al., [157] found out that different mutations in *AFG3L2*, specifically in exon 16, cause SCA28 in different unrelated Italian families. This was the first time that a mitochondrial protein was discovered to cause a form of spinocerebellar ataxia. In later years, more *AFG3L2* mutations, in exons 10, 15 and 16, were linked to SCA28, further confirming the crucial role of this protease in the development of the disease [157, 161-163].

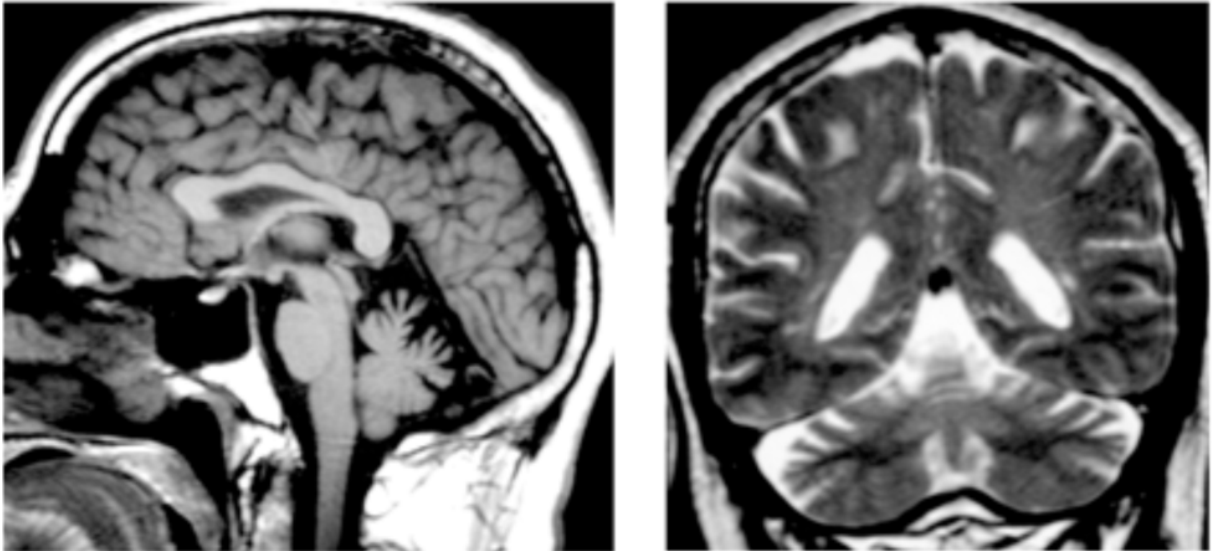


Figure 1.3: Cerebellar atrophy in SCA28 affected patient. Sagittal and coronal MRI scans of patient affected by SCA28 [155].

Autosomal recessive spastic ataxia neuropathy syndrome (SPAX5), caused by homozygous mutations in *AFG3L2*, is characterized by early-onset spasticity, ambulation impairment, dystonia, myoclonic epilepsy, oculomotor apraxia and cerebellar ataxia [158]. However, the symptoms have a variable severity, as observed by Muona et al., [159]. *In vitro* functional studies on yeasts showed that the mutation studied by Pierson and colleagues induces reduced, but not abolition, of the *m*-AAA protease homooligomers, and impaired assemble of both the homo and heterooligomers [158]

In order to understand the pathology development and the functional impairment caused by *AFG3L2* dysfunction, several murine models were generated [139, 151, 164-167]. Animals carrying a null mutation in the *Afg3l2* gene, obtained by ectopic insertion in exon 14 of the murine leukemia virus insertion 66, in heterozygosis (*Afg3l2*^{+/*Emv66*}) manifest a progressive motor impairment with imbalance, mitochondrial dysfunction and cerebellar Purkinje neurons degeneration starting at 4 months of age, whereas the spinal cord was unaffected [168]. The concomitant knockout of *Spg7* in these animals (*Spg7*^{-/-};*Afg3l2*^{+/*Emv66*}) induces a severe phenotype featuring ataxia, imbalance and tremor. Moreover affected animals develop an

axonopathy, faster than the *Spg7*^{-/-} mice and cerebellar degeneration which occurs faster than in the *Afg3l2*^{+/*Emv66*} [151]. In the *Afg3l2*^{*Emv66/Emv66*} null mutant, where the AFG3L2 protein is completely absent, homozygosis leads to complete paralysis by postnatal day 16. The same phenotype was observed in animals carrying an amino acid mutation where an arginine residue was substituted by a glycine residue in position 389, in the AAA domain. In both models of SPAX5, carrying the homozygous depletion of AFG3L2, animals displayed spinal cord reduced axonal diameter and myelinated densities. Moreover, loss of large axons was observed, mostly due to developmental problems, as there is no sign of inflammation or reactive astrogliosis [164].

The Purkinje neurons (PCs) of the cerebellum appear to be sensitive to *Afg3l2* mutations, also because of their high AFG3L2 protein levels [151, 157]. Almajan and colleagues [165] used a conditional knockout model, which targets PCs specifically using the L7 promoter to induce recombination *via* the Cre-LoxP system. Flanking exons 4 and 5 of the *Afg3l2* gene with two LoxP site (*Afg3l2*^{fl/fl}) allowed the selective deletion of the protein only in PCs. The cells developed respiratory deficiency and reduced mitochondrial ribosomal assembly, accompanied by mitochondrial morphological abnormalities and subsequent neuronal electrophysiological alterations and death. To complete the scene, reactive astrogliosis and neuroinflammation also occurred. *Afg3l2* downregulation in primary neuronal cultures showed that mitochondrial anterograde transport is reduced due to tau hyper-phosphorylation [166]. However, the mechanism leading to cellular death is still elusive. Ca²⁺ concentration dysregulation seems to be implicated: according to Maltecca et al., [169, 170] *Afg3l2* deficient mitochondria at the synaptic buttons are incapable of buffering Ca²⁺. The ion intracellular concentration increases in PCs following synaptic stimulation, and it activates calpains triggering a cell death mechanism called dark cell degeneration, as in semithin sections dying cells appear darker. Previously observed following glutamatergic excitotoxicity, dark cell degeneration causes

cytoplasmic condensation, vacuolated cytosol, chromatin aggregation but not apoptotic bodies and no signs of phagocytosis [171]. Dark cell degeneration was also observed in a conditional *Afg3l2* knockout mouse model targeting myelinating cells in a *Afg3l1* null background (*Afg3l1*^{-/-}) [167]. *Afg3l1*^{-/-}: *Afg3l2*^{fl/fl} mice were crossed with a Cre recombinase line driven by a proteolipid protein promoter (PLP-Cre^{wt/tg}), which gives specificity for myelinating cells. While *Afg3l2*^{fl/fl}: PLP-Cre^{wt/tg} and *Afg3l1*^{-/-} mice do not show any phenotype up to 60 weeks, *Afg3l1*^{-/-}: *Afg3l2*^{fl/fl}: PLP-Cre^{wt/tg} manifest an early-onset impaired motor coordination, reduced body-weight and hair-greying. Mitochondria in targeted cells are highly fragmented and swollen with abnormal cristae morphology. Moreover, targeted cell loss and axonal abnormal myelination were observed. Despite the neurons have properly functional *m*-AAA proteases, animals manifest phenotype upon *m*-AAA protease dysfunction in myelinating cells, suggesting that glial cells dysfunction contributes to the neuronal demise [167].

The assumption that Ca²⁺-mediated cell death could be the cause of PCs degeneration, seemed to find further proof in the work published by König and colleagues [138]. In fact, the authors showed that upon *Afg3l2* deletion the EMRE-MCU gate-less complex is constitutively activated and mitochondria are flooded with excessive Ca²⁺, inducing the MPTP opening and massive release of the ion in the cytosol. This may lead to Ca²⁺-mediated cell death, being it apoptosis or dark cell degeneration. To further prove the Ca²⁺-mediated cell death, Maltecca et al., [170] used two different strategies, based on the rationale that increased Ca²⁺ concentrations in PCs are due to glutamatergic stimulation from the granule cells. In order to reduce it, they crossed the *Afg3l2*^{+ /Emv66} mice with a line expressing a loss of function mutation of the metabotropic glutamate receptor 1 (mGluR1), in heterozygosis. The second strategy consisted in the administration to *Afg3l2*^{+ /Emv66} mice of the antibiotic ceftriaxone, which increases the expression of EAAT2 receptors on astrocytes. In both cases, the authors were able to rescue the phenotype of *Afg3l2*^{+ /Emv66} mice. Recently, a work from Patron et al., [139] aimed to ultimately

confirm or deny Ca^{2+} dysregulation as causative for PC death with a direct approach: *Afg3l2*^{fl/fl}:L7-*Cre*^{wt/tg} mice were crossed with *Mcu*^{fl/fl} mice. Despite the reduced MCU levels and Ca^{2+} uptake by mitochondria, PCs fate was unchanged when compared to *Afg3l2*^{fl/fl}:L7-*Cre*^{wt/tg} mice. This observation, according to the authors, rules out the possibility that Ca^{2+} imbalance *per se* is the cause of neuronal cell death in case of *m*-AAA protease impairment.

1.4 Mitochondrial function in astrocytes

The distribution of the mitochondrial network in astrocytes was debated over the years. Protoplasmic astrocytes have many processes, and one single astrocyte can ensheat 100,000 synapses in rodents [172]. However, their diameter varies between 20-200 nm in the peripheral astrocytic processes (PAPs). Considering mitochondrial diameter in other cell types could reach 1 μm [173], it seemed unrealistic for PAPs to have mitochondria. However, it was extensively shown that astrocytes have an extended mitochondrial network in their PAPs [173-175].

Studies using FACS and acutely isolated astrocytes provided evidences of the predominant glycolytic profile of these cells [33, 45, 176]. The glycolytic profile of astrocytes is supported by studies showing that the pyruvate dehydrogenase kinase 4 (PDHK4) is highly expressed in astrocytes. PDHK4 phosphorylates the pyruvate dehydrogenase (PDH) and decreases its activity, favoring the conversion of pyruvate in lactate and decreasing OXPHOS activity [176, 177]. Therefore, it is necessary to understand what, beside OXPHOS, mitochondrial are needed for in astrocytes.

Despite the lack of excitability, meant as neuronal-like response, astrocytes react to neuronal activity with Ca^{2+} fluctuations. Despite the amplitude and the purpose of the varying calcium concentrations can differ, it was shown that small Ca^{2+} signaling microdomains occur in concomitant presence of mitochondria [178, 179]. The reason for mitochondrial localization at the place of the microdomains could be the requirement of ATP to fuel the pumps in charge of moving Ca^{2+} in various compartments inside and outside the cell. In fact, it was shown that increased Ca^{2+} concentration within the matrix is associated with increased ATP production rate in cardiac mitochondria [173]. Furthermore, nanomolar elevations of cytosolic calcium induce increased activation of the aspartate-glutamate carrier 1, which leads to increased NADH levels in mitochondria. This is suspected to increase mitochondrial respiration *via*

OXPPOS in a glutamate-dependent fashion [180]. In addition, it was shown that mitochondria are localized in proximity of astrocytes glutamate transporters EAATs [181]. EAAT2 transports inside astrocytes a molecule of glutamate together with Na^+ and transports K^+ outside the cell. The ions gradient is maintained by the Na^+/K^+ ATPase which, using the energy provided by ATP hydrolysis, pushes sodium outside the cell and potassium inside [182]. The Na^+/K^+ ATPase activity requires high amounts of ATP to fulfill its activity. It was proposed that the glutamate transported inside astrocytes by the EAATs is partially used to refuel the neuronal pools, but it is also partially converted to α -ketoglutarate and used for producing ATP *via* OXPPOS, to provide localized energy substrate for the Na^+/K^+ ATPase activity [183].

Mitochondria Ca^{2+} buffering can actually contribute to the astrocytic Ca^{2+} microdomains by releasing the ion *via* the $\text{Na}^+/\text{Ca}^{2+}$ exchanger NCLX or *via* the opening of the MPTP [173]. Mitochondrial relevance in regulation of Ca^{2+} transients was proposed. In fact, administration of the proton uncoupler carbonyl cyanide p-trifluoromethoxy-phenylhydrazone (FCCP), which causes the dissipation of mitochondrial membrane potential, induces not only the rate decay of the astrocytic Ca^{2+} transients, but also the increased spatial propagation of spontaneous transients as well as the increase of their amplitude [104, 178]. Furthermore, Ca^{2+} is required for mitochondria movement. These organelles accumulate in areas with elevated activity or high-energy demand, and it was previously reported that neuronal activity, glutamate uptake and inverse directionality of the NCLX block mitochondrial transport [181, 184]. In fact, mitochondrial movement requires the adaptor mitochondrial Rho-GTPase proteins 1 and 2 (Miro1 and 2). The role of these proteins is to tether mitochondria to the motor proteins kinesin and dynein, which move the organelles along the microtubule network. The tethering occurs at low calcium concentration in astrocytes, and when intracellular Ca^{2+} increases following the N-methyl-D-aspartate receptor (NMDAR) activation on astrocytes surface, miro proteins disassemble from the motor complex anchoring mitochondria to the activated area [178, 185].

The fact that mitochondria are located at the spot of ~85% Ca^{2+} spontaneous microdomains, hinted to the hypothesis that they contribute to the intracellular ion-mediated signaling in the PAPs. To test this, Agarwal et al [186] blocked the MPTP using cyclosporine A and rotenone, and this reduced the spontaneous microdomains by 35%. Moreover, when adding picrotoxin to induce neuronal activation, they could detect reduced Ca^{2+} release from mitochondria, demonstrating that mitochondria in astrocytes are involved in the generation of calcium microdomains.

1.4.1 Mitochondrial dysfunction in astrocytes and diseases

In case of trauma or neurodegeneration, astrocytes are essential responders, and their mitochondrial network changes along with their activity: Motori and colleagues [174] revealed that, following stab wound injury on mice forebrain, mitochondrial network in astrocytes varies depending on their localization. In fact, astrocytes localized in the core lesion displayed a heavily fragmented mitochondrial network, whereas astrocytes in the penumbra area (i.e. the scar forming region) showed an elongated mitochondrial network, compared to the tubular network of the contralateral uninjured brain region. They also showed that the changes in the core lesion resolved within 10 days from the surgery, but in the penumbra area the mitochondrial network in astrocytes remained elongated up to 10 days. The altered mitochondrial dynamics are caused by pro-inflammatory stimuli, such as $\text{IL-1}\beta$, which also induce increased glycolytic rate and reactive oxygen species (ROS) production in fragmented mitochondria. Finally, the authors showed that mitophagic elimination of fragmented mitochondria restored the tubular network in the core-lesion area [174].

Despite mitochondrial important role in astrocytic function and response to injury, very little is known about mitochondrial dysfunction in astrocytes and its relevance for neurodegeneration. Recently, two murine models of mitochondrial dysfunction in astrocytes have been published,

showing how astrocytic response to mitochondrial dysfunction is complicated [34, 187]. To evaluate the effect of impaired mitochondrial respiration in astrocytes, Supplie and colleagues generated a conditional mouse model in which the cytochrome c oxidase subunit COX10 was specifically depleted in adult astrocytes [34]. The assumption was that astrocytes, being considered glycolytic cells, survive OXPHOS deficiency. Indeed, this was the case, as mice did not display any phenotype. Further analysis did not show any cerebellar abnormality, nor cell death or neuroinflammation. Despite cerebellar astrocytes showed extensive OXPHOS deficiency, they survived by upregulation of aerobic glycolysis.

Mitochondrial respiration seems to be dispensable for astrocytes survival. However, mitochondrial function in astrocytes is not limited to ATP production. Therefore, targeting different mitochondrial functions could reveal that these organelles are indeed essential for astrocytes survival. The Twinkle helicase is essential for mtDNA replication [188], and mutations in the gene encoding it causes the Alpers-Huttenlocher syndrome, characterized by cortical necrosis and spongiotic changes [189]. Ignatenko and colleagues worked on different murine models of Twinkle helicase knockout. While the full body knockout model was not compatible with life, conditional models targeting specifically neurons or astrocytes survived birth and developed till adulthood. However, both mouse models featured a neurodegenerative phenotype. Interestingly, the astrocyte-specific murine model showed the neurological impairment earlier than the neuronal-specific knockout, developing OXPHOS deficiency, secondary neuronal damage, inflammation and, importantly, spongiotic encephalopathy, which was not developed in the neuronal-specific line. The neuronal-specific knockouts showed signs of respiratory deficiency in neurons, apoptosis, reactive astrogliosis and inflammation. Despite the development, at 4-5 months, of the neurological phenotype was early-onset in the astrocyte-specific model compared the neuronal-specific model, animals survived for an additional 4-5

months. The neuronal-specific mouse model on the other hand showed a late-onset phenotype, at 7-8 months, which quickly developed leading to death in less than two months [187].

To conclude, mitochondrial function in astrocytes is essential for OXPHOS, Ca²⁺ homeostasis, cell death inhibition as for other cells. Moreover, mitochondrial dysfunction in astrocytes is detrimental and potentially lethal, as it is for neurons, and goes beyond the respiratory efficiency.

2 AIM

The aim of my thesis is understanding the contribution of astrocytes to the development of neuronal phenotypes associated with *m*-AAA protease dysfunction. I divided the aim in 3 questions:

- Is the *m*-AAA protease dysfunction lethal for astrocytes, as it is for neurons?
- What is the effect of astrocytic *m*-AAA protease impairment in the cerebellum?
- Does astrocytic *m*-AAA protease dysfunction affect PCs intrinsic properties and morphology?

Of note, the murine models, as well as the cell culture experiments were mostly aimed to understand the pathophysiological causes of neuronal death upon *m*-AAA protease deficiency. The mechanism underlying neuronal death remains elusive. The *m*-AAA protease deficiency equals a death sentence for certain neuronal populations and it is crucial to understand how to revert neuronal damage. Moreover, different *m*-AAA protease subunits are linked to differential neuronal susceptibility, probably because different neuronal subpopulations have increased expression of one subunit respect to the other. In fact, it was shown that PCs express high levels of AFG3L2, while pyramidal neurons of the cortex express high levels of paraplegin [157, 190]. Furthermore, it cannot be excluded that different *m*-AAA subunit composition could cause selectivity for undetermined substrates, exponentially threatening specific neuronal subpopulations.

However, it has to be considered that in human diseases caused by *m*-AAA protease dysfunction, neurons are not the only cells affected. The pathophysiological alterations in glial cells could also cause an additional stress on neurons, worsening the already serious condition of the cells. It was shown that alleviating the glutamatergic stimulation on PCs by increasing

the EAAT2 receptors on astrocytes ameliorates the phenotype in the SCA28 mouse model [170]. This finding suggests that astrocytes may have an unrecognized role in the development of the neurodegenerative disorders caused by *m*-AAA protease dysfunction in humans.

3 MATERIAL AND METHODS

3.1 Mouse models

Animal experiments took place in accordance with European (EU directive 86 /609/EEC), German (TierSchG), institutional guidelines and local authorities (Landesamt für Natur, Umwelt und Verbraucherschutz Nordrhein-Westfalen, Germany). Animals were kept in single ventilated cages, under 12h:12h day/night cycles. Food and water were provided *ad libitum* and animals were monitored for signs of motor impairment and distress.

3.1.1 Astrocyte-specific *Afg3l2* knock-out line (*astro-L2 KO*)

Mice carrying two LoxP sites flanking exons 4 and 5 of *Afg3l2* (*Afg3l2^{fl/fl}*) gene were previously described [165, 167]. This conditional mouse line was crossed with the inducible GFAP-CreERT line (hGFAP-Cre^{tg/wt}) [191]. The GFAP promoter gives specificity for targeting astrocytes, when induced after post-natal day 7 (P7) *via* tamoxifen injection. To minimize stress reaction on pups, intraperitoneal tamoxifen injections were administered to lactating mothers for five consecutive days. Control animals (Ctrl) used were hGFAP-Cre^{wt/wt} littermates. Furthermore, to visualize mitochondrial morphology and to identify targeted cells, we crossed the *astro-L2 KO* mouse line with the ROSA26^{+SmY} mice (mtYFP^{tg/+}) [165, 167, 192].

3.1.2 Astrocyte specific *m-AAA* protease ablation mouse model (*astro-DKO*)

In order to obtain total ablation of the *m-AAA* protease, *astro-L2 KO* mice were crossed with full body *Afg3l1* knock out mice (*Afg3l1^{-/-}*). This mouse line was previously described [167] and does not show any phenotype up to 60 weeks. In this case control animals were *Afg3l1^{-/-}* littermates (L1^{-/-}) Furthermore, to visualize mitochondrial morphology and targeted cells, astro-

DKO mice were crossed with the ROSA26^{+SmY} mice. The GFAP-Cre recombinase was induced as previously described.

3.2 Tamoxifen injection procedure

To induce the Cre-mediated recombination, intraperitoneal injection of tamoxifen (T5648, Sigma) was performed on lactating mothers. The drug was dissolved in a mixture of corn oil (Sigma) and pure ethanol 9:1, at the concentration of 20 mg/ml. Prior the injection, the mothers were weighted and the amount of tamoxifen used was calculated in order to administer 1 mg/10 g of body-weight/day.

3.3 Behavioral analysis

3.3.1 Rotarod assay (performed by Steffen Hermans)

To assess motor coordination, male and female astro-L2 KO mice and their respective controls were tested on a rotarod apparatus (TSE system) at 8, 32 and 62 weeks. Animals were trained for 1 minute on the steadily rotating rod at a speed of 4 rpm. During the actual test, animals were placed on the accelerating rod, starting with a speed of 4 rpm, with constant acceleration of 7.2 rpm up to a maximum of 300 seconds. The latency to fall was recorded. Three trials were performed on the same day, 15 minutes apart from each other.

3.3.2 Ataxic score evaluation

The ataxic score evaluation was performed as described previously [193]. It consists of four different tests and observations: ledge test, hind limbs clasp test, gait and kyphosis evaluation. Animals were scored 0 to 3, according to table 1, and the sum of the evaluations of each test determined the final score. Both male and female astro-DKOs and L1^{-/-} mice were tested.

Table 1 - Ataxic phenotype score evaluation.				
Score	Ledge test	Hind limb test	Gait	Kyphosis
0	no balance lost while walking-lower itself back into the cage gracefully	hind limbs outward	move normally, bodyweight supported by all the limbs and both hind limbs participating	straightened spine while walking, no persistent kyphosis
1	foot slips but overall coordinated	one retracted limb more than 50% of suspended time	tremors, limp while walking	mild kyphosis but straightened spine
2	no hind limb grasp, land on its head	both hind limbs partially retracted more than 50% of time	sever tremor and limp, lowered pelvis, feet away from the body	persistent but mild kyphosis
3	fall or nearly-refuses to move and shake	entirely retracted for more than 50% of the time	difficulty in moving, abdomen touching the ground	persistent pronounced kyphosis walking or sitting

3.4 Tissue collection

3.4.1 Transcardial perfusion

Animals were anesthetized with an intraperitoneal injection of a ketamine/xylazin mixture (100 mg/10 mg per kg of bodyweight). Once unconscious, the abdominal cavity was opened to expose the heart. The needle was inserted in the left ventricle and the vena cava was severed close to the heart junction, so that the blood and the perfusion solutions could flow out of the body. Animals that were up to 4 weeks old were transcardially perfused with a 21 G scalp vein

set, while older animals were perfused with a 18 G scalp vein set (Ecoflo). Mice were first perfused with 1X phosphate buffer saline (PBS) for 5 minutes, then with 4% paraformaldehyde (PFA) in 1X PBS for an additional 5 minutes. Afterwards, organs were removed and placed in 4% PFA or in 2% glutaraldehyde.

3.4.2 Cervical dislocation

When fresh tissue was required, mice were euthanized *via* cervical dislocation. The tissues were placed either in sucrose 15% for 4 hours, or post-fixed in 4% PFA for 24 hours or directly frozen in liquid nitrogen and stored at -80°C.

3.5 Histological analyses

3.5.1 Immunofluorescence stainings on free floating sections

Tissues taken from transcardially perfused mice, were embedded in 6% agar and cut in 30 µm sagittal slices using a vibratome (VS1000, Leica). Sections were washed in tris-buffered saline (TBS) and post fixed with methanol. Permeabilization and blocking buffer was prepared with 0.4% Triton X-100 (Fluka), and 10% goat serum in TBS and sections were incubated for 1 hour at room temperature (RT). Afterwards, sections were placed in the primary antibody solution (0.4% Triton X-100, and 5% goat serum in TBS) with single primary antibody or a combination of two antibodies (table 2) O/N at 4°C. Sections were then washed in TBS and incubated at RT for 2 hours with the secondary antibody solution (5% goat serum in TBS), with single antibody or a combination of two different ones (table 3). Following additional TBS washes and DAPI incubation (1:1000), sections were mounted on glass slides with Fluoro Save reagent (Calbiochem) and left for drying at 4°C O/N. Fluorescence images were acquired using Axio-Imager M2 microscope equipped with Apotome 2 (Zeiss) and processed using the software AxioVision SE64 Rel. 4.9.1. For quantifications, 3 to 7 images from each staining were

manually counted using ImageJ software. At least 3 animals for each genotype at each time point were used for the experiments. The antibodies used are listed in table 2 and 3.

Table 2 – Primary antibodies for immunofluorescence stainings			
Antibody	Company	Catalogue #	Concentration
Calbindin	SWANT	300	1:500
EAAT1	Miltenyi	5684	1:1000
EAAT2	BD Transduction	611654	1:1000
GFAP	Cell Signaling	3670	1:500
GFP	Aves	GFP-1020	1:500
NG2	Millipore	AB5320	1:250
Iba1	Wako	019-19741	1:2000
S100	DAKO	Z0311	1:2000
SMI31	Covance	SMI-31R	1:500
SOX2	Abcam	979559	1:700
vGlut2	SySy	135402	1:500

α -chicken Alexa Fluor 488	Jackson Immuno research	703-545-155	1:500
α -mouse Alexa Fluor 488	Molecular Probes	A-11029	1:1000
α -mouse Alexa Fluor 546	Molecular Probes	A-21143	1:1000
α -rabbit Alexa Fluor 488	Molecular Probes	A-11034	1:1000
α -rabbit Alexa Fluor 546	Molecular Probes	A-11035	1:2000
α -guinea pig Alexa Fluor 647	Molecular Probes	A32728	1:1000
α -rabbit Alexa Fluor 594	Molecular Probes	A-21207	1:1000
Streptavidin, Alexa Fluor 633 conjugated	Thermos Fisher	S21375	1:400

3.5.2 Electron microscopy (performed by Esther Barth)

The cerebellum was dissected and post fixed in 2% glutaraldehyde (Sigma) in 0.12 M phosphate buffer at 4°C. The tissue was immerse in freshly prepared 2% glutaraldehyde the day before the embedding. The tissue was then immerse in 1% osmium tetroxide (Sigma) for up to 4 hours, dehydrated in ethanol gradient (50-100%) and propylene oxide. Once the embedding in Epon (Fluka) was solidified, the tissue was trimmed with an ultramicrotome (EM UC, Leica) and 1 μ m sections were cut and stained with 1% toluidine blue for light microscopy. Furthermore, 70 nm ultrathin sections were stained with 160 mM sodium hydroxide, 2% uranyl acetate (Plano GMBH), 3.52% sodium citrate (Electron microscopy sciences), 2.66% lead citrate (Electron

microscopy sciences). For imaging, the transmission electron microscope (JEOL JEM2100PLUS) equipped with GATAN OneView camera was used.

Synapses were counted manually on acquired pictures (10000X) using ImageJ software.

3.5.3 Immunohistochemistry on paraffin sections

Following 4% PFA post-fixation, tissues were dehydrated in ethanol gradient (70-100%) and xylene. The tissues were then embedded in paraffin, and cut in 5 μ m sagittal slices using a microtome (RM2255, Leica). Selected sections were then deparaffinized with xylene and ethanol incubations, washed in PBS. Endogenous peroxidases were quenched by incubation in peroxidase quenching buffer (0.04 M NaCitrate, 0.121 M Na₂HPO₄, 0.013 M NaN₃ and 3% H₂O₂). Following rinse in water, sections were boiled in 10mM NaCitrate buffer containing 0.05% Tween-20 (pH 6) for 20 minutes, and cooled for additional 40 minutes to induce epitope retrieval. Permeabilization and blocking was performed with 1% albumin, 0.1% Triton X-100 and 0.05% Tween-20. The cleaved caspase 3 Asp175 (Cell Signaling, 9661; 1:500) primary antibody incubation was performed O/N at 4°C in permeabilization and blocking buffer, together with Avidin D and Biotin from the Vectastain Blocking kit. Secondary biotinylated anti-Rabbit (Vector, BA-1000) antibody was then applied with Avidin D and Biotin from the ABC Kit Vectastain Elite. The staining was then visualized using the DAB chromogen and its substrate (Vector Laboratories). Three animals at each time-point were used for each genotype. The slides were then scanned with a slide scanner (SCN400, Leica) and analyzed with the software Aperio ImageScope (v12.3.2.8013). Positively stained cells were manually counted from 3 to 4 cerebellar sections/animal.

3.5.4 COX-SDH histochemistry

Animals were sacrificed *via* cervical dislocation, followed by cerebella dissection, the samples were immersed in 15% glucose for 4 hours and then in 30% sucrose O/N at 4°C. To facilitate

the cutting procedure, the tissue was embedded in OCT (Tissue Tek), frozen in dry ice and stored at -80°C till use. The cryostat (CM1850, Leica) was set at -21°C and tissues were equilibrated inside the machine for 20 minutes before cutting. 3 to 4 parallel sections of 10 µm were placed on each slide and kept at -80°C until the COX-SDH histochemistry was performed. On the experimental day, selected sections were air dried for 1 hour and then covered with COX solution: 5 mM 3,3 diaminobenzidine tetrahydrochloride (Sigma-Aldrich), 500 µM cytochrome c (Sigma-Aldrich) and Bovine catalase 2 mg/ml (Sigma-Aldrich). The slides were incubated for 40 minutes at 37°C in a humidified chamber. Following quick washes in PBS, the sections were covered with SDH solution composed of 1.875 mM nitroblue tetrazolium (Sigma-Aldrich), 1.3 M sodium succinate (Sigma-Aldrich), 2 mM phenazine methosulphate (Sigma-Aldrich) and 100 mM sodium azide (Sigma-Aldrich). The incubation took place at 37°C in a humidified chamber for up to 90 minutes. The slides were then scanned with a slide scanner (SCN400, Leica) and analyzed with the software Aperio ImageScope (v12.3.2.8013).

3.6 Molecular Biology

3.6.1 Genotyping and recombination assessment

Genomic DNA was usually extracted from ear-punches and used for genotyping. However, to assess recombination in different tissues, genomic DNA was also extracted from livers, tails, forebrains and cerebella where indicated. The tissue was incubated O/N in lysis buffer (50 mM Tris-HCl pH 8, 100 mM NaCl, 100 mM EDTA pH 8, 0.5% SDS and 1 mg/ml proteinase K) at 55°C. Following 10,000 g centrifugation at RT for 10 minutes, the supernatant was collected in a new tube. DNA precipitation was performed in 100% ethanol at 15,000 g centrifugation at 4°C. The precipitated DNA was washed in 70% ethanol and centrifuged again at 15,000 g at 4°C. The DNA was resuspended in 500 µl of TE buffer (10 mM Tris-HCl pH 8, 1 mM EDTA pH 8). For each sample, 7.5 µl of EmeraldAMP MAX PCR Master Mix (TaKaRa) were mixed

with 1 μ l of each primer (10mM) and 0.5 μ l of DNA. The final volume was adjusted to 15 μ l by adding autoclaved water. The PCR program is reported in table 4, while the primers used are reported in table 5.

Table 4 - PCR program for genotyping and recombination assessment		
Temperature	Time	Number of cycles
95 °C	2 minutes	1
95 °C	15 seconds	34
58 °C	30 seconds	
72°C	45 seconds	
72°C	5 minutes	1

Table 5 - PCR primers			
Locus	Primer name	Sequence (5'-3')	Amplicon size (bp)
<i>Afg3l2</i>	Wt/fl FW	TTGGTTTTGTATGTGTTAGGTCAG	Wt1: 387;
	Wt/fl RV	GCCTGCACAGCTCCATGAT	Fl: 506
	Δ RV	ATTTGGAGCTGCGGGTTAG	Wt2: 1325 Δ : 467

<i>Afg311</i>	Wt/KO FW	GCATTGCACAGTCATTTTCAGG	Wt: 272 KO: 509
	Wt RV	GCCGTGGGTAATGTTTGTTC	
	KO RV	TGGACAGGGCATTATGATGC	
<i>ROSA26</i>	Mt-YFP1	AAAGTCGCTCTGAGTTGTTAT	Wt: 583 Tg: 250
	Mt-YFP2	GCGAAGAGTTTGTCTCAACC	
	Mt-YFP3	GGAGCGGGAGAAATGGATATG	
<i>CRE</i>	Cre1 (TL-7677)	GAACCTGATGGACATGTTTCAGG	Tg: 320
	Cre2 (TL-7678)	AGTGCGTTCGAACGCTAGAGCCT	
	House-keeping1 (TL-7901)	GGAGCGGGAGAAATGGATATG	Wt: 250
	House-keeping2 (TL-7902)	TGGGCTGGGTGTTAGTCTTA	

Wt= wild type, FW= forward; RV= reverse.

3.6.2 RNA extraction and quantitative real time PCR

Animals were quickly sacrificed *via* cervical dislocation. Brain and forebrain were dissected, snap frozen in liquid nitrogen and stored at -80°C. The tissue was homogenized in Trizol (Thermo Fisher Scientific) using a precooled hand-homogenizer. After adding chloroform, samples were centrifuged at 12,000 g at 4°C for 15 minutes and the aqueous phase of the mixture was transferred to a new tube. The RNA was then precipitated for 10 minutes at 12,000 g centrifugation at 4 °C in isopropanol. The RNA pellet was then washed in 75% ethanol and dried at room temperature. The pellet was resuspended in 50 µl of ultrapure water and store at -80°C till use. SuperScript™ First Strand Synthesis System (Thermo Fisher Scientific) was use to retro-transcribe 2 µg of total RNA. Random hexamer primers were used according to the manufacturer instructions. The resulting cDNA was diluted 1:10 in double distilled water and the real time PCR was performed using the SYBR® green master mix (Thermo Fisher scientific) and 600 nM of each primer (table 7). Duplicates or triplicates of each sample were analyzed for each gene. The Quant Studio 12K Flex Real-Time PCR System thermocycler (Thermo Fisher Scientific) was used with the program indicated in table 6. The fold increase was determined with the formula $2^{(-\Delta\Delta Ct)}$ and *HPRT1* was used for normalization.

Table 6 – PCR program for quantitative real time PCR

Temperature	Time	Number of cycles
95°C	10 minutes	1
95°C	15 seconds	40
65°C	1 minute	

95°C	15 seconds	1
60°C	1 minute	1
95°C	15 seconds	1

Table 7 – Quantitative real time PCR primers

Primer name	Sequence 5'-3'
HPRT1 forward	TCCTCCTCAGACCGCTTTT
HPRT1 reverse	CATAACCTGGTTCATCGC
TNF α forward	CTTCTGTCTACTGAACTTCGGG
TNF α reverse	CAGGCTTGTCACTCGAATTTTG
IL-1 β forward	GAAATGCCACCTTTTGACAGTG
IL-1 β reverse	TGGATGCTCTCATCAGGACAG
IL-6 forward	TAGTCCTTCCTACCCCAATTTC
IL-6 reverse	TTGGTCCTTAGCCACTCCTTC
PSAT1 forward	AGTGGAGCGCCAGAATAGAA
PSAT1 reverse	CTTCGGTTGTGACAGCGTTA

PHGDH forward	GACCCCATCATCTCTCCTGA
PHGDH reverse	GCACACCTTTCTTGCACTGA
MTHFD2 forward	CTGAAGTGGGAATCAACAGTGAG
MTHFD2 reverse	GTCAGGAGAAACGGCATTGC
Fadd forward	CGCCGACACGATCTACTG
Fadd reverse	GGCCAGTCTTTTCCAGTCTC
RIPK1 forward	GGAAGGATAATCGTGGAGGC
RIPK1 reverse	AAGGAAGCCACACCAAGATC
RIPK3 forward	ACCCACCGAATCCAATG
RIPK3 reverse	AGTTCCAATCTGCACTTCAG
MLKL forward	ACTGTGAACTTGGAACCCTG
MLKL reverse	TGCTGATGTTTCTGTGGAGTG
ZBP1 forward	TGTTGACTTGAGCACAGGAG
ZBP1 reverse	TTCAGGCGGTAAAGGACTTG
BAK forward	TGATATTAACCGGCGCTACG
BAK reverse	AGCTGATGCCACTCTTAAATAGG

PUMA forward	AGGAAGATCGGAGACAAAGTG
PUMA reverse	AGCACACTCGTCCTTCAAG
MCL1 forward	TTGTAAGGACGAAACGGGAC
MCL1 reverse	TCTAGGTCCTGTACGTGGAAG

3.7 Biochemistry

3.7.1 Amino acid extraction (performed by Dr Susanne Brodesser)

Snap frozen cerebella from cervically dislocated animals were thawed and weighted. Homogenization of the samples was performed with the Precellys 24 Homogenisator (Peqlab) at 6,500 rpm for 30 seconds in ice-cold acetonitrile/0.3 % formic acid 1:1 (v/v) (10 µl/mg tissue). Protein concentration was determined using bicinchoninic acid. A 1:10 dilution of internal standard mixture of isotope-labeled amino acids (Sigma) was added to the samples. Proteins were then precipitated with methanol *via* a 12000 g centrifugation for 5 minutes at 4°C and the supernatant was dried in autoinjector vials with nitrogen steam. The dried amino acids extracts were derivatized with 6-aminoquinolyl-N-hydroxysuccinimidyl carbamate and the AccQ-Tag Ultra Derivatization Kit (Waters).

3.7.2 Liquid Chromatography -Electrospray Ionization Tandem Mass Spectrometry (performed by Dr Susanne Brodesser)

In order to evaluate amino acid levels, samples were treated for Liquid Chromatography coupled to Electrospray Ionization Tandem Mass Spectrometry (LC-ESI-MS/MS) with a Core-Shell Kinetex C18 column (150 mm × 2.1 mm ID, 2.6 µm particle size, 100 Å pore size, Phenomenex) and the QTRAP 6500 triple quadrupole/linear ion trap mass spectrometer

(SCIEX) was used for detection. The liquid chromatography (1260 Infinity Binary LC System, Agilent) was performed at 40°C with a rate flow of 0.4 ml/minute, a mobile water phase with 0.1% formic acid and acetonitrile containing 0.1% of formic acid (AFsolution). The latter was used for column equilibration for 1 minute. Sample injection was accompanied with linear changes in AF solution from 3% to 95% and back to 3% for a total time of 18.4 minutes. For derivatized amino acids evaluation, the positive ion mode was used, together with their specific Multiple Reaction Monitoring (MRM) transitions (Waters). For integration of the chromatogram peaks of internal standards and endogenous amino acid derivatives, the software Analyst ver. 1.6.3 (SCIEX) was used. Serially diluted synthetic amino acid standard solutions within the range of 0.0 to 27.5 pmol on column were used to quantify endogenous amino acids. Each dilution was charged with known amount of isotope-labeled internal standards. Linearity and correlation coefficients (R²) of the calibration curves were obtained *via* linear regression analysis. R² of the calibration curves were >0.99. Normalization of endogenous amino acids was calculated to the wet weight of the tissue.

3.7.3 Protein extraction for western blot

Animals underwent quick cervical dislocation and the forebrain and cerebellum were snap frozen in liquid nitrogen and stored at -80°C till use. Lysis occurred in RIPA buffer containing 50 mM Tris-HCl pH7.4, 150 mM NaCl, 5 mM EDTA, 1% Triton X-100, 1% sodium deoxycholate, 0.1% SDS, and protease cocktail inhibitor (P2714, Sigma) on ice using a Potter S homogenizer (Sartorius) at 1000 rpm. Following the homogenization, the lysates were kept at 4°C for 30 minutes and additionally centrifuged at 20000 g for 30 minutes at 4°C. The supernatant was transferred to a new tube and the protein concentration analyzed using the Bradford assay (Bio-Rad Laboratories). The proteins were diluted to the desired concentration in SDS-sample buffer containing 50 mM Tris-HCl pH 6.8, 2 % SDS, 10 % glycerol, 0.004 %

bromophenol blue and 1 % of β -mercaptoethanol. Samples were then boiled for 5 minutes at 95°C and stored at -20°C.

3.7.4 Western Blot

50 μ g of proteins were resolved in 10% poly-acrylamide gels containing 0.1% SDS in running buffer (25 mM Tris, 192 mM glycine, 0.1% SDS) at constant 30 mA per gel. A protein marker was also used to identify the size of protein bands (PageRuler™ Plus Prestained Protein ladder, Thermo Fisher Scientific). Afterwards, proteins were transferred onto 0.45 μ m PVDF membrane (GE Healthcare) in blotting buffer (25 mM Tris, 192 mM glycine and 20% methanol) at constant 300 mA for 90 minutes at 4°C. To assess that the transfer occurred and evaluate the homogeneous protein concentration of the samples, the membranes were stained with the Ponceau solution containing 0.1% Ponceau S in 5% acetic acid. Following short reactivation in methanol and a quick wash in TBST (0.1% Tween 20 in TBS), the membranes were first incubated in 5% milk (in TBST) at RT for 1 hour, and then in primary antibody at 4°C O/N. After 3 10-minute washes in TBST, the membranes were incubated for 1 hour at RT with secondary antibodies diluted in 5% milk. After 3 more 10-minute washes in TBST, the membranes were incubated with enhanced chemiluminescent (ECL) detection reagents (GE Healthcare) and developed using X-ray films (FUJIFILM). Antibodies used are listed in table 8.

Table 8 – Antibodies for Western blot				
	Antibody	Company	# Catalogue	Dilution
Primary antibodies	Gephyrin/3B11	Schwarz lab	Home-made	1:50
	α -RIPK3	Cell Signalling,	15828S	1:1000
	α -Pan-actin	Millipore	MAB1501R	1:4000
Secondary antibodies	HRP-linked α -mouse IgG	Sigma-Aldrich	A9044	1:20000
	HRP-linked α -rabbit IgG	Sigma-Aldrich	A0545	1:10000

3.8 Electrophysiological recordings (performed by Dr Simon Hess)

4 weeks old $L1^{-/-}$ and astro-DKO mice (25-33 days of age) were anesthetized with isoflurane (AbbVie Deutschland GmbH and Co KG) and decapitated. Cerebella were quickly dissected and 300 μ m sagittal slices were cut with a microtome (HM-650, Thermo Fisher) in a 4°C, carbogenated (95% O₂ and 5% CO₂) glycerol-based modified artificial cerebrospinal fluid (GaCSF) containing 250 mM Glycerol, 2.5 mM KCl, 2 mM MgCl₂, 1.2 mM NaH₂PO₄, 10 mM HEPES, 21 mM NaHCO₃, 5 mM glucose (pH 7.2), with ~310 mOsm. Sections were then transferred to a carbogenated artificial cerebrospinal fluid (aCSF) and kept for 20 minutes at 35°C. aCSF composition was the following: 125 mM NaCl, 2.5 mM KCl, 2 mM MgCl₂, 2 mM CaCl₂, 1.2 mM NaH₂PO₄, 21 mM NaHCO₃, 10 mM HEPES, and 5 mM glucose (pH 7.2) resulting in an osmolarity of ~310 mOsm. Sections were acclimatized at RT for minimum 30 minutes before recording. Experimental chambers were filled with 3 ml continuously superfused with aCSF (2 ml·min⁻¹). Experiments were carried out at 32°C. A fixed-stage upright

microscope was used to visualize neurons in the slices (BX51WI; Olympus). PCs were identified by their location within the cerebellar cortex. Current clamp recordings were obtained with a modified ELC03-XS amplifier (NPI Electronic) controlled by the PatchMaster software (version 2.32; HEKA). Data were sampled every 20 μ s (50 kHz) with a CED 1401 using Spike2 (both Cambridge Electronics). Perforated patch clamp was performed as previously described [165, 194, 195]. Briefly, ATP and GTP free patching pipettes were filled with a solution containing 128 mM Kgluconate, 10 mM KCl, 10 mM HEPES, 0.1 mM EGTA, 2 mM MgCl₂ (pH 7.3) with an osmolarity of \sim 300 mOsm. Furthermore, 0.02% tetraethylrhodamine-dextran (D3308, Invitrogen) and amphotericin-containing internal solution (\sim 200-250 μ g \cdot ml⁻¹; G4888; Sigma). Amphotericin was dissolved in dimethyl sulfoxide (final concentration: 0.1 - 0.3%; DMSO; D8418, Sigma) and was added to the modified pipette solution shortly before use. The aCSF containing 10⁻⁴ M picrotoxin (P1675; Sigma-Aldrich), 5 x 10⁻⁵ M D-AP5 (A5282; Sigma-Aldrich), and 10⁻⁵ M CNQX (C127; Sigma-Aldrich) allowed to shut off synaptic glutamatergic and GABAergic stimuli. Membrane resistance was evaluated *via* injection of hyperpolarizing current pulses. Evoked action potential firing was evaluated *via* injection of depolarizing currents (100 pA to 1000 pA in 100pA increments; 1.5s duration), determining the number of action potentials. Recorded cells were labeled with 1% biocytin (B4261, Sigma), fixed with Roti-Histofix (P0873, Carl Roth) and incubated with Alexa Fluor 633- conjugated streptavidin for 2 hours and fluorescent images were acquired with a confocal microscope (SP-8, Leica).

3.9 Statistical analysis

Two-tailed unpaired Student's *t* test was applied to data sets using the software GraphPrism, v.6.07. Graphs represent mean \pm standard deviation (SD) or mean \pm standard error of the mean (SEM). When statistically significant, the *p* value is indicated in the graphs.

For electrophysiological studies, data analysis was performed with Spike2 (Cambridge Electronics) Igor Pro and GraphPad Prism v5.0b.

4 RESULTS

4.1 Specific targeting of Bergmann glia in the mouse cerebellum with an inducible GFAP-driven Cre-LoxP system

To analyze the astrocyte-specific effect of *m*-AAA protease dysfunction, I took under consideration two different aspects: which animal model to use, and how to induce the desired mutations in the cell type of interest. As animal model, I decided to use mice because of the structural similarities between mouse and human brains. Moreover, murine models recapitulating the *m*-AAA protease-related human diseases SCA28, SPAX5 and HSP were previously published [152, 168].

Considering my aim to target astrocytes and no other cell types, I decided to use a conditional knockout system. Cre recombinase is largely used to specifically induce deletion of portions of genes [196]. This enzyme, derived from bacteriophage P1, is able to induce site-specific recombination between two DNA recognition sites (LoxP) [197]. Nowadays, the Cre-LoxP system is widely used to target specific cell types within organisms. To achieve the specificity required, it is necessary to use a cell type specific-promoter upstream to the Cre sequence. In order to target astrocytes, I decided to use the human GFAP promoter (hGFAP). The advantage of this promoter is that it is expressed mainly in astrocytes after postnatal day 7. The disadvantage is that before that, it is expressed also in neuronal precursors [198]. To overcome the expression of the recombinase in precursors, I used an inducible form of Cre recombinase, downstream to the hGFAP promoter (hGFAP-Cre^{tg/wt}) [191]. In the hGFAP-Cre^{tg/wt} mouse line, animals carry a Cre recombinase fused to modified estrogen receptors (CreER): their task is to translocate the recombinase to the nucleus, where it can act on the DNA. The receptors need to bind a specific drug, called tamoxifen, to move to the nucleus. The advantage of this system is that I have control over the Cre recombinase activity and the resulting recombination.

Moreover, in order to visualize which cells are indeed targeted following the recombination, I crossed hGFAP-Cre^{tg/wt} mice with the mitochondrial conditional reporter line expressing the yellow fluorescent protein (YFP) fused with a mitochondria targeting sequence (MTS) in the ROSA26 (ROSA26^{+SmY}) locus. The stop codon on the ROSA26 locus is flanked by two LoxP sites, and, following Cre recombinase activation, the stop codon is removed and the mitochondrial YFP (mtYFP) is translated [192]. To induce the Cre recombinase, tamoxifen administration was performed on lactating mothers, starting when pups were 7 days old, once/day for 5 consecutive days (Fig. 4.1A).

Chow and colleagues demonstrated that astrocytes of the cerebellum (CB) are highly targeted with the hGFAP-Cre^{tg/wt} [191]. The cerebellar cortex is composed of three different layers. The most internal is the granule cells layer (GCL), where the glutamatergic granule neurons (GCs) reside. The Purkinje cell layer (PCL) contains the GABAergic PCs, which are located one close to the other in a monolayer. Finally, the molecular layer (ML) is the area where the synaptic contact between GC axons (parallel fibers) and the PC dendrites occurs. The PCL contains also the cell bodies of specialized radial astrocytes, called Bergmann glia (BG). These cells send their projections in the ML, and modulate the synaptic signals on the PC dendrites [199] (Fig. 4.1B).

The expression of the mtYFP highlights targeted cells, facilitating their identification. I used specific markers for PCs, parallel fibers and BG to perform immunofluorescence staining on cerebellar slices. PCs were stained with calbindin, a Ca²⁺-binding protein highly expressed in their cell body and dendrites [200]. Parallel fibers were stained with an antibody against phosphorylated neurofilament H and M, SMI31 [201]. BG was stained using the S100 marker, a Ca²⁺-binding protein expressed in glial cells that marks both cell body and projections of BG [202, 203]. The mtYFP signal perfectly co-localized with the S100 staining of BG, whereas no co-localization was detected between mtYFP and calbindin, nor SMI31 (Fig. 4.1C-E).

Therefore, I could conclude that BG are highly targeted with the designated hGFAP-Cre^{wt/tg}, and that the mtYFP is a reliable tool to visualize both targeted cell and mitochondrial morphology.

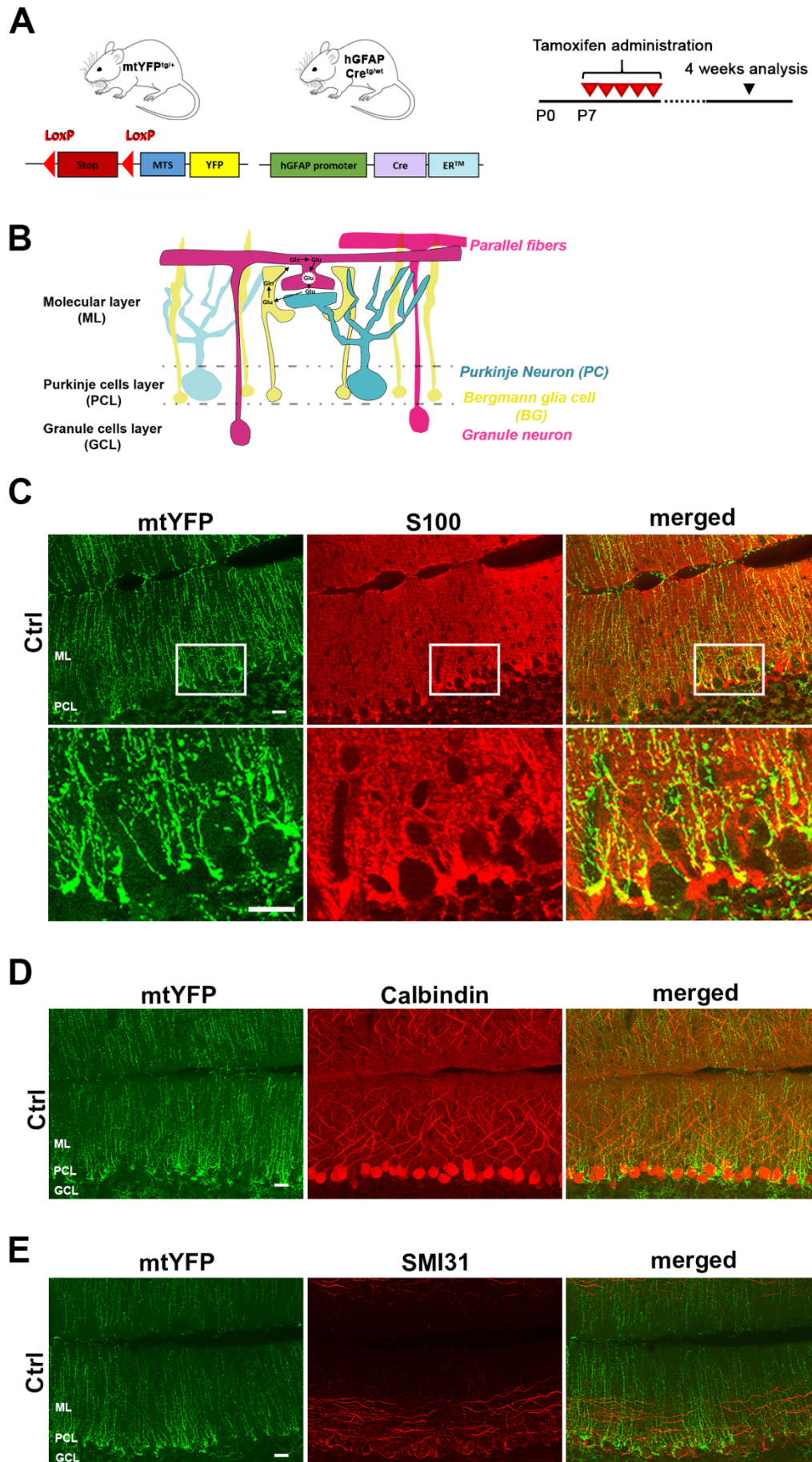


Figure 4.1: hGFAP promoter successfully targets astrocytes and not neurons when tamoxifen is administered starting at P7. (A) Strategy used to obtain transgenic mouse line expressing mtYFP in astrocytes. Lactating mothers (hGFAP-Cre^{wt/wt}) were injected with tamoxifen as indicated in the scheme (B) Schematic representation of the three layers of the cerebellar cortex and the 3 cell types under analysis. BG uptake glutamate (Glut) from the synaptic cleft, convert it to glutamine (Gln) and transport it to GCs, which use it produce Glut and restore their vesicles. (C-E) Immunofluorescence staining of cerebellar sections. mtYFP endogenous signal is represented in green, markers for astrocytes (S100), PCs (calbindin) and parallel fibers (SMI31) are indicated in red. Co-localization was detected only between mtYFP and S100 staining. n=3, scale bars= 20 μ m.

4.2 Generation of two mouse models of *m*-AAA dysfunction in astrocytes

The fact that the GFAP-Cre is active in the BG is of relevance as mutations in AFG3L2 in humans cause cerebellar atrophy [155, 157]. In a previous study, Almajan and colleagues reported the use of a conditional mouse line, in which exons 4 and 5 of the *Afg3l2* gene were flanked by two LoxP sites (*Afg3l2*^{fl/fl}), and a Cre recombinase under the L7 promoter allowed to specifically induce the recombination on PCs. Upon Cre activation, the cut in the alleles leads to the insertion of a premature stop codon and deletion of the functional protein [165]. To investigate the effect of the *m*-AAA protease dysfunction in astrocytes, and its outcome in the cerebellum, I crossed *Afg3l2*^{fl/fl} mice [165] with the inducible GFAP-Cre mouse line [191], resulting in the following genotype: *Afg3l2*^{fl/fl}: hGFAP-Cre^{tg/wt}, from now on called astro-L2 KO mice. The activation of the Cre recombinase was induced by intraperitoneal tamoxifen administration to the lactating mothers, starting when pups were 7 days old (Fig. 4.2A). To ensure that the recombination occurs, I extracted DNA from the forebrain, cerebellum, tail and liver from astro-L2 KO mice. I used the primers indicated in table 5 as *Afg3l2* wt/fl forward, the *Afg3l2* Δ reverse and the PCR program indicated in table 4. The strategy used is that the *Afg3l2* Δ primer binds to a region downstream to the cutting site. If the recombination occurs,

the PCR product would be a 467 bp band. In case the recombination is unsuccessful, the PCR product is a hardly detectable 1325 bp band. The hGFAP-Cre^{tg/wt} recombines in the forebrain and cerebellum, but not in liver and tail, indicating that the Cre is not active in other organs (Fig. 4.2B).

Astro-L2 KO mice have some residual *m*-AAA protease, as mice express a third *m*-AAA protease subunit called *Afg3l1*. AFG3L1 protein creates homooligomeric complexes and heterooligomeric complexes, together with paraplegin, and can compensate the AFG3L2 deletion [122, 167]. To obtain the complete elimination of the *m*-AAA protease in astrocytes, I crossed the astro-L2 KO mice together with the *Afg3l1* full body knockout (*Afg3l1*^{-/-}) mouse line [167], resulting in the following genotype: *Afg3l1*^{-/-}:*Afg3l2*^{fl/fl}: hGFAP-Cre^{tg/wt} (defined as astro-DKO) (Fig. 4.2C). Animals ablated of the AFG3L1 subunit of the *m*-AAA protease (*L1*^{-/-}) do not show any phenotype up to 60 weeks of age [167], and were used as controls for the astro-DKO mouse line. Animals were then analyzed at different time points, as indicated in figure 4.2 (Fig. 4.2A and C).

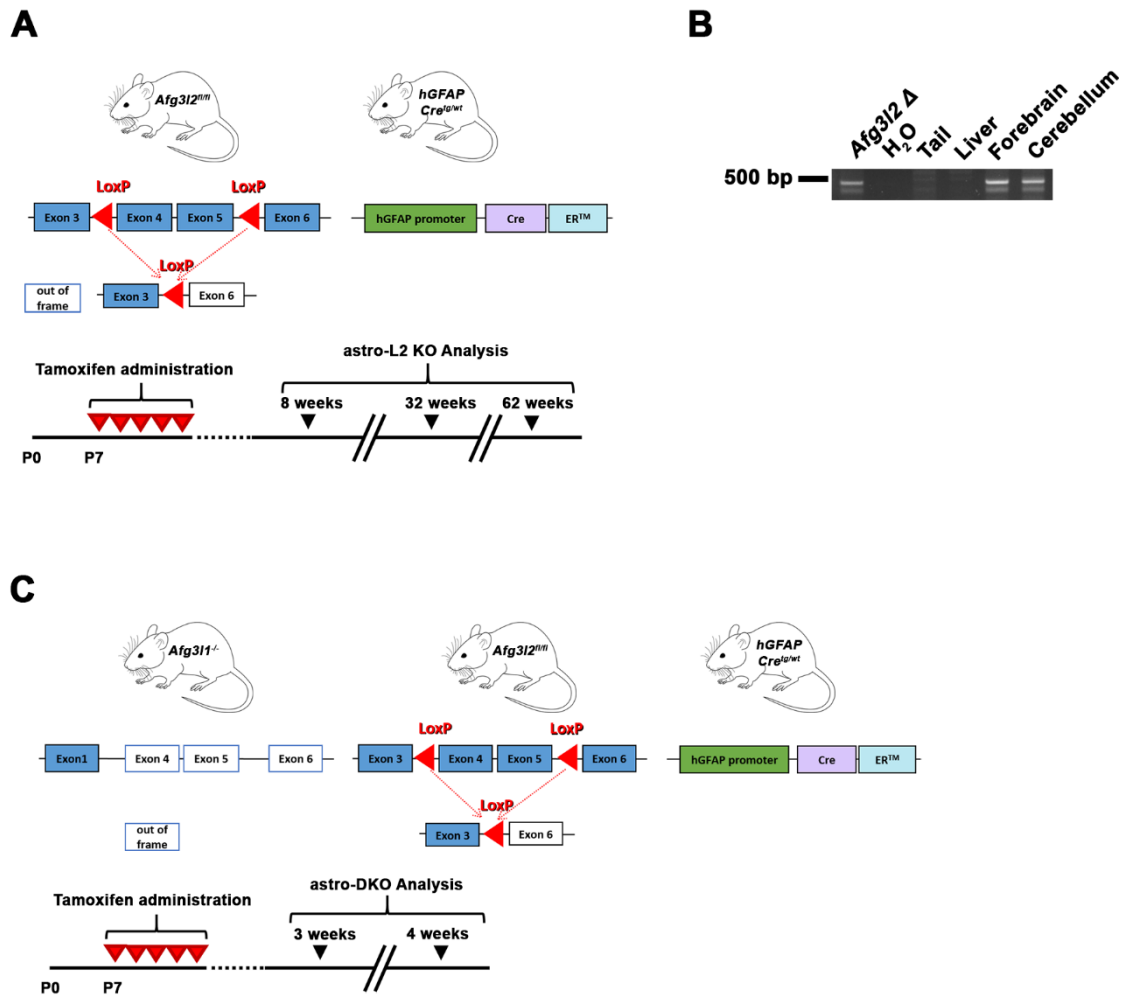


Figure 4.2: Schematic representation of the mouse models studied, the strategy adopted for the Cre induction and the analysis time points. (A) Transgenic mouse lines used to generate the astro-L2 KO mice. Lactating mothers (*Afg3l2^{fl/fl}*) were injected with tamoxifen as indicated in the scheme. The litters were analyzed at 8, 32 or 62 weeks. (B) Recombination assessment from DNA extracted from tail, liver, forebrain and cerebellum of an astro-L2 KO male mouse at 8 weeks. The PCR band at 467 bp shows that recombination occurs only in the forebrain and cerebellum. (C) Transgenic mouse lines used to generate the astro-DKO mice. Lactating mothers (*Afg3l1^{-/-} : Afg3l2^{fl/fl}*) were injected with tamoxifen as indicated in the scheme. The litters were analyzed at 3 and 4 weeks.

4.3 Phenotypical evaluation of astro-L2 KO and astro-DKO mice

To characterize the mouse models, I started to closely monitor the weight of both male and female astro-L2 KO and their control littermates (Ctrl, genotype: *Afg3l2^{fl/fl}*). Both male and female astro-L2 KO have decreased body-weight compared to Ctrl (Fig. 4.3A and B). Despite

this, the animals survive up to 62 weeks of age (latter time point used for the analysis) and do not show a prominent motor impairment by visual inspection. To further investigate any sign of motor impairment hard to detect in animals freely moving in their home cage, I decided to test them with the rotarod assay at different time points (indicated in Fig. 4.2A). The rotarod assay is used to assess motor coordination and can also be used to test memory skills in rodents. It consists of an apparatus provided with a rotating rod on which mice are positioned. While the rod accelerates, the mice have to walk to stay on it, for a maximum of 300 seconds. Sensors on the grid beneath the rod allow to automatically register the latency to fall of the animals. Motor coordination is necessary to maintain the position on the rotating rod [204]. Following a short training, animals were tested 3 times, 15 minutes apart by Steffen Hermans. Astro-L2 KO male mice show a decreased latency to fall, starting at 32 weeks, while female astro-L2 KO animals do not show any motor impairment at any time point analyzed (Fig 4.3 D-H).

The astro-DKO pups were indistinguishable from their $L1^{-/-}$ littermates up to 3 weeks. However, by the fourth week of age astro-DKO animals showed a significant lower body-weight (Fig. 4.3I-J), independent from the sex of the animals. In order to assess ataxia, I performed 4 tests as described by Guyenet and colleagues [193]. The ledge test consists in positioning an animal on the edge of its home cage, and monitoring both how the animal walks and how it descends inside the cage. astro-DKOs were not able to walk on the edge of the home cage, as they had difficulties grasping the surface with their hind limbs, and were so uncoordinated that they were letting themselves fall into the cage. The second test consists in evaluating the curvature of the spine, looking for signs of pronounced kyphosis, which indeed was pronounced in astro-DKOs. The gait evaluation aims to assess if the animals are able to walk, the orientation of the hind limbs and the general ability to move: astro-DKOs walked with the hind limbs at about 45° angle respect to the body, and also were unable to stand on their hind limbs for a prolonged time. Finally, the hind limb clasping consists in holding a mouse by the tail and checking if the

hind limbs are oriented away from the body, or if they are retracted towards the body. The latter was indeed observed in astro-DKOs. Each test received an evaluation score between 0 to 3, with 3 being severely affected. The final score for each animal consists in the sum score of the 4 tests (Fig. 4.3K). astro-DKO mice show a statistically significant increase in the ataxic score, compared to the $L1^{-/-}$ (Fig. 4.3K).

To conclude, both mouse models showed decreased body-weight compared to the respective controls, and these data suggest that *m*-AAA protease dysfunction in astrocytes is enough to induce a motor impairment in affected animals.

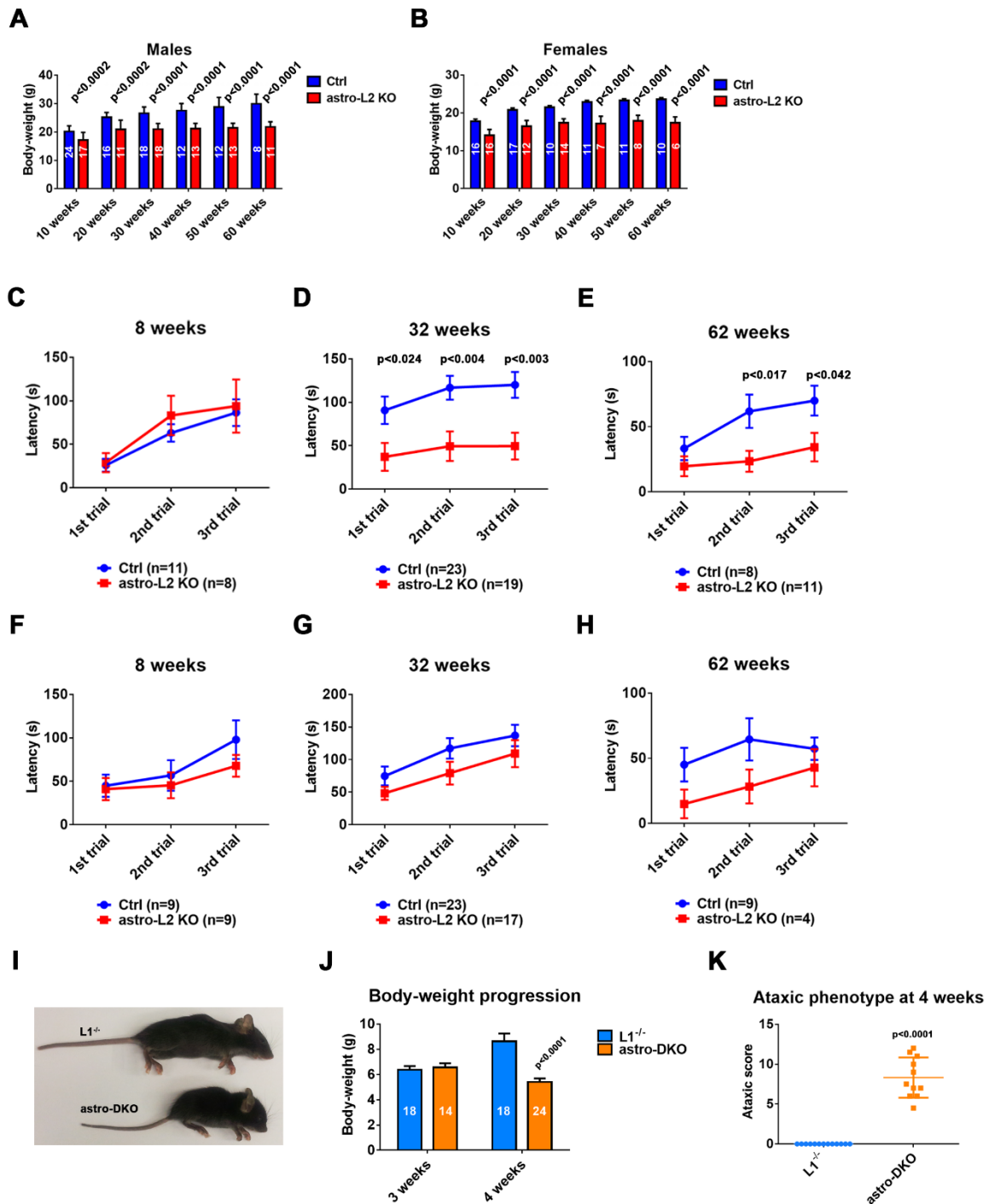


Figure 4.3: *m*-AAA protease impairment and ablation in astrocytes lead to neurological phenotypes. (A-B) Body-weight evaluation of male and female mice. n is indicated in the columns. (C-H) Males and females latency to fall off the rotarod at different time points. n is indicated in the legend for each group at each time point. (I) Picture showing a $L1^{-/-}$ and an astro-DKO mice at 4 weeks. (J) Body-weight evaluation of $L1^{-/-}$ and astro-DKOs at 3 and 4 weeks. n is indicated in the columns. (K) Ataxic score evaluation. Each dot represent one animal. Data represent mean \pm SEM, the *p* value was calculated with the Student's t-test, and is indicated on the respective graphs when ≤ 0.05 .

4.4 *m*-AAA protease depletion induces mitochondrial fragmentation, aberrant cristae morphology and loss of targeted cells

An extensive amount of evidences shows that *m*-AAA protease impairment, or loss, leads to mitochondrial fragmentation and aberrant cristae morphology [117, 164, 165, 167-170]. It has been proposed that the reason behind this is that the *m*-AAA protease dysfunction induces hyper-activation of OMA1, which, by cleavage of mitochondrial pro-fusion protein OPA1, shifts the mitochondrial fusion/fission balance towards fission [116-118]. In order to evaluate mitochondrial morphology in astro-L2 KO and astro-DKO mice, I crossed both lines together with the mtYFP reporter line. The expression of mtYFP is controlled by the Cre recombinase as previously described (Fig. 4.1A) [191], allowing me to directly monitor mitochondrial morphology and distribution in the ML. The mtYFP signal clearly shows mitochondrial fragmentation in both models, compared to the respective control animals (Fig. 4.4 A and B). Interestingly, the organelles appear fragmented prior to the development of the motor phenotype (Fig. 4.3 C-E and J-K). Moreover, mitochondrial distribution appeared altered in both models: the mtYFP signal in Ctrl animals of both models (in Fig. 4.4A, genotype *Afg3l2*^{wt/fl} : hGFAP-Cre^{tg/wt}) appears stretched all over the extension of the ML, whereas in astro-L2 KOs and astro-DKOs the mtYFP signal does not reach the upper part of the ML in the latter time-points analyzed. This suggests that mitochondria are retracted from BG projections or that the entire projection is retracted and does not reach the upper part of the ML.

Another advantage of using a reporter line is that the fate of targeted cells can be monitored. By manual counting of mtYFP-positive (mtYFP⁺) cell bodies, I could show that targeted cells in the astro-L2 KO and astro-DKO models are decreased at 32 weeks and 4 weeks, respectively (Fig. 4.4 C and D), hinting to the possibility that targeted cells die. In the astro-L2 KO line, the number of targeted cells is comparable to Ctrl animals at 8 weeks. However, mitochondrial

fragmentation is already visible at 3 weeks (Fig. 4.4A). This means that mitochondria in targeted cells are fragmented for several weeks before animals manifest the motor impairment. In contrast, the motor impairment in astro-L2 KOs correlates with the demise of targeted cells.

To better characterize mitochondrial morphological changes, I performed ultrastructural analysis of BG mitochondria, together with Esther Barth. Visual identification of the PCL was possible due to the higher electron-density of their cytoplasm compared to other cells, and due to their size, as they are bigger than other cells in the CB [199]. BG cells were also easy to identify because of their localization close to the PCs, and their nuclear structure [199]. BG of both KO lines showed aberrant mitochondria in their cytosol. In line with previous reports on neurons and oligodendrocytes depleted of *Afg3l2*, mitochondria are not only fragmented, but also depleted of cristae, swollen and less electron-dense compared to the respective controls (Fig. 4.4 E and F) [165, 167]. Interestingly, I was not able to find any aberrant mitochondria in BG of astro-L2 KO mice at 62 weeks, further hinting to the targeted cell death over time.

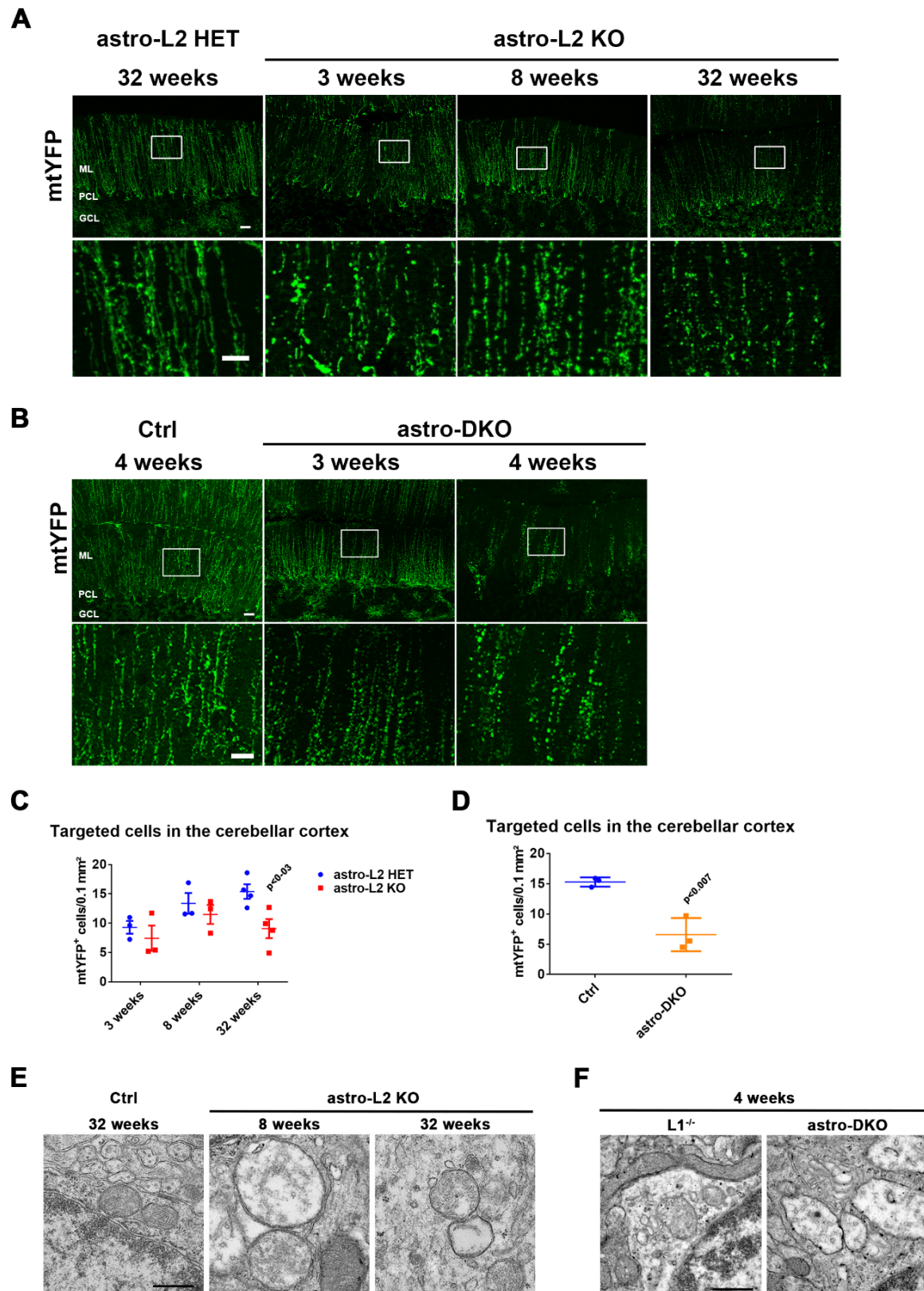


Figure 4.4: *m*-AAA protease depletion causes mitochondrial abnormalities and loss of targeted cells. (A-B) mtYFP endogenous signal shows early mitochondrial fragmentation in astro-L2 KO and

heterozygous mice (astro-L2 HET), and astro-DKO mice. $n=3$ for each group at each time point. Scale bar= 20 μm ; scale bar enlargements= 10 μm . (C-D) Quantification of mtYFP⁺ cell bodies in the PCL. Dots represent n , data is indicated as mean \pm SEM, p value was obtained by Student's t-test and indicated in the graphs when ≤ 0.05 . (E-F) Ultrastructural analysis of BG mitochondria in astro-L2 KO and astro-DKOs compared to the respective controls. $n\geq 3$ for each group at each time point. Scale bar=500 nm.

4.5 *m*-AAA protease function is necessary for BG survival

The decreased number of targeted cells quantified *via* the mtYFP signal, together with the limited expansion of the fluorescent signal through the ML, suggested that BG morphology might be affected. In order to evaluate it, I stained CB sections with an antibody against the calcium-binding protein S100. BG structure appeared different in males and females astro-L2 KO at 62 weeks, as if the females have a delayed phenotype (Fig. 4.5A and S1). This correlates with the absence of motor impairment observed in females. Therefore, I mainly focused on males for the analysis, but performed most of the CB stainings on females as well at 62 weeks (Fig. S1 and 2). BG projections in astro-L2 KO males appeared comparable to Ctrl at 8 weeks: the cell bodies located in the PCL and the projections elongated across the longitudinal plane of the ML, in line with what I detected with the mtYFP signal. However, at 32 weeks some BG cell bodies seemed to migrate into the ML, and the projections appeared shorter and not reaching the edge of the ML. The translocation of BG has been reported also in the vanishing white matter disease (VWM) [205]. The shorter projections in astro-L2 KO observed with the S100 marker recapitulated the results from the mtYFP endogenous signal, which showed a retracted pattern (Fig. 4.4A). At 62 weeks of age, the situation seemed to worsen, as there were more BG cell bodies in the ML in the astro-L2 KO cerebella. I counted the S100-positive (S100⁺) cell bodies in the PCL to validate the results obtained from the mtYFP⁺ cells quantification. The number of S100⁺ cells was, indeed, reduced at 32 weeks, but surprisingly it was again comparable to the controls at 62 weeks (Fig. 4.5B).

Intrigued by the sudden increase in the S100⁺ cells number at 62 weeks, I decided to stain cerebellar slices with an antibody against the transcription factor SOX2 (Fig. 4.5A). In fact, it has been shown that SOX2 is expressed in neural stem and progenitor cells, glial precursors and proliferating astrocytes [206, 207]. I observed an increased number of SOX2⁺ cells in astro-L2 KO mice at 8 weeks, compared to Ctrl. This suggests that there is ongoing proliferation already at this age. However, at 32 weeks of age the number of SOX2⁺ cells is still slightly higher in the astro-L2 KO compared to the Ctrl, but quite reduced compared to the 8 weeks-old mice (Fig.4.5C). This indicates a proliferation process ongoing at early stages of the phenotype development that either slows down before 32 weeks or it is hardly detected because of cell death. However, the proliferation continued over time, as the number of SOX2⁺ and S100⁺ cells in astro-L2 KO mice at 62 weeks were comparable to the respective Ctrl.

In the astro-DKO line, BG marked with S100 appeared comparable to control animals at 3 weeks, but at 4 weeks the BG appeared highly deteriorated, with short processes and cell body displacement towards the ML (Fig. 4.5D and G). The S100⁺ cell count showed the reduction in the number of BG cell bodies lying in the PCL at 4 weeks, but interestingly the cell loss started already at 3 weeks, before animals show any phenotype when compared to L1^{-/-} (Fig. 4.5E). Moreover, SOX2 staining (Fig. 4.5D) nicely reflected the S100 data: at 3 weeks I could not detect any major difference between L1^{-/-} and astro-DKOs, but at 4 weeks the SOX2⁺ cells appeared reduced in number (Fig.4.5F), and translocated to the ML as well (Fig. 4.5H). Overall, it seems that the BG phenotype in astro-DKOs develops much faster than the astro-L2 KO. However, in both cases, targeted cells die. The conclusion is that astrocytes *in vivo* do not survive *m*-AAA protease depletion.

SOX2⁺ cell bodies in the PCL. Dots indicate the n, data represent mean±SEM, *p* value was obtained with Student's t-test and indicated in the graphs when ≤ 0.05 . (G-H) Distribution of S100 and SOX2⁺ cells across the PCL and the ML. n is indicated on the bars.

4.6 The GFAP promoter does not target NG2 precursor cells

The sudden increase in targeted cells between 3 and 8 weeks in astro-L2 KO cerebella may be due to astrocyte proliferation, as most of the S100⁺ cells and mtYFP endogenous signal co-localize (Fig. 4.1C). However, another possibility is that precursor cells may be targeted and proliferate. To test this hypothesis, I looked up for progenitors that have been reported to differentiate in BG. Nerve/glial antigen 2 positive cells (NG2⁺) count as 5-8% of the total cells in the CNS [208, 209]. Research conducted to identify the fate of NG2⁺ progenitors revealed that they could differentiate in both oligodendrocytes and in BG in late stages of cerebellar development [210]. Therefore, I stained cerebellar slices of 3 and 8 week-old astro-L2 HET mice expressing mtYFP with an antibody against NG2, and anti-GFP antibody that detects the mtYFP. I could not detect any co-localization between NG2⁺ cells and GFP⁺ cells, further confirming that the models I used are astrocyte-specific in the CB at 3 or 8 weeks (Fig. 4.6).

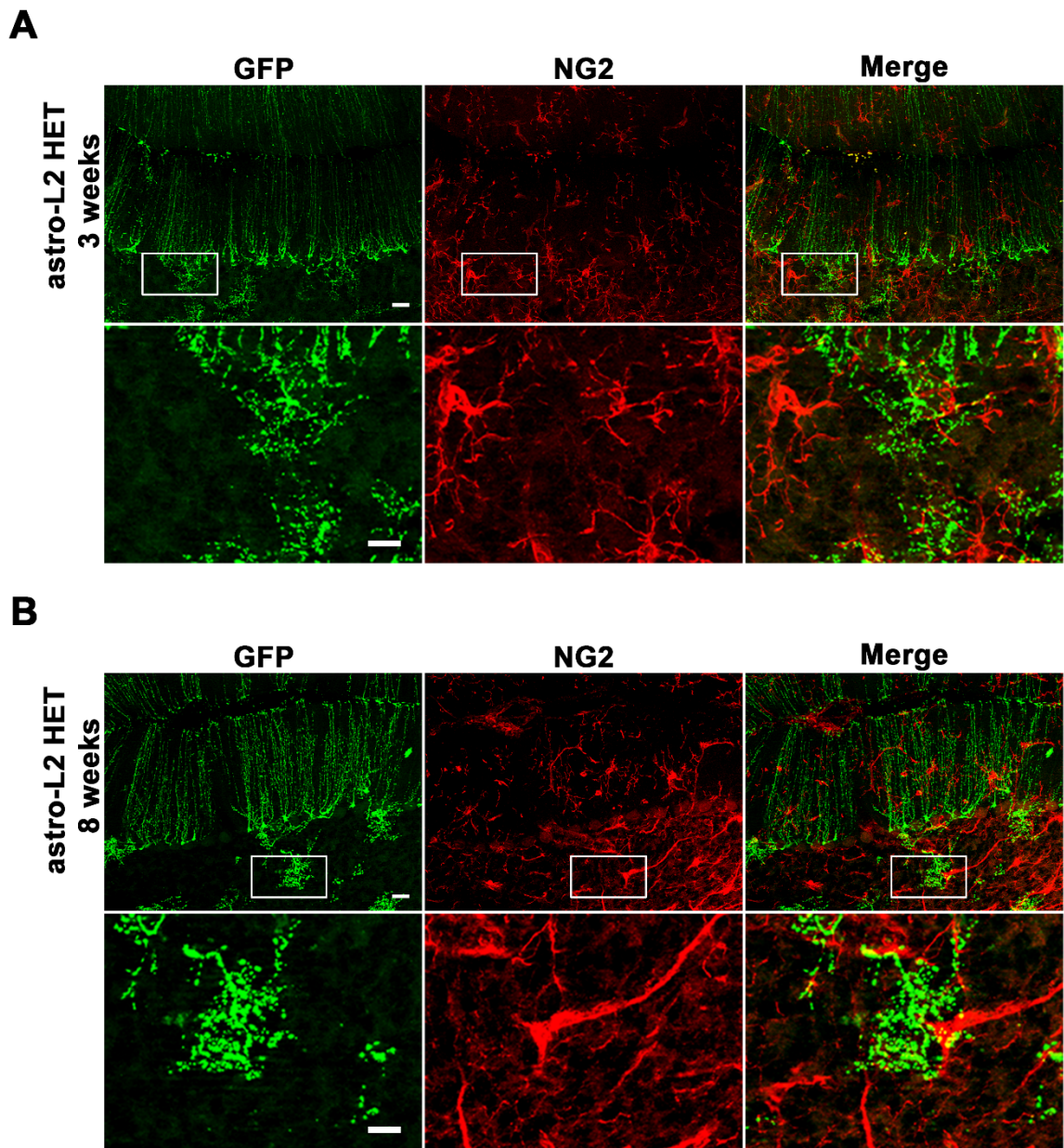


Figure 4.6: Targeted cells are not NG2⁺ precursor cells. (A-B) Immunofluorescence staining on cerebellar slices against NG2 and mtYFP. n=3 for each group. Scale bar= 20 μ m; scale bar enlargement= 10 μ m

4.7 Regulation of mitochondrial functions in astrocyte-specific *m*-AAA protease deficient mouse models

4.7.1 *m*-AAA protease deficiency does not alter respiratory efficiency in targeted BG

Due to its role in degradation of respiratory complexes subunits [146] and activation of MRPL32 [211], a component of the mitochondrial ribosomal machinery, *m*-AAA protease dysfunction was suspected to cause mitochondrial respiratory deficiency. Studies conducted to shed light onto this hypothesis showed that *m*-AAA protease dysfunction leads to reduced respiration in different cell types like neurons and oligodendrocytes [123, 146, 165, 167, 211]. It has been also shown that knocking out *Cox10* (encoding for a subunit of complex IV) or *Twinkle* (encoding for the Twinkle helicase, important for mtDNA replication) in astrocytes leads to impaired mitochondrial respiration [34, 187]. However, the result of the two deletions is very different: *Cox10*-deficient cells, in fact, survive by aerobic glycolysis in absence of glial pathology or neurodegeneration, while *Twinkle*-deficient astrocytes induce spongiotic degeneration of brain parenchyma, secondary neuronal degeneration and microgliosis. Thus, to test the effect of *m*-AAA dysfunction in mitochondrial respiratory capability in astrocytes, I performed the COX-SDH staining of cerebellar slices from both astro-L2 KOs and astro-DKOs (and their relative controls) at different time points. This histochemical technique allows to check for respiratory dysfunction due to mtDNA impairment [212]. The enzymes tested with this method are usually the succinate dehydrogenase (SDH), which is entirely encoded by nuclear DNA, and the cytochrome c oxidase (COX), which is partially encoded by mtDNA. In case of defective mtDNA transcription or mitochondrial translation impairment, COX does not function, whereas the SDH carries out its activity. In healthy conditions, the COX substrate diaminobenzidine (DAB) is converted to brown indamine that deposits inside mitochondria. The SDH substrate nitroblue tetrazolium (NBT), on the other hand, is converted to blue

formazan. In case of respiratory deficiency caused by impaired mtDNA transcription or translation, mitochondria appear blue, because the COX lacks its mitochondrial encoded subunits to properly function [212]. Previous reports showed that *Afg3l2*-depleted neurons have COX deficiency and, therefore, impaired mitochondrial respiration [165]. Moreover, *m*-AAA protease impairment is also associated with decreased mitochondrial translation and respiratory chain assembly [140, 146, 165, 211].

The COX-SDH staining on cerebellar slices of both astro-L2 KOs and astro-DKO, surprisingly, did not reveal any respiratory impairment in BG cells (Fig. 4.7A and B). This interesting result demarks a separation between the *m*-AAA protease dysfunction in astrocytes and respiratory efficiency.

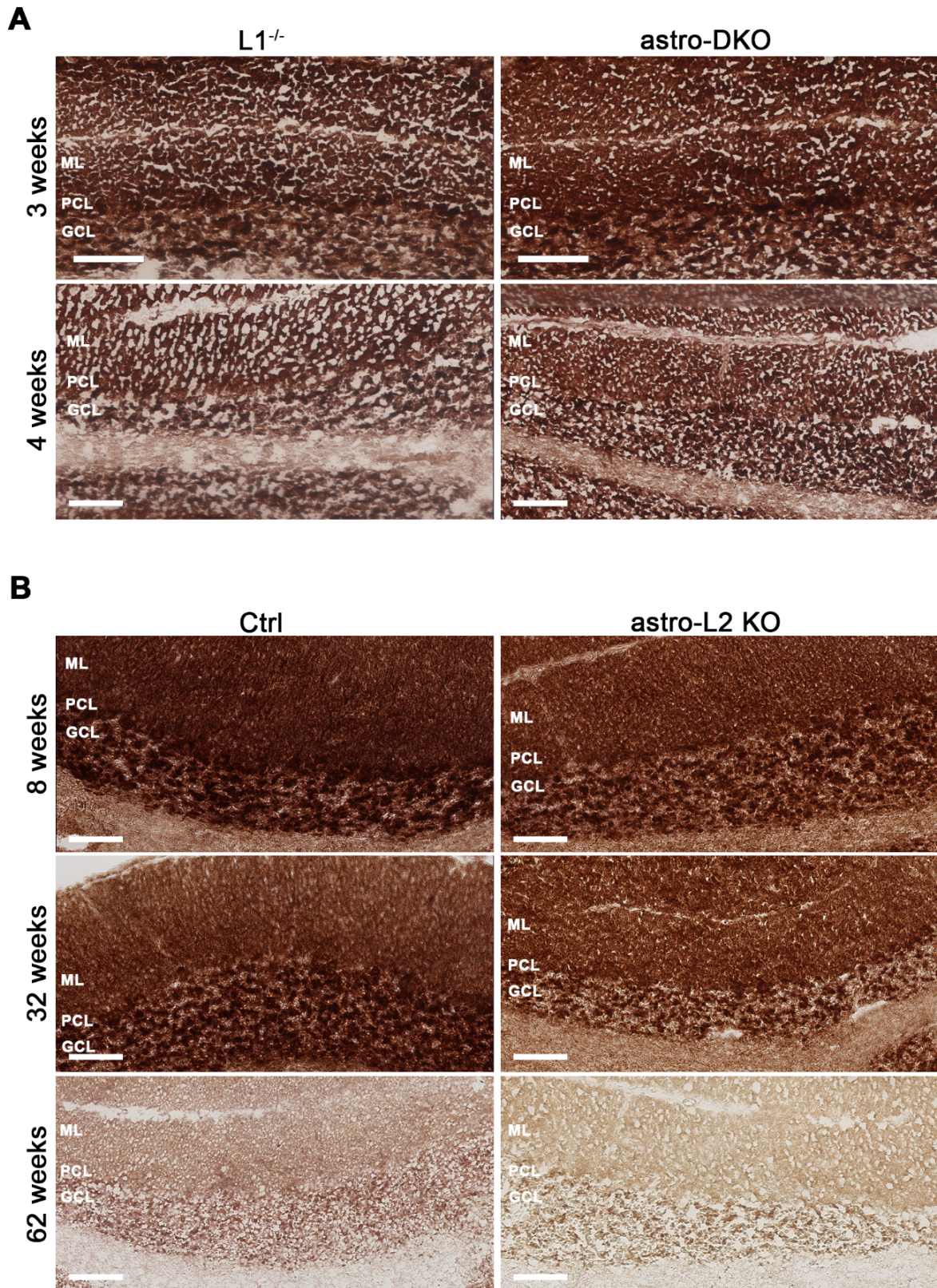


Figure 4.7: *m*-AAA protease ablation does not cause respiratory deficiency in astrocytes. (A-B) COX-SDH staining on cerebellar slices show no signs of COX deficiency at any time point analyzed in both astro-DKO and astro-L2 KO mice. n=3 for each group at each time point, scale bar= 100 μ m.

4.7.2 *m-AAA protease ablation induces metabolic stress response*

Mitochondrial stress response is common in mitochondrial diseases [213]. It has been shown that in case of mtDNA replication defects, deoxynucleotide (dNTP) pools could be insufficient and/or unbalanced. This, rather than oxidative phosphorylation defects, leads to the integrated mitochondrial stress response which results in upregulation of the regulatory enzyme of the one-carbon folate cycle, the methylene-tetrahydrofolate dehydrogenase 2 (MTHFD2) and *de novo* serine and glutathione synthesis induction [214]. Upstream of the MTHFD2 activation is the induction of the mechanistic target of rapamycin 1 (mTORC1), connecting metabolic response and cell growth pathways [213, 215]. To verify whether the mitochondrial stress response is induced, I tested if enzymes involved in serine biosynthesis, the phosphoglycerate dehydrogenase (PHGDH) and phosphoserine aminotransferase 1 (PSAT1), and MTHFD2 were upregulated in astro-DKOs at 3 and 4 weeks. I focused on the astro-DKO line as it develops a strong and early-onset phenotype. Indeed, quantitative real time PCR results from total cerebellar RNA isolation confirmed that in astro-DKOs at 3 weeks the integrated stress response is induced, and it worsen at 4 weeks (Fig. 4.8A). To further confirm the induction of serine biosynthesis, I checked the amino acid levels from total cerebellar lysates of 3 and 4 weeks old astro-DKO animals (Fig. 4.8B and C) in collaboration with Dr Susanne Brodesser. I could detect increased amounts of several amino acids, including serine, threonine, proline and glycine, which were also reported to be upregulated in muscles of mice carrying a dominant Twinkle helicase defect, which develop mitochondrial myopathy [214].

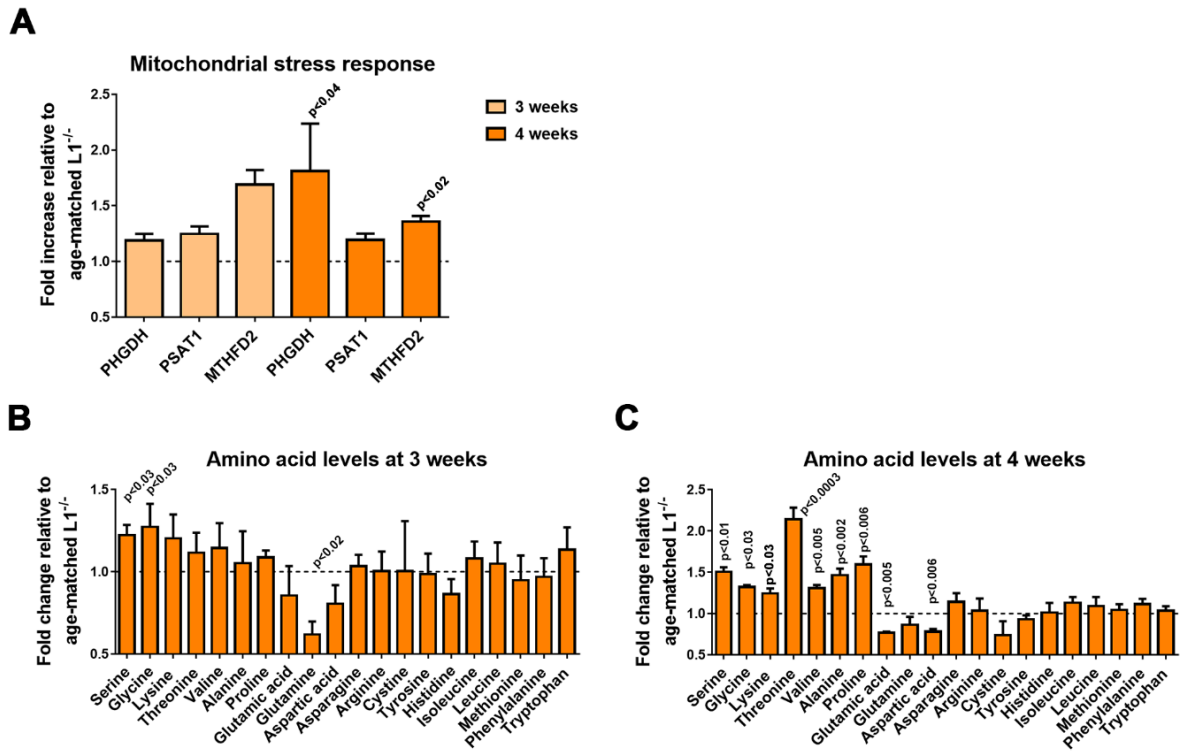


Figure 4.8: Metabolic stress response is induced by *m*-AAA protease dysfunction in astrocytes. (A) mRNA levels, expressed as fold increase, of serine metabolism involved enzymes at 3 and 4 weeks in astro-DKO cerebella, compared to age-matched $L1^{-/-}$ animals. $n \geq 2$ for each group at each time point. (B-C) Amino acid levels in astro-DKO at 3 and 4 weeks compared to age-matched $L1^{-/-}$. $n \geq 3$ for each group at each time point. Data represent mean \pm SD, p value obtained by Student's t -test is reported on the graph when <0.05 .

4.8 Glutamate transport is affected in *m*-AAA protease deficient astrocytes

When I checked for amino acid levels in astro-DKO at 3 and 4 weeks, I could detect upregulation of those involved in mitochondrial stress response, as well as downregulation of glutamate and glutamine (Fig. 4.8B and C). This is in line with the evidences indicating astrocytes involvement in glutamate uptake and recycling [43]. In fact, glutamate is released from the presynaptic neurons and binds glutamate receptors on the dendrites of postsynaptic neurons. To avoid excitotoxicity, glutamate must stay in the synaptic cleft for a limited amount of time. Its removal is operated by transporters expressed on astrocyte surface EAAT1 and 2,

also referred to as glutamate-aspartate transporter (GLAST) and glutamate transporter 1 (GLT1), respectively [216, 217]. Once inside astrocytes, glutamate is converted into glutamine by the glutamine synthetase, and shuttled to neurons for glutamate synthesis [218-220]. Therefore, I checked the expression of both EAAT1 and 2 in astro-L2 KO and astro-DKOs. At 4 weeks of age astro-DKO mice manifest a dramatic reduction of both transporters compared to $L1^{-/-}$ (Fig. 4.9A). These data further confirm the low glutamate and glutamine levels: due to lack of transporters, glutamate cannot be recycled. At 3 weeks of age, however, I could not detect any major difference between groups for each transporters.

Intrigued by the results on the astro-DKOs, I tested the same antibodies on the astro-L2 KOs (Fig. 4.9B). Surprisingly, EAAT1 levels are unaffected compared to control animals at any time point analyzed. EAAT2 on the other hand, appeared patchy and not uniformly distributed in the ML at 32 and 62 weeks, suggesting a lower expression of this glutamate transporter in BG, likely impairing glutamate transport. However, EAAT1 levels are unchanged, and it can compensate for the EAAT2 loss.

The results obtained from the astro-L2 KO cerebella suggest that *m*-AAA protease dysfunction could differentially affect the expression of the two EAATs.

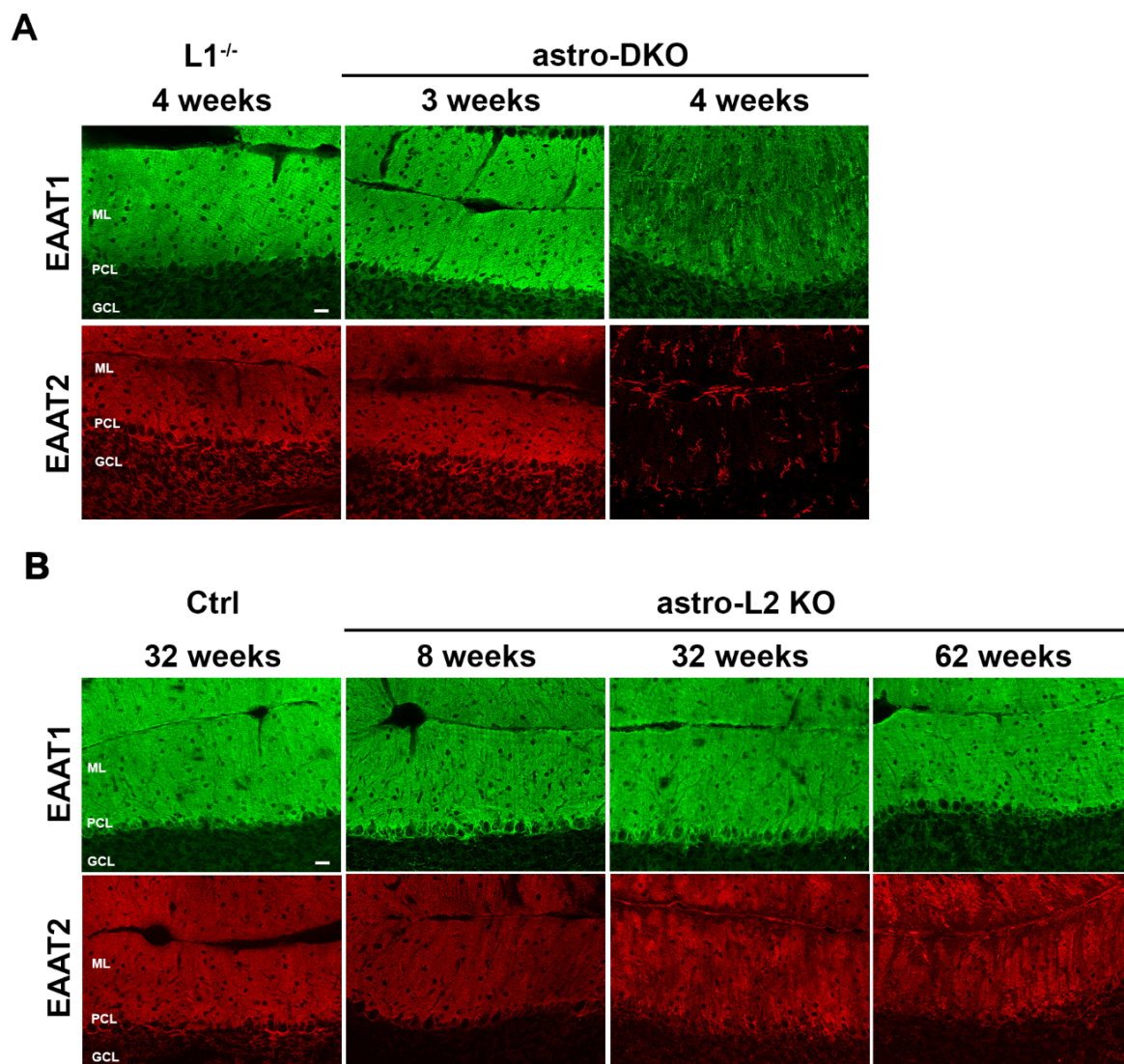


Figure 9: Glutamate transporters are downregulated upon *m*-AAA dysfunction in astrocytes. (A-B) Immunofluorescence staining of cerebellar slices against glutamate transporters EAAT1 and 2. $n=3$ for each group at each time point, scale bar= 20 μm .

4.9 *m*-AAA protease deficiency causes cell autonomous reactive astrogliosis

GFAP is normally used as a generic marker for astrocytes [4, 221], and it is upregulated during a reactive astrogliosis [12, 222]. In case of injury or neurodegeneration, reactive astrocytes remove debris, dead cells, phagocyte synapses and repair the blood-brain barrier. Furthermore, they confine the injured areas and create a scar to avoid spreading of the damage to unaffected

brain areas [53-55, 223]. In order to evaluate whether *m*-AAA protease deficiency causes reactive astrogliosis, I stained cerebellar slices of both mouse models with an anti-GFAP antibody. Interestingly, astro-L2 KO mice show a mild reactive phenotype only at 32 weeks, which gets resolved by 62 weeks (Fig. 4.10A). This is in line with what I observed with the S100⁺ cells counts: at 32 weeks there is a reduction of BG cells, but by 62 weeks, the number of BG cells is comparable to Ctrl (Fig. 4.5A and B). It could be that in this model, reactive astrocytes remove dead cells and proliferate to replenish the reduced pool of BG cells, and stop once they fulfill their duty. In astro-DKO mice, I could detect a mild reactive astrogliosis at 3 weeks, which became more pronounced at 4 weeks (Fig. 4.10B). Again, the comparison to the S100⁺ cell counts is necessary: S100⁺ cells are already mildly reduced at 3 weeks, and strongly reduced one week later. It is possible to speculate that the degree of reactivity may depend on BG loss. In astro-DKOs, because cells die rather fast, it is necessary to quickly remove them. In addition, dying cells must be replaced, thus reactivity may be a mean to replenish the pool of BG.

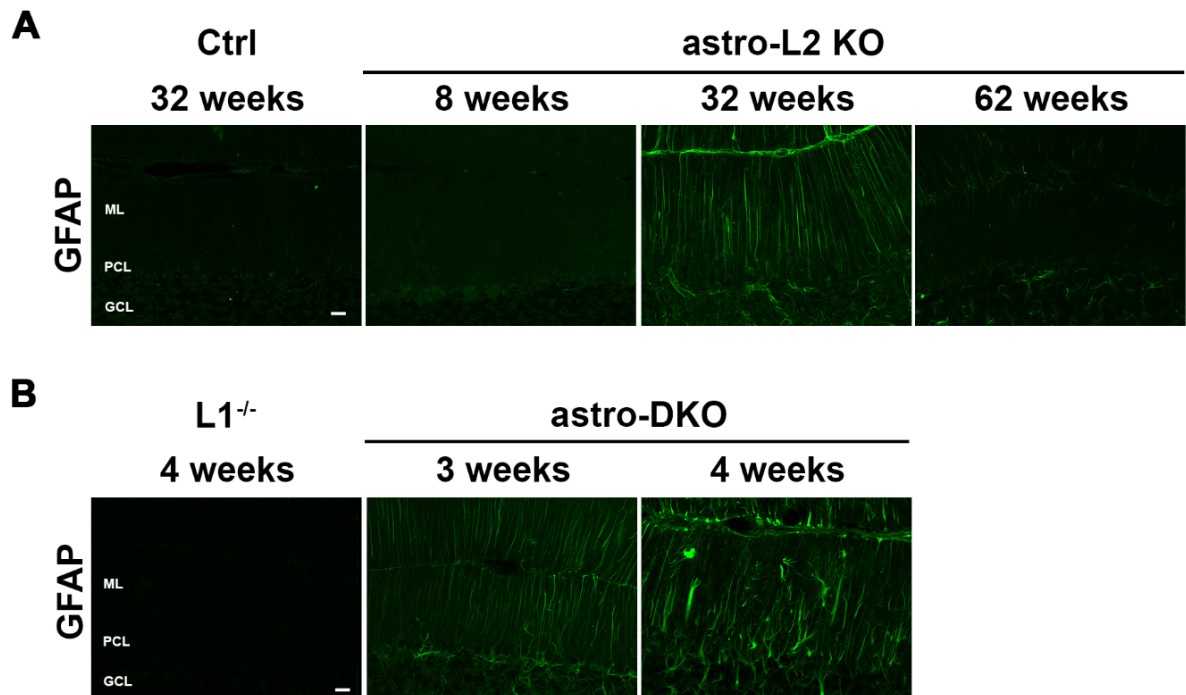


Figure 4.10: *m*-AAA protease dysfunction in astrocytes leads to reactive astrogliosis. (A-B) Immunofluorescence staining of cerebellar slices against GFAP. $n=3$ for each group at each time point, scale bar= 20 μm .

However, what is the identity of these reactive cells? An alternative hypothesis is that reactive astrogliosis is triggered by the mitochondrial dysfunction within the same cell, rather than being induced in healthy untargeted cells reacting to environmental stimuli. To discriminate the origin of reactive cells, I took advantage of the mtYFP reporter and stained cerebellar slices for both GFAP and GFP. Remarkably, most of the reactive cells in astro-L2 KOs appear to be mtYFP⁺ (Fig. 4.11A), suggesting that indeed this is a cell autonomous effect caused by the dysfunction of mitochondria, rather than an attempt by untargeted cells to replenish the BG pool. However, some untargeted cells are reactive, indicating that the reactive astrogliosis in this model is both cell and non-cell autonomous. Therefore both the self-reactivity and the replenishing theories are still applicable and need further investigation.

In the astro-DKO model, most of the cells at 4 weeks were untargeted, but it could be due to the fact that at the 4 weeks time point, targeted cells are mostly dead (Fig. 4.11B).

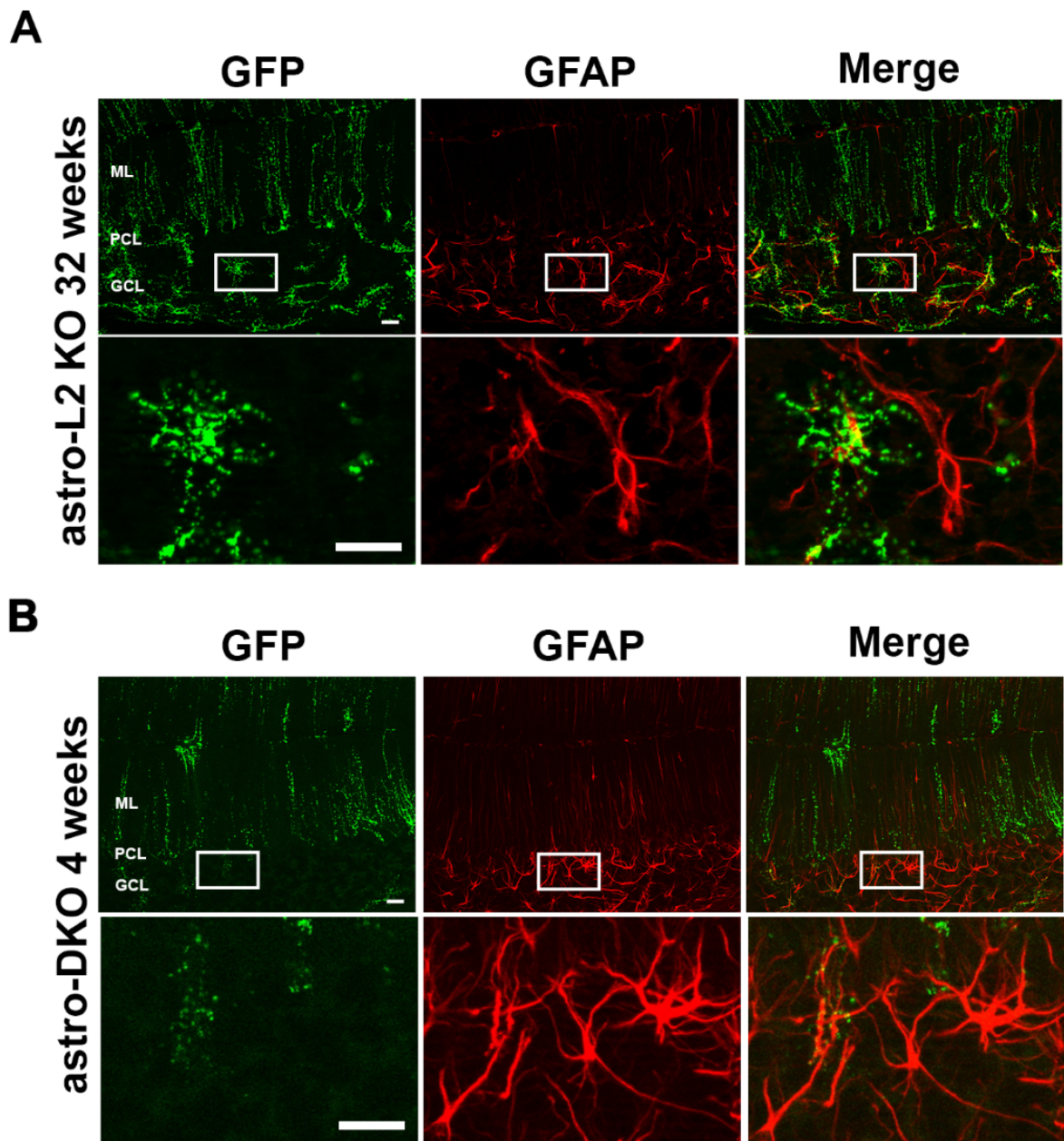


Figure 4.11: Reactive astrocytes belong to both target and untargeted pools. (A-B) Immunofluorescence staining against mtYFP and GFAP. $n=3$ for each group. Scale bar= 20 μm , scale bar enlargement= 20 μm .

4.10 *m*-AAA protease depletion causes neuroinflammation

Considering the strong reactive astrogliosis and the cell loss observed in astro-DKO mice at 4 weeks, it seems reasonable that microglia cells are activated. Despite the unclear dynamics, it seems that cytokines released by microglia can activate toxic reactive astrocytes, but it is hard

to discriminate the chicken and the egg, because they are activated in same situations at very close time [12, 63]. Therefore, I decided to test microglia activation using the ionized calcium binding adaptor molecule 1 (Iba1) [224], a microglia-specific calcium-binding protein upregulated in activated microglia (Fig. 4.12A). Microglia activation was detected at 4 weeks, after the first signs of reactive astrogliosis at 3 weeks (Fig. 4.10B). Moreover, TNF- α and interleukines are upregulated in astro-DKOs at 4 weeks, further confirming an ongoing inflammatory process (Fig. 4.12B). The morphology of activated microglia reminds that of EAAT2⁺ cells in astro-DKOs at 4 weeks (Fig.4.9A). To assess whether these are astrocytes or microglia cells expressing EAAT2, I co-stained cerebellar sections with both Iba1 and EAAT2 markers. Interestingly, I detected a perfect co-localization between the two antibodies in astro-DKOs at 4 weeks (Fig. 4.12C). This means that EAAT2 glutamate transporter is expressed in microglial cells, rather than in BG. EAAT2 expression in microglial cells has been reported previously. In case of neurotoxic stimuli, and incapability of astrocytes to uptake glutamate, microglia upregulates EAAT2 to remove the neurotransmitter from the extracellular environment [225, 226].

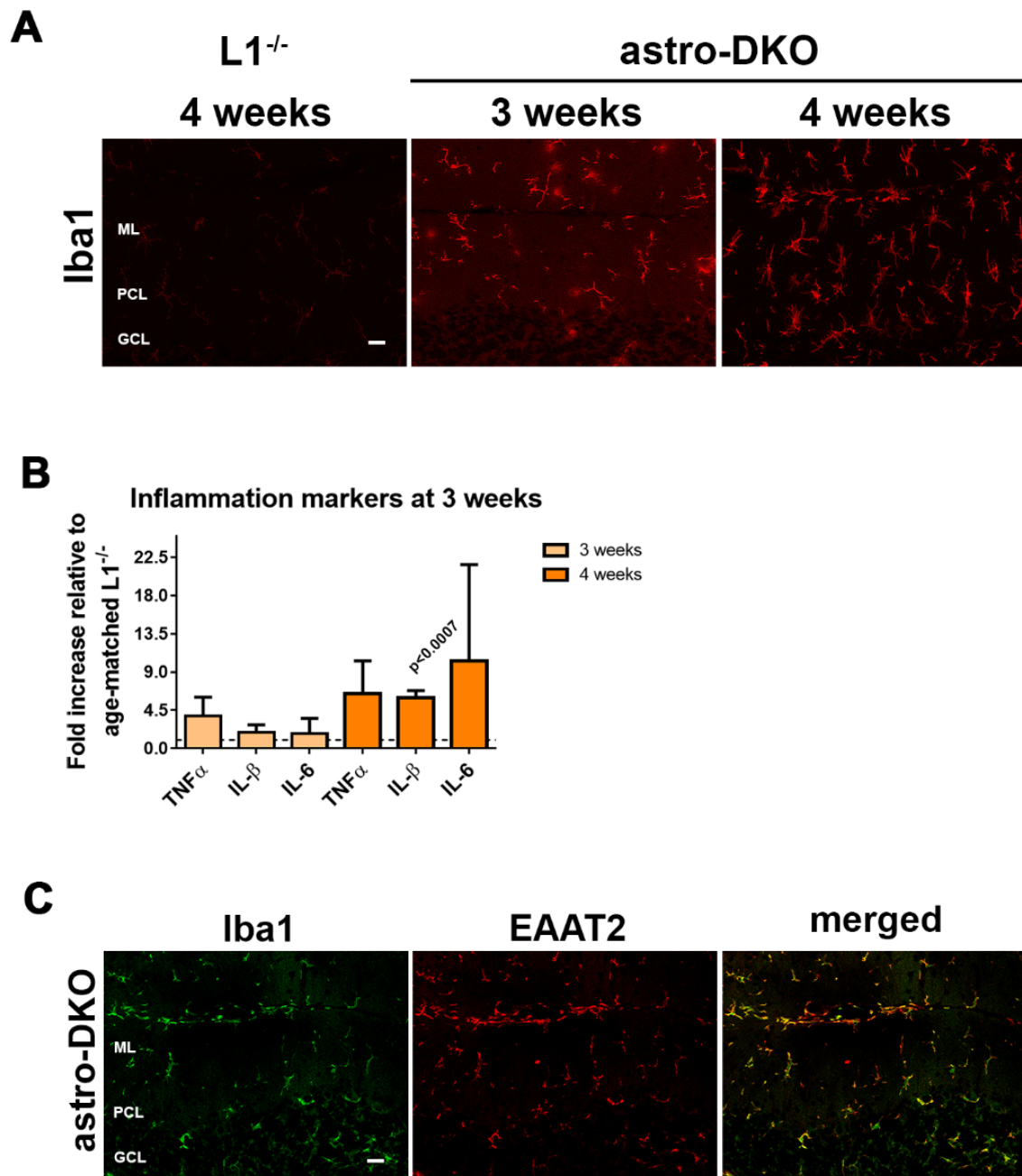


Figure 4.12: Depletion of the *m*-AAA protease induces inflammation. (A) Immunofluorescence staining against microglia marker Iba1 in cerebellar slices of L1^{-/-} and astro-DKO mice. n=3 for each group at each time point. (B) mRNA levels of inflammatory markers, expressed as fold increase, from astro-DKO cerebella, normalized to age-matched L1^{-/-}. n \geq 2 for each group at each time point. Data represent mean \pm SD, *p* value obtained by Student's t-test is reported on the graph when <0.05. (C) Immunofluorescence staining against microglia marker Iba1 and glutamate transporter EAAT2. n=3. Scale bars=20 μ m.

As microglia were activated in astro-DKO mice, I wondered if it was the case also for the astro-L2 KO mice. I stained cerebellar slices with Iba1 but I could not detect any microglial activation (Fig.4.13). Interestingly, these results suggest that reactive astrogliosis occurs prior to microglia activation.

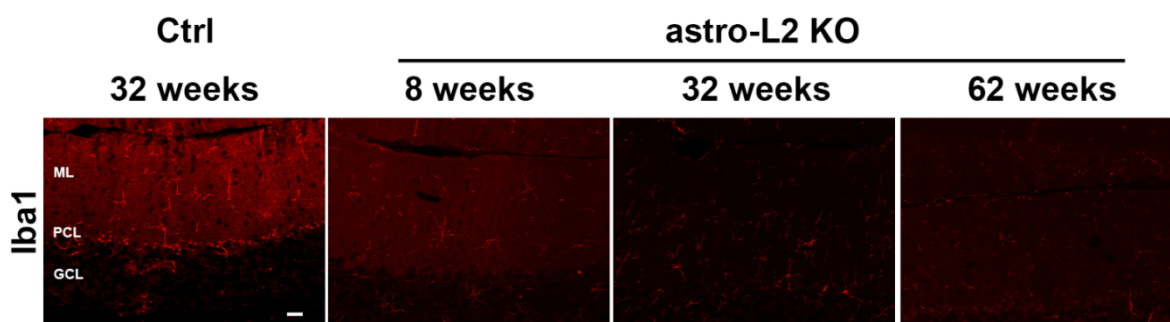


Figure 4.13: Astro-L2 KOs do not show signs of microglial activation. Immunostaining against microglia marker Iba1. n=3 for each group at each time point, scale bar= 20 μ m.

4.11 Astrocyte-specific *m*-AAA protease ablation causes morphological and electrophysiological abnormalities in PCs

To establish if neurons were secondarily affected by mitochondrial dysfunction in astrocytes, I stained PCs with calbindin (a Ca^{2+} binding protein expressed in PCs) and SMI31 that targets parallel fibers. Astro-L2 KO animals show PCs cell bodies tightly packed one close to the other, at 32 and 62 weeks. In some cases, PCs cell bodies were also slightly towards the ML. Moreover, the dendritic tree of PCs in astro-L2KOs appears disorganized, as the primary branches are bent rather than straight toward the ML. I could not detect any major difference in the parallel fibers (Fig. 4.14A).

In astro-DKOs the situation was different: at 3 weeks there were no differences in the appearance of both PCs and parallel fibers compared to the $L1^{-/-}$. However, at 4 weeks, PCs appeared quite disrupted, with abnormal dendrites, small cell bodies that in some cases are more towards the ML than the PCL (Fig. 4.14B).

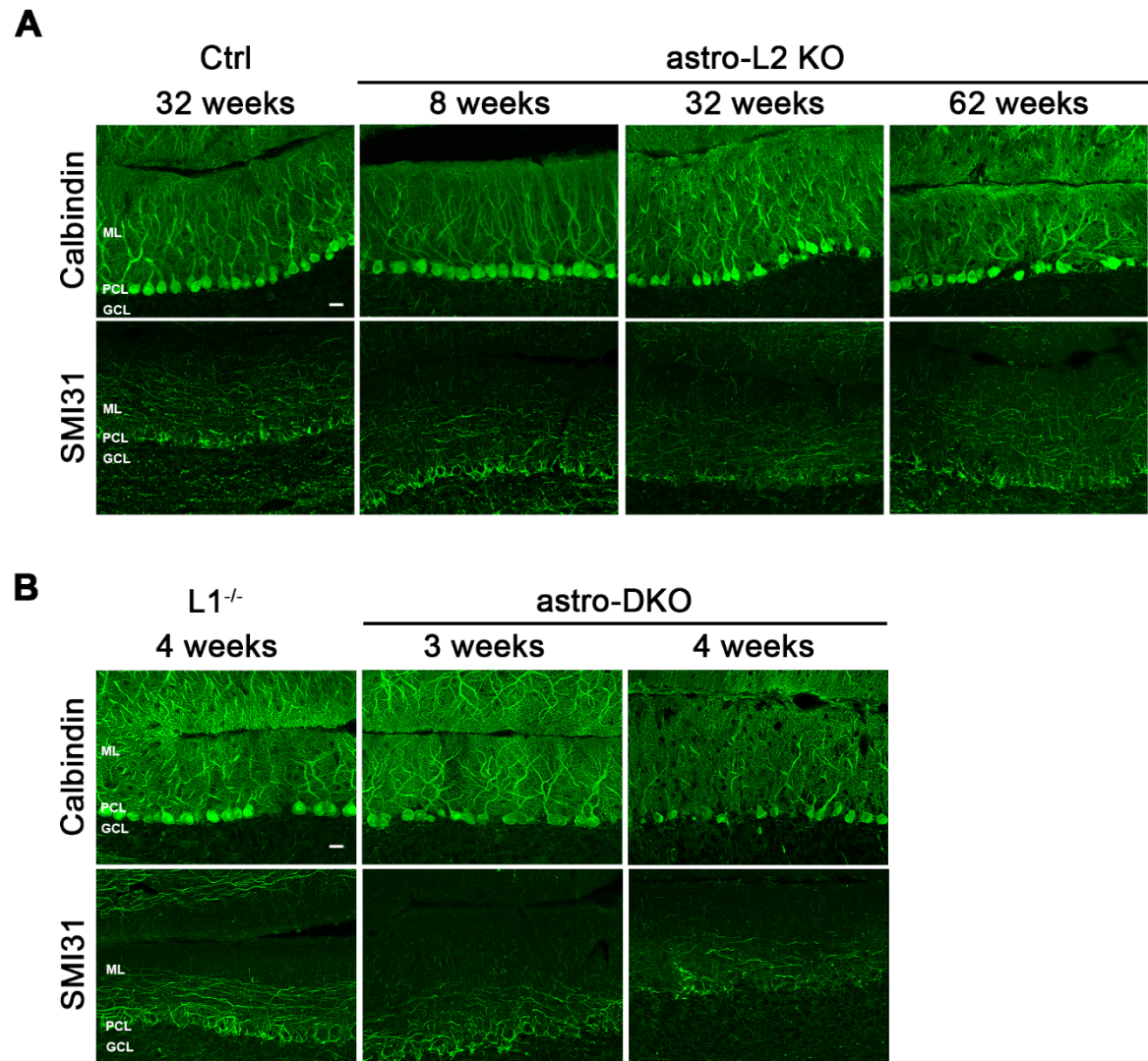


Figure 4.14: *m*-AAA protease dysfunction in astrocytes leads to PC morphological abnormalities.

(A-B) Immunofluorescence stainings for PC marker calbindin and parallel fiber marker SMI31 in cerebellar slices of astro-L2 KOs and astro-DKOs and relative controls. $n=3$ for each group at each time point. Scale bar=20 μm .

To further elucidate the effect on PCs in the more severe astro-DKO mouse model, I collaborated with Dr Simon Hess to perform electrophysiological recordings on cerebellar slices from animals at 4 weeks. Freshly dissected CB were cut in slices and kept in aCSF. A cocktail of different inhibitors of glutamatergic and GABAergic stimuli was used to abolish any neuronal activation induced by surrounding cells. In resting conditions, perforated patch clamp on PCs of L1^{-/-} animals confirmed that these cells have a pattern of spontaneous activity [227, 228]. Following the recordings in resting conditions, PCs from L1^{-/-} show a regular firing

pattern at 4 weeks (Fig. 4.15A, lower panel). However, this was not the case for astro-DKO PCs. In fact, there was almost no recording of spontaneous activity, as quantified in Fig. 4.15B. Following the recordings, measured cells were visualized at the microscope with biocytin-labeling. The lower dendritic arborization of astro-DKO PCs compared to the L1^{-/-} can be noticed (Fig. 4.15A, upper panel). Then, hyper-polarizing current pulses were used to evaluate membrane resistance. Interestingly PCs of astro-DKO mice showed a higher cell input resistance than the respective controls (Fig. 4.15C), suggesting ion channels changes. Moreover, when stimulated with electric pulses, the neuronal response was lower than in L1^{-/-}, as indicated from the current-frequency plot with a shallower slope for the astro-DKOs compared to the L1^{-/-}. The number of spikes was quite reduced in astro-DKOs (Fig. 4.15D).

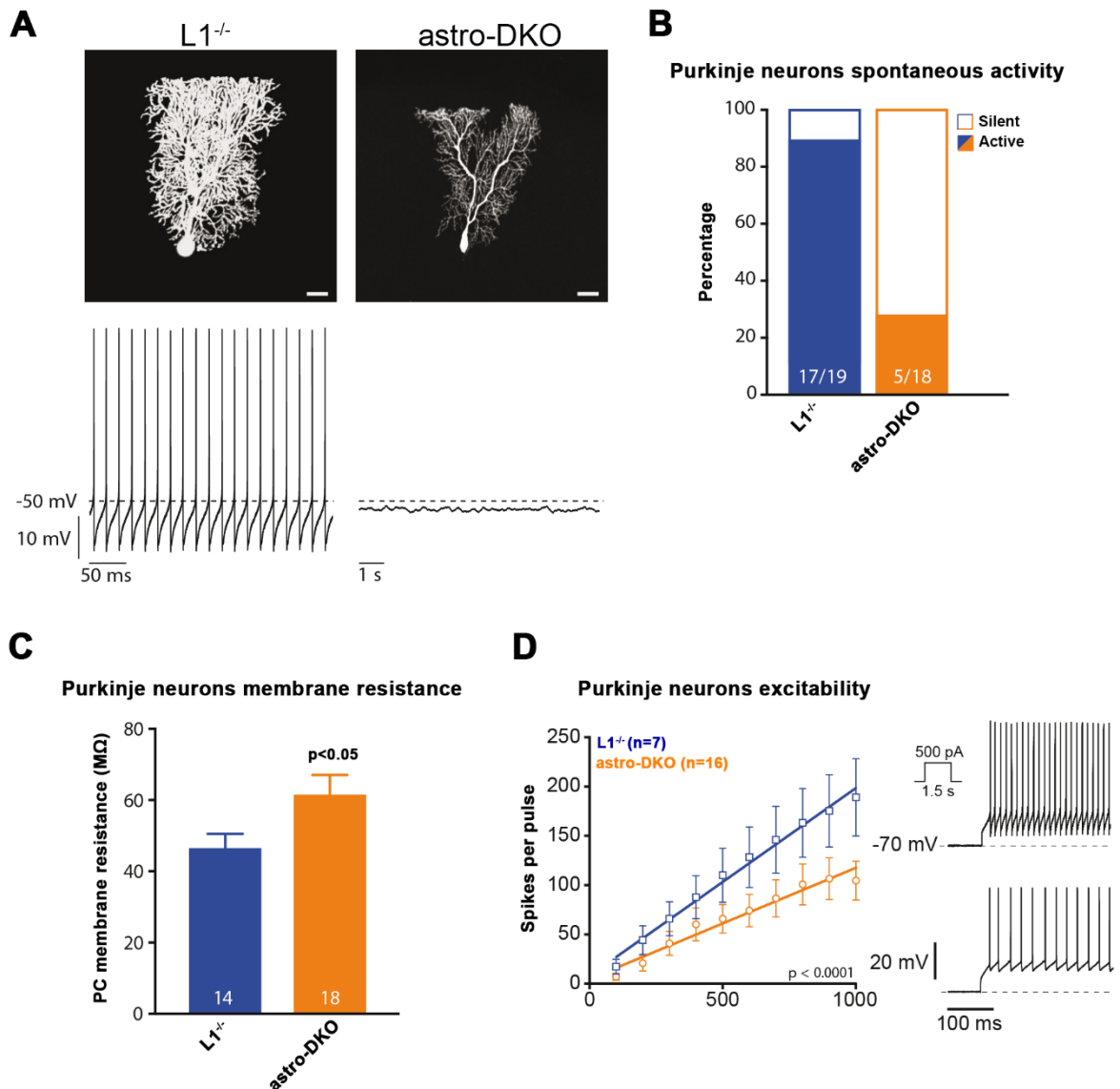


Figure 4.15: *m*-AAA protease dysfunction causes electrophysiological abnormalities in PCs. (A) Stained PCs and respective spontaneous activity ephys of L1^{-/-} and astro-DKOs. (B) Percentage of spontaneously active versus silent neurons in L1^{-/-} and astro-DKOs. The number of neurons analyzed is indicated in the bars. (C) Membrane resistance indicated in mega ohm (MΩ). The number of neurons analyzed is indicated in the bars. Data represents mean±standard deviation (SD), *p* value was obtained by Student's t-test and is indicated when < 0.05. (D) Evaluation of excitability of PCs, expressed as spikes per pulse. The number of neurons analyzed is indicated in the graph. On the left side, example of ephys from L1^{-/-} (upper) and astro-DKO (lower) PCs. Animals were tested at 4 weeks of age, *n* ≥ 3 for each group.

Considering the morphological alterations in PCs caused by BG dysfunction, I decided to evaluate whether the synapses on PCs were also affected. Electron microscopy images were

acquired in random areas of the ML. I counted the active synapses, identified as areas of increased electron density where the membranes of pre and postsynaptic buttons were visible, often showing synaptic vesicles. The quantification did not show any significant difference in the synaptic density in astro-L2 KOs and astro-DKOs (Fig. S3 and S5C).

In the ML, it is possible to identify two different types of synapses occurring at the PC dendrites. In fact, synapses between PCs and climbing fibers (axons deriving from neurons located in the olivary nuclei) can be identified using vesicular glutamate transporter 2 (vGlut2). Synapses between PCs and parallel fiber express, instead, the vesicular glutamate transporter 1 (vGlut1) transporter [229]. I used an antibody against vGlut2 marker on cerebellar slices, as it is easier to quantify because of the lower expression. While in the astro-L2 KO mouse model I could not detect any difference between astro-L2 KOs and Ctrl (Fig. S4), in the astro-DKOs the number of vGlut2 puncta are significantly increased compared to $L1^{-/-}$ (Fig. S5A and B). This could hint to an alteration in the synaptic trim operated through glial cells [230, 231]. Overall, mitochondrial dysfunction that targets solely astrocytes has a deep impact on PC morphology and electrophysiological properties. Neurons are known to be affected by astrocyte dysfunction [187, 232, 233]. However, this is the first time that a mitochondrial protease ablation, which is not causing OXPHOS deficiency, selectively removed from astrocytes causes neuronal degeneration.

4.12 *m*-AAA protease ablation in astrocytes causes upregulation of necroptotic markers, but not apoptosis

As previously discussed, targeted cells disappear over time in both KO models. According to the most recent theories concerning *Afg3l2* deletion, it could be due to calpain-mediated cell death or apoptosis [138, 170]. In both hypothesis, calcium handling is abnormal, and it could either cause activation of calpain enzymes or being buffered excessively by mitochondria,

leading to MPTP opening and apoptosis induction. To shed light on this matter, I decided to test whether there was activation of caspase 3 (cleaved-caspase 3), one of the most used markers for apoptosis [234]. In both models, I could not detect an increased number of cleaved-caspase 3⁺ cells while counting all the positive cells in each section analyzed (Fig. 4.16A and B). Focusing only on the astro-DKOs and L1^{-/-}, as astro-DKOs manifest a stronger phenotype, I tried to detect calpain activation by western blot on total cerebellar lysates. Gephyrin is known as target of activated calpains, and it is cleaved forming a 48 kDa fragment called E-domain, recognized by the 3B11 antibody [235]. Gephyrin is a glycine and GABA receptors anchoring protein expressed in both neurons and astrocyte [236, 237]. Astro-DKOs do not show any increased cleavage of gephyrin, which looks comparable to the L1^{-/-} levels (Fig.4.16C). I therefore excluded calpain activation as cell death in astro-DKOs. I then decided to check for necroptosis, a pathway that combines apoptosis and necrosis features, and apoptosis with a different approach: I analyzed mRNA levels of both apoptotic and necroptotic markers from total cerebellar extracts (Fig. 4.16D). I used different necroptosis markers reported in literature. Fas-associated protein with death domain (FADD) is an adaptor protein involved in caspases cascade activation [238]. The receptor-interacting serine/threonine protein kinases 1/3 (RIPK1 and 3) are mediators of necroptosis [239]. The pseudokinase mixed lineage kinase domain-like (MLKL) has been reported to induce necroptosis following RIPK3-mediated phosphorylation [240]. Z-DNA binding protein 1 (ZBP1) activates RIPK3 upstream to MLKL [241]. As marker for apoptosis, I used the Bcl-2 homologous antagonist/killer (BAK), a pro-apoptotic regulator [242]; the p53 upregulated modulator of apoptosis (PUMA) [243] and myeloid cell leukemia 1 protein (MCL1), a pro-survival regulator of apoptosis [244]. Confirming the cleaved-caspase3 results(Fig. 4.16 B), I could not detect upregulation of apoptotic markers, except PUMA, which could also be involved in necroptosis [245]. On the contrary, necroptosis markers were upregulated, indicating ongoing necroptosis in the tissue (Fig. 4.16 D). I could also detect increased protein levels of RIPK3 in total cerebellar lysates, further confirming the quantitative

real time PCR results (Fig. 4.16E). Necroptosis markers were all highly increased. However, I cannot claim that necroptosis is the occurring death pathway for targeted cells. In fact, these markers are upregulated in activated microglia [246, 247], which is present in this mouse model, thus further investigation is required.

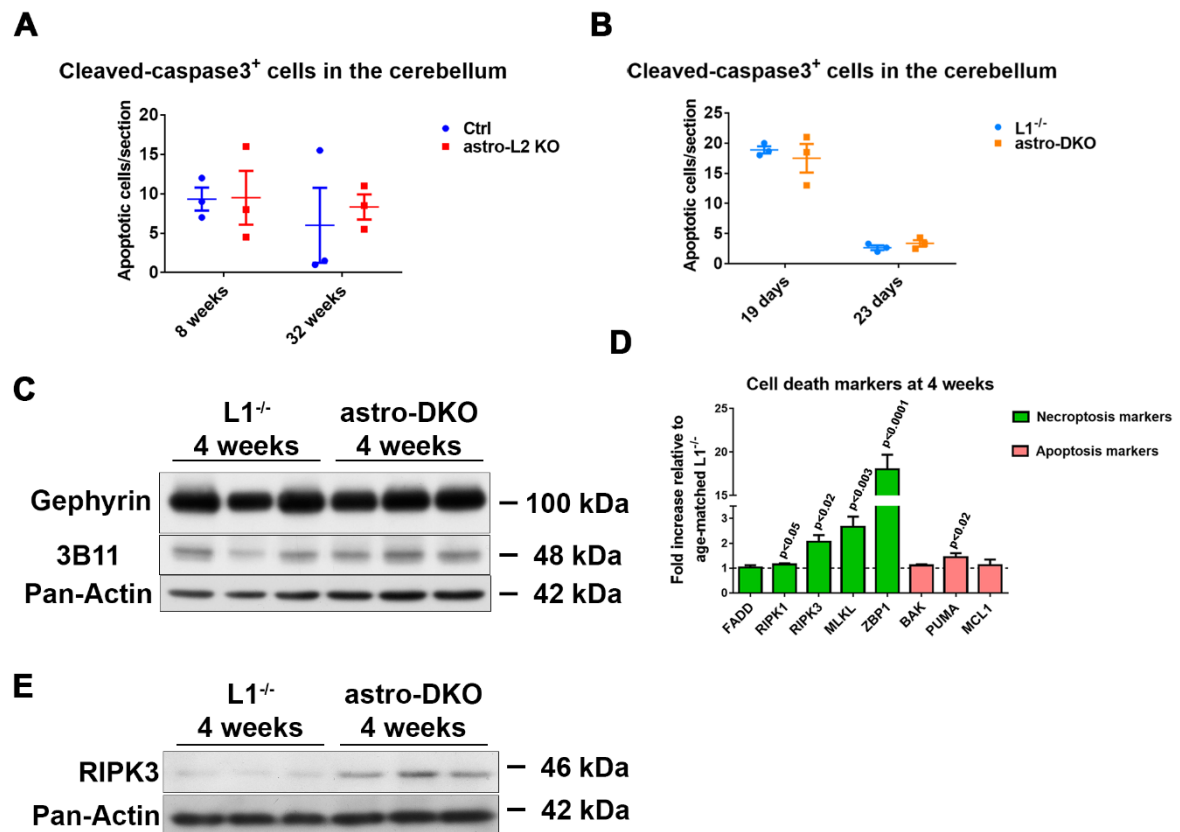


Figure 4.16: *m*-AAA protease depletion causes upregulation of necroptotic markers. (A-B) Quantification of immunohistochemistry against the apoptosis marker cleaved-caspase 3. Dots represent the n. Data are presented as mean±SEM. (C) Western blot from total cerebellar lysates for gephyrin full length (target of calpain) and 3B11 (cleavage product of calpain targeting gephyrin) and pan-actin as a loading control. (D) mRNA level of necroptotic and apoptotic markers, expressed as fold increase to the age-matched L1^{-/-}. n=3 for each group, data represent mean±SD, *p* value obtained with Student's *t*-test is indicated when < 0.05. (E) Western blot against RIPK3 (necroptotic marker) which is upregulated in astro-DKOs at 4 weeks.

5 DISCUSSION

5.1 Conditional KO mouse models as a tool for understanding the contribution of glial cells to neurodegeneration

The pleiotropic functions of the *m*-AAA protease give it an important role within mitochondrial homeostasis. In fact, due to the range of targets, its function is directly or indirectly correlated with many mitochondrial processes such as translation, mtDNA maintenance, respiration, fusion-fission balance, mitophagy and protein quality control [114, 119, 133, 134, 139]. *m*-AAA protease dysfunction leads to mitochondrial impairment and neuronal death, and in humans it is associated with different neurodegenerative diseases, with a different neuronal target depending on the mutated subunit [114, 123, 133, 156, 211]. Interestingly, the focus of researchers has been understanding the mechanisms leading to neuronal death, as all the diseases caused by *m*-AAA protease dysfunctions are considered neuronal-diseases. Indeed, a PC-specific *Afg3l2*-KO mouse model showed that PCs die within few weeks, reinforcing the idea that neurons are highly susceptible to *m*-AAA protease deficiency and that they die in a cell-autonomous fashion [165]. However, the contribution of glial cells to neuronal welfare should not be underestimated. In fact, *m*-AAA protease ablation specifically in myelinating cells induces improper axonal myelination and death of targeted cells, resulting in the development of a motor defect [167]. Moreover, the finding by Maltecca et al., [170] that reducing synaptic stimulation of PCs actually ameliorates the phenotype of a SCA28 mouse model, suggests an important contribution of glial cells in the development of the phenotype. Indeed, the group showed that induction of EAAT2 expression in astrocytes with ceftriaxone treatment improves the ataxic symptoms. In addition, the contribution of glial cells in the development of neurodegenerative diseases has recently been taken under consideration. Beside that there are neurodegenerative diseases caused by glial cells dysfunction, such as the Alexander disease [66, 67], the use of conditional mouse models have shed some light on the

contribution of glial cells to the development of neurodegeneration. Ignatenko et al., [187] recently showed, by the means of conditional Twinkle helicase KO in neurons or astrocytes, that mtDNA loss in neurons leads to a sudden neurodegeneration between 7 and 8 months. However, mtDNA loss specifically in astrocytes leads to a much earlier phenotype development, which includes also spongiosis, a symptom observed in patients affected by mitochondrial encephalopathies such as Alpers–Huttenlocher and Leigh syndrome. Moreover, different mouse models in which Parkinson disease related genes were knocked out in astrocytes, showed the incapability of astrocytes to promote dopaminergic neuron survival, causing also the development of motor impairment [248]. In my work, I could indeed detect that *Afg3l2*-KO or *m*-AAA protease ablation in astrocytes is sufficient to induce motor impairment development. My findings suggest that mitochondrial dysfunction impairs astrocytic functions, such as glutamate recycling, without causing respiratory deficiency. Uncoupling mitochondrial respiration from other mitochondrial functions is extremely important. In fact, Supplie and colleagues [34] showed that respiratory deficiency in astrocytes has no detectable effect in cellular viability, and does not cause any secondary phenotype on neurons or motor impairment in the mouse model. In my thesis, I described the effect of *m*-AAA protease dysfunction in astrocytes, which causes mild or severe phenotype on animals in a dose-dependent manner, without inducing any detectable respiratory deficiency (Fig. 4.7). The results obtained during my thesis show that not only *m*-AAA protease impairment in astrocytes leads to cell demise, but also alters PCs morphology and electrophysiological properties, causing a reduced arborization of the dendritic tree, as well as reduced excitability. Moreover, neuroinflammation was detected. The data collected in this work suggest a relevant contribution of astrocytes in the development and progression of SCA28 and SPAX5.

5.2 Gender-specific phenotype delay

As *AFG3L2* gene is located at chromosome 18 in humans [155], both SCA28 and SPAX5 follow the autosomal inheritance mode. However, as only few families have been reported to develop SCA28, and even less SPAX5, it is not yet possible to establish either penetrance or gender effects [249]. Until now, no gender-related peculiarities have been reported. In line with the theoretical equality due to autosomal transmission, male and female astro-DKOs do not show any prominent difference in neither the motor impairment nor the cerebellar phenotype. On the contrary, astro-L2 KO mice manifested gender-specific differences: despite both groups appear to be smaller compared to the relative gender and age-matched controls, astro-L2 KO males have a lower rotarod latency to fall compared to Ctrl starting at 32 weeks of age, whereas females may have a tendency towards worse performance at 62 weeks. This finding suggests that females develop the phenotype at a slower pace. Indeed, it was shown that primary astrocyte cultures from female pup brains proliferate in presence of steroid hormones progesterone and estrogen. These hormones have also the effect of inducing fusion and fission events, therefore affecting mitochondrial dynamics [250]. The same effect was not observed in primary astrocyte cultures obtained from male pups: there was no increased proliferation when treated with estrogen. Moreover, progesterone treatment reduced the total cell number. In addition, the two hormones in male-astrocytes culture differentially affected mitochondrial dynamics: estrogen increased the transcription of fusion/fission genes, whereas progesterone decreased it.

Tamoxifen, used to induce the Cre recombinase translocation to the nucleus, is an estrogen receptor-binding drug. Its effect on endogenous estrogen receptors has been studied and gender differences have been reported especially in kidney diseases, where tamoxifen-inducible CreER systems could give confounding results [251]. However, gender differences are attributed mostly to the promoter used for targeting the recombination to specific subsets of cells, and to

the gene under study [251, 252]. Concerning the AFG3L2 protein-associated phenotypes, no gender-related differences have been reported so far, nor in human nor in mouse models. It was shown that astrocytes reactivity varies in a sex- and estrous-cycle dependent manner in adult animals with brain injuries, and also in primary culture [253, 254]. However, no sex differences related to the GFAP promoter were reported. Therefore, I excluded a tamoxifen- or promoter-related gender difference in astro-L2 KOs. Indeed, the hypothesis that sex hormones can protect astrocytes with mitochondrial dysfunction is intriguing and would need further investigation.

5.3 Mitochondrial morphology, phenotype development and cell death

Mitochondrial morphology is altered in case of *m*-AAA protease dysfunction [152, 165, 167]. It has been shown that *m*-AAA protease dysfunction leads to hyper-activation of OMA1, which in turn processes OPA1. The increased ratio of short OPA1 isoforms over the long OPA1 isoforms is correlated with the increased fragmentation observed in *m*-AAA protease deficient cells [116, 118, 255]. In both mouse models analyzed in this thesis, mitochondria indeed show fragmentation, as observed by the means of mitochondrial reporter lines. Therefore, the findings here reported are in line with the current available literature. An interesting observation is that mitochondrial fragmentation occurs already around 3 weeks in the astro-L2 KO mouse line. However, the motor impairment is detected not earlier than 32 weeks and also the morphological alterations observed in male animals lacking AFG3L2 in astrocytes, such as BG translocation and decreased number and PCs cell bodies almost overlapping, do not develop at an early stage, as at 8 weeks the CB morphology look indistinguishable from Ctrl. Therefore, it is likely that the slow phenotype development is due to an accumulation of dysfunctions. In the astro-DKO mice on the other end, the *m*-AAA protease ablation leads to a sudden death of targeted cells which results in the fast development of an ataxic phenotype. Mitochondrial fragmentation is already visible at 3 weeks, but the motor phenotype cannot be evaluated at this

age, as the cerebellar development is not yet completed and the results obtained could be wrongly interpreted. By visual inspection, $L1^{-/-}$ and astro-DKOs look indistinguishable at 3 weeks.

In all *m*-AAA protease deficient models, mitochondria not only look fragmented, but the cristae morphology is completely disrupted. It was reported that OPA1 can regulate the cristae morphology and, at the same time, preserve cytochrome c inside the cristae. OPA1 cleavage can open the tight junction that allow the cristae structure, resulting in release of cytochrome c and induction of apoptosis [95, 256-258]. Another possible way how *m*-AAA protease dysfunction could affect cristae morphology is through the accumulation of Ca^{2+} ions within the mitochondrial matrix. This would cause MPTP opening, inducing the collapse of the proton gradient and therefore, the dysfunction of the ATP synthesis. The resulting dissipation of the ionic gradient would lead to the swelling of the cristae [139]. Induction of apoptosis seems plausible. However, apoptosis is not induced in either the astro-L2 KO or the astro-DKO mouse models. In fact, mice lacking only AFG3L2 in astrocytes showed fragmented mitochondria as early as at 3 weeks. At 8 weeks BG cells contain mitochondria with highly disrupted cristae, but $S100^{+}$ and $SOX2^{+}$ cells counts failed to reveal cell death at this stage. Moreover, there was no difference in the number of cleaved-caspase 3⁺ cells at 8 weeks nor later at 32 weeks in the astro-L2 KOs. What about the astro-DKOs? The phenotype in this mouse model develops much faster and targeted cells die in few days. However, the cleaved-caspase 3 marker did not show increase at any age analyzed, and real-time quantitative PCR did not reveal upregulation of apoptotic markers.

Another mechanism proposed by Maltecca et al., [168-170] consists in the activation of calpain, due to increased Ca^{2+} influx in the cytosol that would induce calpain-mediated dark cell degeneration in PCs in a SCA28 mouse model. Dark degenerating axons were observed also in the spinal cord of mice lacking the *m*-AAA protease specifically in oligodendrocytes [167]. In

neither of the mouse models studied in this work, dark cell degeneration was observed in the cerebellum. To conclusively exclude the calpain activation, I tested whether the calpain target gephyrin, an anchoring protein for glycine receptors to the cellular membrane of neurons and astrocytes [236, 237], was processed in cerebellar total lysates of astro-DKO mice. If the cleavage occurred, it would be possible to detect both a reduction of the full length gephyrin and the increased amount of the fragment 3B11. This was not the case and therefore I excluded the calpain activation. Necrotic events were not detected either and I decided to test for necroptosis markers upregulation in total cerebellar RNA extracts *via* real time quantitative PCR. Here, I could detect an upregulation of the necroptosis markers at 4 weeks. However, I cannot conclude that necroptosis is the mechanism by which targeted cells die. In fact, at the same time, activated microglia have invaded the cerebellum. It has been reported that reactive microglia upregulate necroptotic markers and could also induce necroptosis in reactive astrocytes, rather than being the *m*-AAA protease deficiency the direct cause of the necroptotic death [246, 247].

A possible way to address which cells are upregulating necroptotic markers is immunofluorescence co-staining against necroptosis markers and astrocytes/microglia markers. Another method would be testing isolated astrocytes from affected animals or primary astrocytes, in which the deletion is induced, using western blotting techniques. However, it could be that once astrocytes are isolated, and not exposed to the extremely dynamic environment that they must monitor, they do not show the same reactivity and death. Another interesting method would be crossing the mouse models presented in this thesis with RIP3-deficient mice [259] and evaluate targeted cells death.

5.4 Mitochondrial dysfunction and BG response

I could successfully induce the Cre recombinase specifically in astrocytes, and BG cells showed a high rate of recombination. As members of the tripartite synapse with parallel fibers and PCs, BG proper function is crucial for synaptic transmission. Astrocytes have a quite dynamic mitochondrial network which is highly sensitive to neuronal activity [185]. In the *m*-AAA protease deficient mouse models, it is possible to notice mitochondrial retraction from the upper extremity of the ML, compared to the respective controls. It could be that dysfunctional mitochondria are targeted for elimination, as the morphology of BG analyzed using the S100 marker does not appear disrupted in the early stages (3 weeks for the astro-DKOs and 8 weeks for the astro-L2 KOs). Possible way to test mitophagy would be performing an immunofluorescence staining against mitophagy or autophagy markers, such as LC3, an autophagosome associated protein, and to quantify co-localization with mtYFP. *In vitro* studies using autophagy blockers could also reveal if fragmented mitochondria are targeted for mitophagy.

Despite mitochondrial fragmentation has been reported as an astrocytic physiological response to glutamate stimulation [185], I observed that following mitochondrial retraction also the BG projections were retracted. Moreover, I observed also that targeted cells expressing the mtYFP were reduced in astro-L2 KOs at 32 weeks and astro-DKOs at 4 weeks. Therefore, I can conclude that, comparable to neurons and oligodendrocytes, *m*-AAA protease dysfunction is not compatible with long term survival of BG. Aberrant BG projections and reduced BG number coincide with the motor impairment development in both mouse models, even if I cannot directly link temporally in a cause-effect fashion the two events.

Despite the *m*-AAA dysfunction in this cell type, BG mitochondria do not show OXPHOS deficiency. In fact, COX-SDH staining did not reveal any respiration defect, even if

mitochondrial morphology is quite disrupted. Moreover, it was shown that astrocyte-specific KO of *Cox10* does impair mitochondrial respiration but does not cause BG demise [34]. These results are in line with the previous literature describing astrocytes as glycolytic cells, rather than cells relying on OXPHOS for energy production. However, mitochondrial dysfunction has been reported to be lethal for astrocytes. A recent study demonstrated that astrocyte-specific KO of the mitochondrial helicase Twinkle causes astrocyte death. mtDNA maintenance is necessary for mitochondrial function and cell survival [187]. Interestingly, despite the *m*-AAA protease is important for elimination of OXPHOS subunits and it is also important for the translation of mtDNA-encoded proteins, targeted cells do not present respiratory deficiency. However, the dysfunction is so severe that causes mitochondrial stress response and cellular demise.

Metabolic stress response has been reported in other mouse model in which mtDNA maintenance was impaired [214, 215]. In fact, mitochondrial dysfunction affects the whole cell metabolism, inducing changes in the cytosolic biosynthetic pathways. Of relevance is the folate cycle, orchestrated between mitochondria and the cytosol: the one-carbon units formed constitute substrates for different biosynthetic pathways, including nucleotide synthesis and methylation reactions. Animals carrying a dominant Twinkle defect show upregulation of enzymes involved in mitochondrial folate cycle such as MTHFD2. Moreover, enzymes responsible for serine *de novo* synthesis, PSAT1 and PHGDH are upregulated. Serine is the mitochondrial primary one-carbon donor, and is used to produce both glycine and methylenetetrahydrofolate. The altered folate cycle causes amino acid imbalance as well as deoxynucleotide triphosphate increase [214]. In the astro-DKO mice at 4 weeks, I was able to detect upregulation of PSAT1, PHGDH and MTHFD2. A further confirmation that this pathway is changed is the amino acids levels detected at both 3 and 4 weeks in the astro-DKOs. In fact, not only serine and glycine, but also threonine and proline are commonly upregulated

during metabolic stress. This is the first indication that *m*-AAA protease deficiency can lead to an overall metabolic rearrangement, therefore adding a new piece to the puzzle.

5.5 Neuroinflammation upon *m*-AAA protease dysfunction in astrocytes

The inflammatory response is normally mediated by immune cells. However, in the CNS, astrocytes have a special role as they can either direct microglia activation or being activated themselves by microglia signaling [57, 58]. Neuroinflammation occurs in case of injury, infection or neurodegenerative disorders. Release of inflammation mediators induces the reactive state in both cell types, which includes hypertrophy, proliferation and release of cytokines to recruit other neuroinflammatory macrophages. In cerebella of astro-DKO mice at 4 weeks, both activated microglia and reactive astrocytes are present. The massive death of BG cells could explain the activation of both cell types to eliminate debris. In astro-L2 KO mice, microglia activation in CB was not observed, and reactive astrogliosis was detected only at 32 weeks, indicating that at 62 weeks the cause disappeared. Both reactive astrogliosis and activated microglia were observed in a mouse model in which *Afg3l2* was deleted specifically in PCs [165]. In this model, both cell types were responding to neuronal damage. While in astro-DKO mice most, but not all, reactive astrocytes were not targeted cells, in 32-week-old astro-L2 KO mice targeted and non-targeted cells displayed reactivity. This interesting difference between the two models can be explained by the fact that most targeted cells were already dead in 4 week-old astro-DKO, therefore the only reactive astrocytes left were the untargeted ones. It would be interesting to understand the mechanism leading to activation of targeted astrocytes: are they responding to other cells damage or to their own dysfunction? Interestingly, at 62 weeks the reactive astrogliosis was not detected anymore in astro-L2 KO mice, most likely due to the disappearance of targeted cells. Concerning microglial activation in the astro-DKO mice at 4 weeks, it is mostly induced following reactive astrogliosis, as the latter was mildly present at 3

weeks. The release of interleukins and cytokines detected in total cerebellar RNA pools could explain the massive microglial activation. However, the fine dynamics of astrocytes/microglia interplay should be further investigated.

Another interesting difference between the astro-L2 KOs and the astro-DKOs is the fact that the first ones survive to the astrocyte-specific *m*-AAA protease dysfunction. In particular, despite the death of targeted cells, at 62 weeks the cerebellum does not present major abnormalities, beside the BG projections abnormalities, with cells moving into the ML rather than staying in the PCL. BG mobilization was also observed in astro-DKOs at 4 weeks. This phenomenon was previously observed in patients and a mouse model for the leukoencephalopathy vanishing white matter (VWM) disease [205]. In the VWM, the displacement is caused by mutation in the gene encoding for the eukaryotic initiation factor 2B, an important translational regulator, and causes an increased expression of the immature astrocytic marker nestin, as well as GFAP. The mechanism leading to BG mobilization is not understood and further studies are required to properly dissect the regulation of BG translocation. Without a reporter line for astro-L2 KOs at 62 weeks, I could not verify if the translocating cells were targeted or not, but the impossibility to detect abnormal mitochondria in 62 weeks old astro-L2 KO animals, directed me to the hypothesis that the translocating cells are not targeted. This observation was also reinforced by the replenished pool of BG in the PCL at 62 weeks. Where are these cells coming from? Already at 8 weeks both astro-L2 KO and HET mice show an increased number of mtYFP positive cells, hinting towards astrocytic proliferation between 3 and 8 weeks. The increased proliferation in astro-L2 KO was further confirmed by the transcription factor SOX2, which is upregulated in proliferating astrocytes. These findings allow the conclusion that both targeted and untargeted astrocytes proliferate already around 8 weeks, but while the deficient ones die over time, the untargeted ones replace

them. Maybe due to the late stage of differentiation the newly inserted BG cells cannot properly anchor themselves in the PCL, and move towards the ML.

BG replenishment poses an important question: which are the progenitor cells differentiating in new BG cells? The mtYFP reporter line showed that targeted cells are not PCs nor granule neurons, and the mtYFP signal perfectly co-localizes with BG markers. However, NG2⁺ cells can give rise to both oligodendrocytes and BG cells [210]. I provided proof that NG2⁺ cells are not targeted. It was not possible to establish whether new BG cells were generated by proliferating BG or by precursor cells.

5.6 Glutamate dysregulation and secondary neuronal phenotype development

When analyzing the amino acid levels from total cerebellar lysates, an interesting finding was the downregulation of glutamine and glutamate in astro-DKOs at 4 weeks. Astrocytes are required for glutamate recycling [37], and mitochondria provide astrocytic glutamate transporters with the energy necessary for their activity, being also localized close to the EAATs [181]. In astro-DKOs, EAAT1 was strongly decreased, while EAAT2 signal was completely absent in BG cells. The residual signal was instead localized to microglia cells. It was previously reported that in case of EAAT2 downregulation in astrocytes, microglia cells upregulate the glutamate transporter expression as a survival mechanism [225, 226]. In contrast, in astro-L2 KOs EAAT1 signal was comparable to Ctrl at any stage observed, but EAAT2 showed overtime a patchy distribution in the ML, which was an indication of not homogeneous coverage of the ML, in line with the BG altered morphology.

The impaired glutamate uptake and recycling *per se* affects neurons in astro-DKOs at 4 weeks causing a secondary neuronal phenotype. Glutamate mishandling by BG has been previously reported to cause secondary neuronal impairment. In fact, ataxin-7 polyglutamine expansion in

astrocytes leads to reduced expression of EAAT1 leading to neurodegeneration [260]. In another study, Sicot et al [261] found that, in a model of myotonic dystrophy, mutant toxic RNA addressed BG rather than neurons, causing EAAT2 lower expression and toxicity of PCs. The phenotype was ameliorated, also in this case, by ceftriaxone administration. In astro-DKO mice at 4 weeks, *m*-AAA protease dysfunction induces non-cell autonomous modifications in both morphology and electrophysiological intrinsic properties of PCs. In fact, PCs showed reduced dendritic arborization. Considering that the synaptic counts did not reveal any major difference between $L1^{-/-}$ and astro-DKO at 4 weeks, the loss of dendritic arborization seemed counterintuitive. However, the vGlut2 puncta counts, which mark climbing fibers synapses, were significantly increased. It could be that while the dendritic arborization is remodeled to selectively reduce the synaptic input from the GCs, climbing fibers synapse increase. The difference between the synaptic counts could be masked this way. What cannot be compensated, though, is the lack of spontaneous activity of PCs, and it could be that the increased climbing fibers synapses are aimed to further stimulate otherwise silent PCs. The increased membrane potential could be a further adaptation mechanism to overcome glutamate hyper-stimulation from both climbing fibers and parallel fibers. It can also indicate that ion channels composition remodeling occurred, making neurons less excitable and affecting the firing rate, even when stimulated with depolarizing currents.

6 CONCLUSIONS

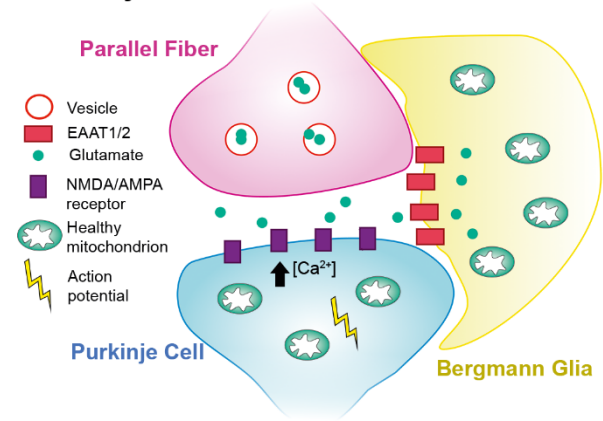
In conclusion, with this thesis I provided evidences that an *m*-AAA protease dysfunction is incompatible with astrocytes survival. Although the dysfunction was limited to astrocytes, both mouse models developed motor impairment and the severity was dose-dependent. This work represents a direct evidence of the BG relevance in the development of *Afg3l2* deficiency-associated motor phenotypes in mouse models. The work proposed is in line with the recent findings by Maltecca et al., König et al., and Patron et al., in which the authors postulated that excitotoxicity on PCs is involved SCA28 development [138, 139, 169, 170]. As BG contribution should also be taken under consideration, I propose an integrated model of the current pathophysiological hypothesis, where BG cells are more than passive bystanders and actively contribute to the development and the progression of the disease.

In a healthy situation, GC axons release glutamate vesicles in the synaptic cleft following an action potential. Glutamate receptors located on the postsynaptic PC dendrites bind glutamate and respond to the synaptic stimulation, signaling to the deep cerebellar nuclei. Meanwhile, glutamate transporters located on the astrocytic surface surrounding the synapse remove the neurotransmitter from the synaptic cleft. Inside astrocytes, glutamate is converted to glutamine by the glutamine synthase and shipped to the GC, where it is converted to glutamate and used to fill the synaptic vesicles.

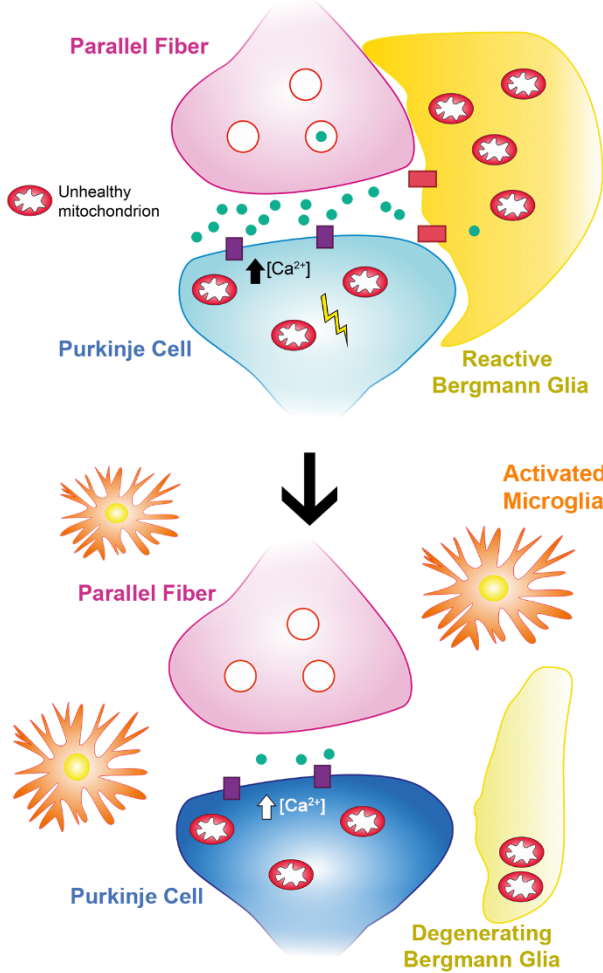
In case of AFG3L2 dysfunction, both PCs and GCs are subjected to mitochondrial dysfunction, which includes respiration deficiency, reduced ATP production and Ca^{2+} mishandling. Moreover, glutamate release from GC further aggravate the Ca^{2+} homeostasis defect caused by impaired mitochondrial function in PCs. BG cells with dysfunctional AFG3L2 are not able to promptly remove glutamate from the synaptic cleft due to the reduction of EAATs expression on the cellular surface. The reduced of glutamate uptake causes further hyper-stimulation of

PCs, and excitotoxicity. With cell death occurring, reactive astrogliosis and microglia activation are induced. Neurons and BG die due to the accumulation of dysfunction and induction of cell death pathways.

Healthy condition



AFG3L2 deficiency



Ca²⁺-mediated cell death

Figure 5.1: Integrated model of SCA28 progression. In healthy conditions, parallel fibers communicate with PCs *via* the neurotransmitter glutamate. BG clean up the synaptic cleft *via* EAATs expressed on its surface, and fueled by mitochondria. In pathogenic conditions, BG reduced EAATs expression causes glutamate uptake impairment. The resulting hyper-stimulation of PCs induces

excitotoxicity and mishandling of Ca^{2+} . The lack of BG support, together with the intrinsic inability to properly process synaptic stimulation, lead to degeneration and cell death of both astrocytes and neurons. These events activate both astrocytes and microglial cells, causing neuroinflammation.

7 BIBLIOGRAPHY

- [1] H. Wolosker, E. Dumin, L. Balan, V.N. Foltyn, d-Amino acids in the brain: d-serine in neurotransmission and neurodegeneration, *The FEBS Journal* 275(14) (2008) 3514-3526.
- [2] M.V. Sofroniew, Molecular dissection of reactive astrogliosis and glial scar formation, *Trends in neurosciences* 32(12) (2009) 638-47.
- [3] J.G. Emsley, J.D. Macklis, Astroglial heterogeneity closely reflects the neuronal-defined anatomy of the adult murine CNS, *Neuron Glia Biol* 2(3) (2006) 175-86.
- [4] M.V. Sofroniew, H.V. Vinters, Astrocytes: biology and pathology, *Acta neuropathologica* 119(1) (2010) 7-35.
- [5] E.A. Bushong, M.E. Martone, Y.Z. Jones, M.H. Ellisman, Protoplasmic astrocytes in CA1 stratum radiatum occupy separate anatomical domains, *The Journal of neuroscience : the official journal of the Society for Neuroscience* 22(1) (2002) 183-92.
- [6] K. Ogata, T. Kosaka, Structural and quantitative analysis of astrocytes in the mouse hippocampus, *Neuroscience* 113(1) (2002) 221-33.
- [7] J. Livet, T.A. Weissman, H. Kang, R.W. Draft, J. Lu, R.A. Bennis, J.R. Sanes, J.W. Lichtman, Transgenic strategies for combinatorial expression of fluorescent proteins in the nervous system, *Nature* 450 (2007) 56.
- [8] M.M. Halassa, T. Fellin, H. Takano, J.H. Dong, P.G. Haydon, Synaptic islands defined by the territory of a single astrocyte, *The Journal of neuroscience : the official journal of the Society for Neuroscience* 27(24) (2007) 6473-7.
- [9] N.A. Oberheim, G.F. Tian, X. Han, W. Peng, T. Takano, B. Ransom, M. Nedergaard, Loss of astrocytic domain organization in the epileptic brain, *The Journal of neuroscience : the official journal of the Society for Neuroscience* 28(13) (2008) 3264-76.
- [10] L.F. Eng, Glial fibrillary acidic protein (GFAP): the major protein of glial intermediate filaments in differentiated astrocytes, *Journal of Neuroimmunology* 8 (1985) 203-214.

-
- [11] L.F. Eng, J.J. Vanderhaeghen, A. Bignami, B. Gerstl, An acidic protein isolated from fibrous astrocytes, *Brain research* 28(2) (1971) 351-354.
- [12] S.A. Liddelow, B.A. Barres, Reactive Astrocytes: Production, Function, and Therapeutic Potential, *Immunity* 46(6) (2017) 957-967.
- [13] N.J. Allen, B.A. Barres, Glia — more than just brain glue, *Nature* 457 (2009) 675.
- [14] C.E. Ribak, W.M. Tong, N.C. Brecha, GABA plasma membrane transporters, GAT-1 and GAT-3, display different distributions in the rat hippocampus, *The Journal of comparative neurology* 367(4) (1996) 595-606.
- [15] N.C. Danbolt, Glutamate uptake, *Progress in neurobiology* 65(1) (2001) 1-105.
- [16] B. Weber, L.F. Barros, The Astrocyte: Powerhouse and Recycling Center, *Cold Spring Harbor perspectives in biology* 7(12) (2015) a020396.
- [17] A. Araque, V. Parpura, R.P. Sanzgiri, P.G. Haydon, Tripartite synapses: glia, the unacknowledged partner, *Trends in neurosciences* 22(5) (1999) 208-15.
- [18] G. Perea, M. Navarrete, A. Araque, Tripartite synapses: astrocytes process and control synaptic information, *Trends in neurosciences* 32(8) (2009) 421-31.
- [19] M.M. Halassa, T. Fellin, P.G. Haydon, The tripartite synapse: roles for gliotransmission in health and disease, *Trends in molecular medicine* 13(2) (2007) 54-63.
- [20] M. Nedergaard, B. Ransom, S.A. Goldman, New roles for astrocytes: redefining the functional architecture of the brain, *Trends in neurosciences* 26(10) (2003) 523-30.
- [21] G. Seifert, K. Schilling, C. Steinhauser, Astrocyte dysfunction in neurological disorders: a molecular perspective, *Nature reviews. Neuroscience* 7(3) (2006) 194-206.
- [22] E. Shigetomi, D.N. Bowser, M.V. Sofroniew, B.S. Khakh, Two forms of astrocyte calcium excitability have distinct effects on NMDA receptor-mediated slow inward currents in pyramidal neurons, *The Journal of neuroscience : the official journal of the Society for Neuroscience* 28(26) (2008) 6659-63.

- [23] L.M. Garcia-Segura, R.C. Melcangi, Steroids and glial cell function, *Glia* 54(6) (2006) 485-98.
- [24] E.M. Powell, H.M. Geller, Dissection of astrocyte-mediated cues in neuronal guidance and process extension, *Glia* 26(1) (1999) 73-83.
- [25] B.A. Barres, The mystery and magic of glia: a perspective on their roles in health and disease, *Neuron* 60(3) (2008) 430-40.
- [26] K.S. Christopherson, E.M. Ullian, C.C. Stokes, C.E. Mallowney, J.W. Hell, A. Agah, J. Lawler, D.F. Moshier, P. Bornstein, B.A. Barres, Thrombospondins are astrocyte-secreted proteins that promote CNS synaptogenesis, *Cell* 120(3) (2005) 421-33.
- [27] G.R. Gordon, S.J. Mulligan, B.A. MacVicar, Astrocyte control of the cerebrovasculature, *Glia* 55(12) (2007) 1214-21.
- [28] J. Schummers, H. Yu, M. Sur, Tuned responses of astrocytes and their influence on hemodynamic signals in the visual cortex, *Science (New York, N.Y.)* 320(5883) (2008) 1638-43.
- [29] X. Yao, S. Hrabetova, C. Nicholson, G.T. Manley, Aquaporin-4-deficient mice have increased extracellular space without tortuosity change, *The Journal of neuroscience : the official journal of the Society for Neuroscience* 28(21) (2008) 5460-4.
- [30] O. Bloch, K.I. Auguste, G.T. Manley, A.S. Verkman, Accelerated progression of kaolin-induced hydrocephalus in aquaporin-4-deficient mice, *Journal of cerebral blood flow and metabolism : official journal of the International Society of Cerebral Blood Flow and Metabolism* 26(12) (2006) 1527-37.
- [31] N.N. Haj-Yasein, G.F. Vindedal, M. Eilert-Olsen, G.A. Gundersen, O. Skare, P. Laake, A. Klungland, A.E. Thoren, J.M. Burkhardt, O.P. Ottersen, E.A. Nagelhus, Glial-conditional deletion of aquaporin-4 (Aqp4) reduces blood-brain water uptake and confers barrier function on perivascular astrocyte endfeet, *Proc Natl Acad Sci U S A* 108(43) (2011) 17815-20.

- [32] J. Badaut, A.M. Fukuda, A. Jullienne, K.G. Petry, Aquaporin and brain diseases(,), *Biochimica et biophysica acta* 1840(5) (2014) 1554-1565.
- [33] D. Lovatt, U. Sonnewald, H.S. Waagepetersen, A. Schousboe, W. He, J.H.-C. Lin, X. Han, T. Takano, S. Wang, F.J. Sim, S.A. Goldman, M. Nedergaard, The Transcriptome and Metabolic Gene Signature of Protoplasmic Astrocytes in the Adult Murine Cortex, *The Journal of Neuroscience* 27(45) (2007) 12255-12266.
- [34] L.M. Supplie, T. Düking, G. Campbell, F. Diaz, C.T. Moraes, M. Götz, B. Hamprecht, S. Boretius, D. Mahad, K.-A. Nave, Respiration-Deficient Astrocytes Survive As Glycolytic Cells *In Vivo*, *The Journal of Neuroscience* 37(16) (2017) 4231-4242.
- [35] J.D. Cahoy, B. Emery, A. Kaushal, L.C. Foo, J.L. Zamanian, K.S. Christopherson, Y. Xing, J.L. Lubischer, P.A. Krieg, S.A. Krupenko, W.J. Thompson, B.A. Barres, A Transcriptome Database for Astrocytes, Neurons, and Oligodendrocytes: A New Resource for Understanding Brain Development and Function, *The Journal of Neuroscience* 28(1) (2008) 264-278.
- [36] A. Herrero-Mendez, A. Almeida, E. Fernandez, C. Maestre, S. Moncada, J.P. Bolanos, The bioenergetic and antioxidant status of neurons is controlled by continuous degradation of a key glycolytic enzyme by APC/C-Cdh1, *Nature cell biology* 11(6) (2009) 747-52.
- [37] E. Lopez-Bayghen, A. Ortega, Glial glutamate transporters: new actors in brain signaling, *IUBMB life* 63(10) (2011) 816-23.
- [38] L. Pellerin, A.K. Bouzier-Sore, A. Aubert, S. Serres, M. Merle, R. Costalat, P.J. Magistretti, Activity-dependent regulation of energy metabolism by astrocytes: an update, *Glia* 55(12) (2007) 1251-62.
- [39] L. Pellerin, P.J. Magistretti, Glutamate uptake into astrocytes stimulates aerobic glycolysis: a mechanism coupling neuronal activity to glucose utilization, *Proceedings of the National Academy of Sciences of the United States of America* 91(22) (1994) 10625-10629.

- [40] L. Pellerin, P.J. Magistretti, Sweet sixteen for ANLS, *Journal of cerebral blood flow and metabolism : official journal of the International Society of Cerebral Blood Flow and Metabolism* 32(7) (2012) 1152-66.
- [41] L. Pellerin, G. Pellegrini, P.G. Bittar, Y. Charnay, C. Bouras, J.L. Martin, N. Stella, P.J. Magistretti, Evidence supporting the existence of an activity-dependent astrocyte-neuron lactate shuttle, *Developmental neuroscience* 20(4-5) (1998) 291-9.
- [42] I. Allaman, M. Bélanger, P.J. Magistretti, Astrocyte–neuron metabolic relationships: for better and for worse, *Trends in neurosciences* 34(2) (2011) 76-87.
- [43] M. Bélanger, I. Allaman, Pierre J. Magistretti, Brain Energy Metabolism: Focus on Astrocyte-Neuron Metabolic Cooperation, *Cell metabolism* 14(6) (2011) 724-738.
- [44] M. Belanger, P.J. Magistretti, The role of astroglia in neuroprotection, *Dialogues in clinical neuroscience* 11(3) (2009) 281-95.
- [45] P.J. Magistretti, I. Allaman, A cellular perspective on brain energy metabolism and functional imaging, *Neuron* 86(4) (2015) 883-901.
- [46] J. Chuquet, P. Quilichini, E.A. Nimchinsky, G. Buzsáki, Predominant enhancement of glucose uptake in astrocytes versus neurons during activation of the somatosensory cortex, *The Journal of neuroscience : the official journal of the Society for Neuroscience* 30(45) (2010) 15298-15303.
- [47] I. Lundgaard, B. Li, L. Xie, H. Kang, S. Sanggaard, J.D.R. Haswell, W. Sun, S. Goldman, S. Blekot, M. Nielsen, T. Takano, R. Deane, M. Nedergaard, Direct neuronal glucose uptake heralds activity-dependent increases in cerebral metabolism, *Nature communications* 6 (2015) 6807-6807.
- [48] C.M. Diaz-Garcia, R. Mongeon, C. Lahmann, D. Koveal, H. Zucker, G. Yellen, Neuronal Stimulation Triggers Neuronal Glycolysis and Not Lactate Uptake, *Cell metabolism* 26(2) (2017) 361-374.e4.

-
- [49] U. Wilhelmsson, E.A. Bushong, D.L. Price, B.L. Smarr, V. Phung, M. Terada, M.H. Ellisman, M. Pekny, Redefining the concept of reactive astrocytes as cells that remain within their unique domains upon reaction to injury, *Proc Natl Acad Sci U S A* 103(46) (2006) 17513-8.
- [50] R.R. Voskuhl, R.S. Peterson, B. Song, Y. Ao, L.B.J. Morales, S. Tiwari-Woodruff, M.V. Sofroniew, Reactive Astrocytes Form Scar-Like Perivascular Barriers to Leukocytes during Adaptive Immune Inflammation of the CNS, *The Journal of Neuroscience* 29(37) (2009) 11511-11522.
- [51] I.B. Wanner, M.A. Anderson, B. Song, J. Levine, A. Fernandez, Z. Gray-Thompson, Y. Ao, M.V. Sofroniew, Glial Scar Borders Are Formed by Newly Proliferated, Elongated Astrocytes That Interact to Corral Inflammatory and Fibrotic Cells via STAT3-Dependent Mechanisms after Spinal Cord Injury, *The Journal of Neuroscience* 33(31) (2013) 12870-12886.
- [52] M.A. Anderson, Y. Ao, M.V. Sofroniew, Heterogeneity of reactive astrocytes, *Neuroscience letters* 565 (2014) 23-29.
- [53] O.E. Tasdemir-Yilmaz, M.R. Freeman, Astrocytes engage unique molecular programs to engulf pruned neuronal debris from distinct subsets of neurons, *Genes & development* 28(1) (2014) 20-33.
- [54] W.-S. Chung, L.E. Clarke, G.X. Wang, B.K. Stafford, A. Sher, C. Chakraborty, J. Joung, L.C. Foo, A. Thompson, C. Chen, S.J. Smith, B.A. Barres, Astrocytes mediate synapse elimination through MEGF10 and MERTK pathways, *Nature* 504 (2013) 394.
- [55] M.A. Anderson, J.E. Burda, Y. Ren, Y. Ao, T.M. O'Shea, R. Kawaguchi, G. Coppola, B.S. Khakh, T.J. Deming, M.V. Sofroniew, Astrocyte scar formation aids central nervous system axon regeneration, *Nature* 532(7598) (2016) 195-200.
- [56] Y.M. Morizawa, Y. Hirayama, N. Ohno, S. Shibata, E. Shigetomi, Y. Sui, J. Nabekura, K. Sato, F. Okajima, H. Takebayashi, H. Okano, S. Koizumi, Reactive astrocytes function as

phagocytes after brain ischemia via ABCA1-mediated pathway, *Nature Communications* 8 (2017) 28.

[57] K. Kierdorf, M. Prinz, Factors regulating microglia activation, *Frontiers in Cellular Neuroscience* 7 (2013) 44.

[58] Y. Shinozaki, K. Shibata, K. Yoshida, E. Shigetomi, C. Gachet, K. Ikenaka, K.F. Tanaka, S. Koizumi, Transformation of Astrocytes to a Neuroprotective Phenotype by Microglia via P2Y1 Receptor Downregulation, *Cell reports* 19(6) (2017) 1151-1164.

[59] L. Mayo, S.A. Trauger, M. Blain, M. Nadeau, B. Patel, J.I. Alvarez, I.D. Mascalfroni, A. Yeste, P. Kivisakk, K. Kallas, B. Ellezam, R. Bakshi, A. Prat, J.P. Antel, H.L. Weiner, F.J. Quintana, Regulation of astrocyte activation by glycolipids drives chronic CNS inflammation, *Nature medicine* 20(10) (2014) 1147-56.

[60] L. Mayo, S.A. Trauger, M. Blain, M. Nadeau, B. Patel, J.I. Alvarez, I.D. Mascalfroni, A. Yeste, P. Kivisäkk, K. Kallas, B. Ellezam, R. Bakshi, A. Prat, J.P. Antel, H.L. Weiner, F.J. Quintana, B4GALT6 regulates astrocyte activation during CNS inflammation, *Nature medicine* 20(10) (2014) 1147-1156.

[61] M. He, H. Dong, Y. Huang, S. Lu, S. Zhang, Y. Qian, W. Jin, Astrocyte-Derived CCL2 is Associated with M1 Activation and Recruitment of Cultured Microglial Cells, *Cellular Physiology and Biochemistry* 38(3) (2016) 859-870.

[62] M. Marella, J. Chabry, Neurons and Astrocytes Respond to Prion Infection by Inducing Microglia Recruitment, *The Journal of Neuroscience* 24(3) (2004) 620-627.

[63] S.A. Liddelow, K.A. Guttenplan, L.E. Clarke, F.C. Bennett, C.J. Bohlen, L. Schirmer, M.L. Bennett, A.E. Münch, W.-S. Chung, T.C. Peterson, D.K. Wilton, A. Frouin, B.A. Napier, N. Panicker, M. Kumar, M.S. Buckwalter, D.H. Rowitch, V.L. Dawson, T.M. Dawson, B. Stevens, B.A. Barres, Neurotoxic reactive astrocytes are induced by activated microglia, *Nature* 541 (2017) 481.

- [64] H. Phatnani, T. Maniatis, Astrocytes in neurodegenerative disease, Cold Spring Harbor perspectives in biology 7(6) (2015).
- [65] B. Wagner, A. Natarajan, S. Grünaug, R. Kroismayr, E.F. Wagner, M. Sibilica, Neuronal survival depends on EGFR signaling in cortical but not midbrain astrocytes, The EMBO journal 25(4) (2006) 752-762.
- [66] A.A. Sosunov, G.M. McKhann, J.E. Goldman, The origin of Rosenthal fibers and their contributions to astrocyte pathology in Alexander disease, Acta neuropathologica communications 5 (2017) 27.
- [67] A.A. Sosunov, E. Guilfoyle, X. Wu, G.M. McKhann, J.E. Goldman, Phenotypic Conversions of “Protoplasmic” to “Reactive” Astrocytes in Alexander Disease, The Journal of neuroscience : the official journal of the Society for Neuroscience 33(17) (2013) 7439-7450.
- [68] U. Gomez-Pinedo, M. Duran-Moreno, S. Sirerol-Piquer, J. Matias-Guiu, Myelin changes in Alexander disease, Neurologia (Barcelona, Spain) (2017).
- [69] L. Wang, T.L. Hagemann, H. Kalwa, T. Michel, A. Messing, M.B. Feany, Nitric oxide mediates glial-induced neurodegeneration in Alexander disease, Nature Communications 6 (2015) 8966.
- [70] G.H. Lee, Hepatic encephalopathy in acute-on-chronic liver failure, Hepatology international 9(4) (2015) 520-6.
- [71] R.G. Nagele, J. Wegiel, V. Venkataraman, H. Imaki, K.C. Wang, J. Wegiel, Contribution of glial cells to the development of amyloid plaques in Alzheimer's disease, Neurobiology of aging 25(5) (2004) 663-74.
- [72] R.G. Nagele, M.R. D'Andrea, H. Lee, V. Venkataraman, H.Y. Wang, Astrocytes accumulate A beta 42 and give rise to astrocytic amyloid plaques in Alzheimer disease brains, Brain research 971(2) (2003) 197-209.

- [73] J.E. Simpson, P.G. Ince, G. Lace, G. Forster, P.J. Shaw, F. Matthews, G. Savva, C. Brayne, S.B. Wharton, Astrocyte phenotype in relation to Alzheimer-type pathology in the ageing brain, *Neurobiology of aging* 31(4) (2010) 578-90.
- [74] R. Pihlaja, J. Koistinaho, T. Malm, H. Sikkilä, S. Vainio, M. Koistinaho, Transplanted astrocytes internalize deposited beta-amyloid peptides in a transgenic mouse model of Alzheimer's disease, *Glia* 56(2) (2008) 154-63.
- [75] R. Pihlaja, J. Koistinaho, R. Kauppinen, J. Sandholm, H. Tanila, M. Koistinaho, Multiple cellular and molecular mechanisms are involved in human Aβ clearance by transplanted adult astrocytes, *Glia* 59(11) (2011) 1643-57.
- [76] J.I. Nagy, W. Li, E.L. Hertzberg, C.A. Marotta, Elevated connexin43 immunoreactivity at sites of amyloid plaques in Alzheimer's disease, *Brain research* 717(1-2) (1996) 173-8.
- [77] X. Mei, P. Ezan, C. Giaume, A. Koulakoff, Astroglial connexin immunoreactivity is specifically altered at Aβ plaques in Aβ precursor protein/presenilin1 mice, 2010.
- [78] H. Takeuchi, H. Mizoguchi, Y. Doi, S. Jin, M. Noda, J. Liang, H. Li, Y. Zhou, R. Mori, S. Yasuoka, E. Li, B. Parajuli, J. Kawanokuchi, Y. Sonobe, J. Sato, K. Yamanaka, G. Sobue, T. Mizuno, A. Suzumura, Blockade of gap junction hemichannel suppresses disease progression in mouse models of amyotrophic lateral sclerosis and Alzheimer's disease, *PLoS One* 6(6) (2011) e21108.
- [79] J.Y. Shin, Z.H. Fang, Z.X. Yu, C.E. Wang, S.H. Li, X.J. Li, Expression of mutant huntingtin in glial cells contributes to neuronal excitotoxicity, *The Journal of cell biology* 171(6) (2005) 1001-12.
- [80] X. Tong, Y. Ao, G.C. Faas, S.E. Nwaobi, J. Xu, M.D. Hausteiner, M.A. Anderson, I. Mody, M.L. Olsen, M.V. Sofroniew, B.S. Khakh, Astrocyte Kir4.1 ion channel deficits contribute to neuronal dysfunction in Huntington's disease model mice, *Nature neuroscience* 17(5) (2014) 694-703.

- [81] J. Bradford, J.-Y. Shin, M. Roberts, C.-E. Wang, X.-J. Li, S. Li, Expression of mutant huntingtin in mouse brain astrocytes causes age-dependent neurological symptoms, *Proceedings of the National Academy of Sciences* 106(52) (2009) 22480-22485.
- [82] J. Bradford, J.Y. Shin, M. Roberts, C.E. Wang, G. Sheng, S. Li, X.J. Li, Mutant huntingtin in glial cells exacerbates neurological symptoms of Huntington disease mice, *The Journal of biological chemistry* 285(14) (2010) 10653-61.
- [83] H.J. Lee, J.E. Suk, C. Patrick, E.J. Bae, J.H. Cho, S. Rho, D. Hwang, E. Masliah, S.J. Lee, Direct transfer of alpha-synuclein from neuron to astroglia causes inflammatory responses in synucleinopathies, *The Journal of biological chemistry* 285(12) (2010) 9262-72.
- [84] Y.J. Song, G.M. Halliday, J.L. Holton, T. Lashley, S.S. O'Sullivan, H. McCann, A.J. Lees, T. Ozawa, D.R. Williams, P.J. Lockhart, T.R. Revesz, Degeneration in different parkinsonian syndromes relates to astrocyte type and astrocyte protein expression, *J Neuropathol Exp Neurol* 68(10) (2009) 1073-83.
- [85] X.-L. Gu, C.-X. Long, L. Sun, C. Xie, X. Lin, H. Cai, Astrocytic expression of Parkinson's disease-related A53T α -synuclein causes neurodegeneration in mice, *Molecular Brain* 3(1) (2010) 1-16.
- [86] A. Pramatarova, J. Laganier, J. Roussel, K. Brisebois, G.A. Rouleau, Neuron-specific expression of mutant superoxide dismutase 1 in transgenic mice does not lead to motor impairment, *The Journal of neuroscience : the official journal of the Society for Neuroscience* 21(10) (2001) 3369-74.
- [87] S. Boillee, C. Vande Velde, D.W. Cleveland, ALS: a disease of motor neurons and their nonneuronal neighbors, *Neuron* 52(1) (2006) 39-59.
- [88] D. Jaarsma, E. Teuling, E.D. Haasdijk, C.I. De Zeeuw, C.C. Hoogenraad, Neuron-Specific Expression of Mutant Superoxide Dismutase Is Sufficient to Induce Amyotrophic Lateral Sclerosis in Transgenic Mice, *The Journal of Neuroscience* 28(9) (2008) 2075-2088.

-
- [89] A.M. Clement, M.D. Nguyen, E.A. Roberts, M.L. Garcia, S. Boillée, M. Rule, A.P. McMahon, W. Doucette, D. Siwek, R.J. Ferrante, R.H. Brown, J.-P. Julien, L.S.B. Goldstein, D.W. Cleveland, Wild-Type Nonneuronal Cells Extend Survival of SOD1 Mutant Motor Neurons in ALS Mice, *Science (New York, N.Y.)* 302(5642) (2003) 113-117.
- [90] E. Dossi, F. Vasile, N. Rouach, Human astrocytes in the diseased brain, *Brain Research Bulletin* 136 (2018) 139-156.
- [91] I.E. Wallin, *Symbioticism and the origin of species*, Williams & Wilkins Company, Baltimore :, 1927.
- [92] A.M. Poole, S. Gribaldo, Eukaryotic Origins: How and When Was the Mitochondrion Acquired?, *Cold Spring Harbor perspectives in biology* 6(12) (2014) a015990.
- [93] A. Karnkowska, V. Vacek, Z. Zubáčová, S.C. Treitli, R. Petrželková, L. Eme, L. Novák, V. Žárský, L.D. Barlow, E.K. Herman, P. Soukal, M. Hroudová, P. Doležal, C.W. Stairs, A.J. Roger, M. Eliáš, J.B. Dacks, Č. Vlček, V. Hampl, A Eukaryote without a Mitochondrial Organelle, *Current Biology* 26(10) (2016) 1274-1284.
- [94] F.N. Low, MITOCHONDRIAL STRUCTURE, *The Journal of Biophysical and Biochemical Cytology* 2(4) (1956) 337-340.
- [95] C. Frezza, S. Cipolat, O. Martins de Brito, M. Micaroni, G.V. Beznoussenko, T. Rudka, D. Bartoli, R.S. Polishuck, N.N. Danial, B. De Strooper, L. Scorrano, OPA1 controls apoptotic cristae remodeling independently from mitochondrial fusion, *Cell* 126(1) (2006) 177-89.
- [96] S. Hoppins, S.R. Collins, A. Cassidy-Stone, E. Hummel, R.M. Devay, L.L. Lackner, B. Westermann, M. Schuldiner, J.S. Weissman, J. Nunnari, A mitochondrial-focused genetic interaction map reveals a scaffold-like complex required for inner membrane organization in mitochondria, *The Journal of cell biology* 195(2) (2011) 323-40.
- [97] C. Glytsou, E. Calvo, S. Cogliati, A. Mehrotra, I. Anastasia, G. Rigoni, A. Raimondi, N. Shintani, M. Loureiro, J. Vazquez, L. Pellegrini, J.A. Enriquez, L. Scorrano, M.E. Soriano,

Optic Atrophy 1 Is Epistatic to the Core MICOS Component MIC60 in Mitochondrial Cristae Shape Control, *Cell reports* 17(11) (2016) 3024-3034.

[98] J.R. Friedman, J. Nunnari, Mitochondrial form and function, *Nature* 505 (2014) 335.

[99] D. De Stefani, M. Patron, R. Rizzuto, Structure and function of the mitochondrial calcium uniporter complex, *Biochimica et Biophysica Acta (BBA) - Molecular Cell Research* 1853(9) (2015) 2006-2011.

[100] T. Finkel, S. Menazza, K.M. Holmstrom, R.J. Parks, J. Liu, J. Sun, J. Liu, X. Pan, E. Murphy, The ins and outs of mitochondrial calcium, *Circulation research* 116(11) (2015) 1810-9.

[101] R. Covian, S. French, H. Kusnetz, R.S. Balaban, Stimulation of oxidative phosphorylation by calcium in cardiac mitochondria is not influenced by cAMP and PKA activity, *Biochimica et biophysica acta* 1837(12) (2014) 1913-1921.

[102] M.R. Duchen, Mitochondria, calcium-dependent neuronal death and neurodegenerative disease, *Pflugers Archiv* 464(1) (2012) 111-121.

[103] B. Pardo, L. Contreras, A. Serrano, M. Ramos, K. Kobayashi, M. Iijima, T. Saheki, J. Satrustegui, Essential role of aralar in the transduction of small Ca²⁺ signals to neuronal mitochondria, *The Journal of biological chemistry* 281(2) (2006) 1039-47.

[104] E. Boitier, R. Rea, M.R. Duchen, Mitochondria exert a negative feedback on the propagation of intracellular Ca²⁺ waves in rat cortical astrocytes, *The Journal of cell biology* 145(4) (1999) 795-808.

[105] H. Vakifahmetoglu-Norberg, A.T. Ouchida, E. Norberg, The role of mitochondria in metabolism and cell death, *Biochemical and Biophysical Research Communications* 482(3) (2017) 426-431.

[106] D. Green, G. Kroemer, The central executioners of apoptosis: caspases or mitochondria?, *Trends in cell biology* 8(7) (1998) 267-71.

- [107] Z. Hao, G.S. Duncan, C.C. Chang, A. Elia, M. Fang, A. Wakeham, H. Okada, T. Calzascia, Y. Jang, A. You-Ten, W.C. Yeh, P. Ohashi, X. Wang, T.W. Mak, Specific ablation of the apoptotic functions of cytochrome C reveals a differential requirement for cytochrome C and Apaf-1 in apoptosis, *Cell* 121(4) (2005) 579-591.
- [108] S.Y.a. Proskuryakov, A.G. Konoplyannikov, V.L. Gabai, Necrosis: a specific form of programmed cell death?, *Experimental cell research* 283(1) (2003) 1-16.
- [109] D.E. Christofferson, J. Yuan, Necroptosis as an alternative form of programmed cell death, *Current opinion in cell biology* 22(2) (2010) 263-8.
- [110] D. Roise, S.J. Horvath, J.M. Tomich, J.H. Richards, G. Schatz, A chemically synthesized pre-sequence of an imported mitochondrial protein can form an amphiphilic helix and perturb natural and artificial phospholipid bilayers, *The EMBO journal* 5(6) (1986) 1327-34.
- [111] N. Pfanner, Protein sorting: recognizing mitochondrial presequences, *Current biology : CB* 10(11) (2000) R412-5.
- [112] J.C. Young, N.J. Hoogenraad, F.U. Hartl, Molecular chaperones Hsp90 and Hsp70 deliver preproteins to the mitochondrial import receptor Tom70, *Cell* 112(1) (2003) 41-50.
- [113] S. Franco-Iborra, M. Vila, C. Perier, Mitochondrial Quality Control in Neurodegenerative Diseases: Focus on Parkinson's Disease and Huntington's Disease, *Front Neurosci* 12 (2018) 342.
- [114] E.I. Rugarli, T. Langer, Mitochondrial quality control: a matter of life and death for neurons, *The EMBO journal* 31(6) (2012) 1336-49.
- [115] P.M. Quiros, T. Langer, C. Lopez-Otin, New roles for mitochondrial proteases in health, ageing and disease, *Nature reviews. Molecular cell biology* 16(6) (2015) 345-59.
- [116] R. Anand, T. Wai, M.J. Baker, N. Kladt, A.C. Schauss, E. Rugarli, T. Langer, The i-AAA protease YME1L and OMA1 cleave OPA1 to balance mitochondrial fusion and fission, *The Journal of cell biology* 204(6) (2014) 919-29.

-
- [117] F. Consolato, F. Maltecca, S. Tulli, I. Sambri, G. Casari, *m*-AAA and *i*-AAA complexes work coordinately regulating OMA1, the stress-activated supervisor of mitochondrial dynamics, *Journal of Cell Science* (2018).
- [118] S. Ehses, I. Raschke, G. Mancuso, A. Bernacchia, S. Geimer, D. Tondera, J.C. Martinou, B. Westermann, E.I. Rugarli, T. Langer, Regulation of OPA1 processing and mitochondrial fusion by m-AAA protease isoenzymes and OMA1, *The Journal of cell biology* 187(7) (2009) 1023-36.
- [119] F. Gerdes, T. Tatsuta, T. Langer, Mitochondrial AAA proteases--towards a molecular understanding of membrane-bound proteolytic machines, *Biochimica et biophysica acta* 1823(1) (2012) 49-55.
- [120] C.M. Haynes, K. Petrova, C. Benedetti, Y. Yang, D. Ron, ClpP mediates activation of a mitochondrial unfolded protein response in *C. elegans*, *Developmental cell* 13(4) (2007) 467-80.
- [121] C.M. Haynes, D. Ron, The mitochondrial UPR – protecting organelle protein homeostasis, *Journal of Cell Science* 123(22) (2010) 3849-3855.
- [122] M. Koppen, M.D. Metodiev, G. Casari, E.I. Rugarli, T. Langer, Variable and tissue-specific subunit composition of mitochondrial m-AAA protease complexes linked to hereditary spastic paraplegia, *Molecular and cellular biology* 27(2) (2007) 758-67.
- [123] L. Atorino, L. Silvestri, M. Koppen, L. Cassina, A. Ballabio, R. Marconi, T. Langer, G. Casari, Loss of m-AAA protease in mitochondria causes complex I deficiency and increased sensitivity to oxidative stress in hereditary spastic paraplegia, *The Journal of cell biology* 163(4) (2003) 777-87.
- [124] G. Kremmidiotis, A.E. Gardner, C. Settasatian, A. Savoia, G.R. Sutherland, D.F. Callen, Molecular and functional analyses of the human and mouse genes encoding AFG3L1, a mitochondrial metalloprotease homologous to the human spastic paraplegia protein, *Genomics* 76(1-3) (2001) 58-65.

- [125] K. N Truscott, B. R Lowth, P. R Strack, D. Dougan, Diverse functions of mitochondrial AAA+ proteins: Protein activation, disaggregation, and degradation, 2010.
- [126] S. Lee, S. Augustin, T. Tatsuta, F. Gerdes, T. Langer, F.T. Tsai, Electron cryomicroscopy structure of a membrane-anchored mitochondrial AAA protease, *The Journal of biological chemistry* 286(6) (2011) 4404-11.
- [127] D. Korbel, S. Wurth, M. Kaser, T. Langer, Membrane protein turnover by the m-AAA protease in mitochondria depends on the transmembrane domains of its subunits, *EMBO reports* 5(7) (2004) 698-703.
- [128] H. Shi, A.J. Rampello, S.E. Glynn, Engineered AAA+ proteases reveal principles of proteolysis at the mitochondrial inner membrane, *Nat Commun* 7 (2016) 13301.
- [129] K. Leonhard, B. Guiard, G. Pellicchia, A. Tzagoloff, W. Neupert, T. Langer, Membrane protein degradation by AAA proteases in mitochondria: extraction of substrates from either membrane surface, *Mol Cell* 5(4) (2000) 629-38.
- [130] C. Merkwirth, T. Langer, Prohibitin function within mitochondria: essential roles for cell proliferation and cristae morphogenesis, *Biochimica et biophysica acta* 1793(1) (2009) 27-32.
- [131] C. Merkwirth, S. Dargazanli, T. Tatsuta, S. Geimer, B. Lower, F.T. Wunderlich, J.C. von Kleist-Retzow, A. Waisman, B. Westermann, T. Langer, Prohibitins control cell proliferation and apoptosis by regulating OPA1-dependent cristae morphogenesis in mitochondria, *Genes & development* 22(4) (2008) 476-88.
- [132] G. Steglich, W. Neupert, T. Langer, Prohibitins Regulate Membrane Protein Degradation by the m-AAA Protease in Mitochondria, *Molecular and cellular biology* 19(5) (1999) 3435-3442.
- [133] P. Martinelli, E.I. Rugarli, Emerging roles of mitochondrial proteases in neurodegeneration, *Biochimica et biophysica acta* 1797(1) (2010) 1-10.
- [134] S.E. Glynn, Multifunctional Mitochondrial AAA Proteases, *Frontiers in Molecular Biosciences* 4(34) (2017).

- [135] L. Stiburek, J. Cesnekova, O. Kostkova, D. Fornuskova, K. Vinsova, L. Wenchich, J. Houstek, J. Zeman, YME1L controls the accumulation of respiratory chain subunits and is required for apoptotic resistance, cristae morphogenesis, and cell proliferation, *Molecular biology of the cell* 23(6) (2012) 1010-23.
- [136] E. Guélin, M. Rep, L.A. Grivell, Afg3p, a mitochondrial ATP-dependent metalloprotease, is involved in degradation of mitochondrially-encoded Cox1, Cox3, Cob, Su6, Su8 and Su9 subunits of the inner membrane complexes III, IV and V, *FEBS Letters* 381(1) (1996) 42-46.
- [137] H. Arlt, R. Tauer, H. Feldmann, W. Neupert, T. Langer, The YTA10-12 complex, an AAA protease with chaperone-like activity in the inner membrane of mitochondria, *Cell* 85(6) (1996) 875-85.
- [138] T. König, S.E. Troder, K. Bakka, A. Korwitz, R. Richter-Dennerlein, P.A. Lampe, M. Patron, M. Muhlmeister, S. Guerrero-Castillo, U. Brandt, T. Decker, I. Lauria, A. Paggio, R. Rizzuto, E.I. Rugarli, D. De Stefani, T. Langer, The m-AAA Protease Associated with Neurodegeneration Limits MCU Activity in Mitochondria, *Mol Cell* 64(1) (2016) 148-162.
- [139] M. Patron, H.G. Sprenger, T. Langer, m-AAA proteases, mitochondrial calcium homeostasis and neurodegeneration, *Cell research* (2018).
- [140] F. Bonn, T. Tatsuta, C. Petrunaro, J. Riemer, T. Langer, Presequence-dependent folding ensures MrpL32 processing by the m-AAA protease in mitochondria, *The EMBO journal* 30(13) (2011) 2545-56.
- [141] K. Esser, B. Tursun, M. Ingenhoven, G. Michaelis, E. Pratje, A Novel Two-step Mechanism for Removal of a Mitochondrial Signal Sequence Involves the mAAA Complex and the Putative Rhomboid Protease Pcp1, 2002.
- [142] T. Tatsuta, S. Augustin, M. Nolden, B. Friedrichs, T. Langer, m-AAA protease-driven membrane dislocation allows intramembrane cleavage by rhomboid in mitochondria, *The EMBO journal* 26(2) (2007) 325-335.

-
- [143] I.E. Suppanz, C.A. Wurm, D. Wenzel, S. Jakobs, J.M. Shaw, The m-AAA Protease Processes Cytochrome c Peroxidase Preferentially at the Inner Boundary Membrane of Mitochondria, *Molecular biology of the cell* 20(2) (2009) 572-580.
- [144] S. Duvezin-Caubet, M. Koppen, J. Wagener, M. Zick, L. Israel, A. Bernacchia, R. Jagasia, E.I. Rugarli, A. Imhof, W. Neupert, T. Langer, A.S. Reichert, OPA1 Processing Reconstituted in Yeast Depends on the Subunit Composition of the m-AAA Protease in Mitochondria, *Molecular biology of the cell* 18(9) (2007) 3582-3590.
- [145] M. Koppen, F. Bonn, S. Ehses, T. Langer, Autocatalytic processing of m-AAA protease subunits in mitochondria, *Molecular biology of the cell* 20(19) (2009) 4216-4224.
- [146] H. Arlt, G. Steglich, R. Perryman, B. Guiard, W. Neupert, T. Langer, The formation of respiratory chain complexes in mitochondria is under the proteolytic control of the m-AAA protease, *The EMBO journal* 17(16) (1998) 4837-47.
- [147] N. Chrestian, N. Dupré, Z. Gan-Or, A. Szuto, S. Chen, A. Venkitachalam, J.-D. Brisson, J. Warman-Chardon, S. Ahmed, S. Ashtiani, H. MacDonald, N. Mohsin, K. Mourabit-Amari, P. Provencher, K.M. Boycott, D.J. Stavropoulos, P.A. Dion, P.N. Ray, O. Suchowersky, G.A. Rouleau, G. Yoon, Clinical and genetic study of hereditary spastic paraplegia in Canada, *Neurology: Genetics* 3(1) (2017) e122.
- [148] K.R. Denton, C. Xu, H. Shah, X.-J. Li, Modeling axonal defects in hereditary spastic paraplegia with human pluripotent stem cells, *Frontiers in Biology* 11(5) (2016) 339-354.
- [149] G. Casari, M. De Fusco, S. Ciarmatori, M. Zeviani, M. Mora, P. Fernandez, G. De Michele, A. Filla, S. Coccozza, R. Marconi, A. Dürr, B. Fontaine, A. Ballabio, Spastic Paraplegia and OXPHOS Impairment Caused by Mutations in Paraplegin, a Nuclear-Encoded Mitochondrial Metalloprotease, *Cell* 93(6) (1998) 973-983.
- [150] F. Brugman, H. Scheffer, J.H. Wokke, W.M. Nillesen, M. de Visser, E. Aronica, J.H. Veldink, L.H. van den Berg, Paraplegin mutations in sporadic adult-onset upper motor neuron syndromes, *Neurology* 71(19) (2008) 1500-5.

-
- [151] P. Martinelli, V. La Mattina, A. Bernacchia, R. Magnoni, F. Cerri, G. Cox, A. Quattrini, G. Casari, E.I. Rugarli, Genetic interaction between the m⁻AAA protease isoenzymes reveals novel roles in cerebellar degeneration, *Human molecular genetics* 18(11) (2009) 2001-2013.
- [152] F. Ferreira, A. Quattrini, M. Pirozzi, V. Valsecchi, G. Dina, V. Broccoli, A. Auricchio, F. Piemonte, G. Tozzi, L. Gaeta, G. Casari, A. Ballabio, E.I. Rugarli, Axonal degeneration in paraplegin-deficient mice is associated with abnormal mitochondria and impairment of axonal transport, *Journal of Clinical Investigation* 113(2) (2004) 231-242.
- [153] G. Mancuso, E. Barth, P. Crivello, E.I. Rugarli, Alternative splicing of *Spg7*, a gene involved in hereditary spastic paraplegia, encodes a variant of paraplegin targeted to the endoplasmic reticulum, *PLoS One* 7(5) (2012) e36337.
- [154] S. Shanmughapriya, S. Rajan, N.E. Hoffman, A.M. Higgins, D. Tomar, N. Nemani, K.J. Hines, D.J. Smith, A. Eguchi, S. Vallem, F. Shaikh, M. Cheung, N.J. Leonard, R.S. Stolakis, M.P. Wolfers, J. Ibetti, J.K. Chuprun, N.R. Jog, S.R. Houser, W.J. Koch, J.W. Elrod, M. Madesh, SPG7 is an Essential and Conserved Component of the Mitochondrial Permeability Transition Pore, *Molecular cell* 60(1) (2015) 47-62.
- [155] C. Cagnoli, C. Mariotti, F. Taroni, M. Seri, A. Brussino, C. Michielotto, M. Grisoli, D. Di Bella, N. Migone, C. Gellera, S. Di Donato, A. Brusco, SCA28, a novel form of autosomal dominant cerebellar ataxia on chromosome 18p11.22–q11.2, *Brain : a journal of neurology* 129(1) (2006) 235-242.
- [156] C. Cagnoli, G. Stevanin, A. Brussino, M. Barberis, C. Mancini, R.L. Margolis, S.E. Holmes, M. Nobili, S. Forlani, S. Padovan, P. Pappi, C. Zaros, I. Leber, P. Ribai, L. Pugliese, C. Assalto, A. Brice, N. Migone, A. Durr, A. Brusco, Missense mutations in the AFG3L2 proteolytic domain account for approximately 1.5% of European autosomal dominant cerebellar ataxias, *Human mutation* 31(10) (2010) 1117-24.
- [157] D. Di Bella, F. Lazzaro, A. Brusco, M. Plumari, G. Battaglia, A. Pastore, A. Finardi, C. Cagnoli, F. Tempia, M. Frontali, L. Veneziano, T. Sacco, E. Boda, A. Brussino, F. Bonn, B.

Castellotti, S. Baratta, C. Mariotti, C. Gellera, V. Fracasso, S. Magri, T. Langer, P. Plevani, S. Di Donato, M. Muzi-Falconi, F. Taroni, Mutations in the mitochondrial protease gene AFG3L2 cause dominant hereditary ataxia SCA28, *Nature genetics* 42(4) (2010) 313-21.

[158] T.M. Pierson, D. Adams, F. Bonn, P. Martinelli, P.F. Cherukuri, J.K. Teer, N.F. Hansen, P. Cruz, J.C. Mullikin For The Nisc Comparative Sequencing Program, R.W. Blakesley, G. Golas, J. Kwan, A. Sandler, K. Fuentes Fajardo, T. Markello, C. Tiffit, C. Blackstone, E.I. Rugarli, T. Langer, W.A. Gahl, C. Toro, Whole-exome sequencing identifies homozygous AFG3L2 mutations in a spastic ataxia-neuropathy syndrome linked to mitochondrial m-AAA proteases, *PLoS genetics* 7(10) (2011) e1002325.

[159] M. Muona, S.F. Berkovic, L.M. Dibbens, K.L. Oliver, S. Maljevic, M.A. Bayly, T. Joensuu, L. Canafoglia, S. Franceschetti, R. Michelucci, S. Markkinen, S.E. Heron, M.S. Hildebrand, E. Andermann, F. Andermann, A. Gambardella, P. Tinuper, L. Licchetta, I.E. Scheffer, C. Criscuolo, A. Filla, E. Ferlazzo, J. Ahmad, A. Ahmad, B. Baykan, E. Said, M. Topcu, P. Riguzzi, M.D. King, C. Ozkara, D.M. Andrade, B.A. Engelsens, A. Crespel, M. Lindenau, E. Lohmann, V. Saletti, J. Massano, M. Privitera, A.J. Espay, B. Kauffmann, M. Duchowny, R.S. Møller, R. Straussberg, Z. Afawi, B. Ben-Zeev, K.E. Samocha, M.J. Daly, S. Petrou, H. Lerche, A. Palotie, A.-E. Lehesjoki, A recurrent de novo mutation in KCNC1 causes progressive myoclonus epilepsy, *Nature genetics* 47 (2014) 39.

[160] C. Cagnoli, C. Mariotti, F. Taroni, M. Seri, A. Brussino, C. Michielotto, M. Grisoli, D. Di Bella, N. Migone, C. Gellera, S. Di Donato, A. Brusco, SCA28, a novel form of autosomal dominant cerebellar ataxia on chromosome 18p11.22-q11.2, *Brain : a journal of neurology* 129(Pt 1) (2006) 235-42.

[161] C. Mariotti, A. Brusco, D. Di Bella, C. Cagnoli, M. Seri, C. Gellera, S. Di Donato, F. Taroni, Spinocerebellar ataxia type 28: A novel autosomal dominant cerebellar ataxia characterized by slow progression and ophthalmoparesis, *The Cerebellum* 7(2) (2008) 184-188.

-
- [162] U. Edener, J. Wollner, U. Hehr, Z. Kohl, S. Schilling, F. Kreuz, P. Bauer, V. Bernard, G. Gillessen-Kaesbach, C. Zuhlke, Early onset and slow progression of SCA28, a rare dominant ataxia in a large four-generation family with a novel AFG3L2 mutation, *European journal of human genetics* : EJHG 18(8) (2010) 965-8.
- [163] A.M. Lobbe, J.S. Kang, R. Hilker, H. Hackstein, U. Muller, D. Nolte, A novel missense mutation in AFG3L2 associated with late onset and slow progression of spinocerebellar ataxia type 28, *Journal of molecular neuroscience* : MN 52(4) (2014) 493-6.
- [164] F. Maltecca, A. Aghaie, D.G. Schroeder, L. Cassina, B.A. Taylor, S.J. Phillips, M. Malaguti, S. Previtali, J.L. Guenet, A. Quattrini, G.A. Cox, G. Casari, The mitochondrial protease AFG3L2 is essential for axonal development, *The Journal of neuroscience : the official journal of the Society for Neuroscience* 28(11) (2008) 2827-36.
- [165] E.R. Almajan, R. Richter, L. Paeger, P. Martinelli, E. Barth, T. Decker, N.G. Larsson, P. Kloppenburg, T. Langer, E.I. Rugarli, AFG3L2 supports mitochondrial protein synthesis and Purkinje cell survival, *The Journal of clinical investigation* 122(11) (2012) 4048-58.
- [166] A.K. Kondadi, S. Wang, S. Montagner, N. Kladt, A. Korwitz, P. Martinelli, D. Herholz, M.J. Baker, A.C. Schauss, T. Langer, E.I. Rugarli, Loss of the m-AAA protease subunit AFG3L2 causes mitochondrial transport defects and tau hyperphosphorylation, *The EMBO journal* 33(9) (2014) 1011-1026.
- [167] S. Wang, J. Jacquemyn, S. Murru, P. Martinelli, E. Barth, T. Langer, C.M. Niessen, E.I. Rugarli, The Mitochondrial m-AAA Protease Prevents Demyelination and Hair Greying, *PLoS genetics* 12(12) (2016) e1006463.
- [168] F. Maltecca, R. Magnoni, F. Cerri, G.A. Cox, A. Quattrini, G. Casari, Haploinsufficiency of AFG3L2, the gene responsible for spinocerebellar ataxia type 28, causes mitochondria-mediated Purkinje cell dark degeneration, *The Journal of neuroscience : the official journal of the Society for Neuroscience* 29(29) (2009) 9244-54.

-
- [169] F. Maltecca, D. De Stefani, L. Cassina, F. Consolato, M. Wasilewski, L. Scorrano, R. Rizzuto, G. Casari, Respiratory dysfunction by AFG3L2 deficiency causes decreased mitochondrial calcium uptake via organellar network fragmentation, *Human molecular genetics* 21(17) (2012) 3858-3870.
- [170] F. Maltecca, E. Baseggio, F. Consolato, D. Mazza, P. Podini, S.M. Young, Jr., I. Drago, B.A. Bahr, A. Puliti, F. Codazzi, A. Quattrini, G. Casari, Purkinje neuron Ca²⁺ influx reduction rescues ataxia in SCA28 model, *The Journal of clinical investigation* 125(1) (2015) 263-74.
- [171] P. Barenberg, H. Strahlendorf, J. Strahlendorf, Hypoxia induces an excitotoxic-type of dark cell degeneration in cerebellar Purkinje neurons, *Neuroscience Research* 40(3) (2001) 245-254.
- [172] N.A. Oberheim, T. Takano, X. Han, W. He, J.H. Lin, F. Wang, Q. Xu, J.D. Wyatt, W. Pilcher, J.G. Ojemann, B.R. Ransom, S.A. Goldman, M. Nedergaard, Uniquely hominid features of adult human astrocytes, *The Journal of neuroscience : the official journal of the Society for Neuroscience* 29(10) (2009) 3276-87.
- [173] J.G. Jackson, M.B. Robinson, Regulation of mitochondrial dynamics in astrocytes: Mechanisms, consequences, and unknowns, *Glia* 66(6) (2018) 1213-1234.
- [174] E. Motori, J. Puyal, N. Toni, A. Ghanem, C. Angeloni, M. Malaguti, G. Cantelli-Forti, B. Berninger, K.K. Conzelmann, M. Gotz, K.F. Winklhofer, S. Hrelia, M. Bergami, Inflammation-induced alteration of astrocyte mitochondrial dynamics requires autophagy for mitochondrial network maintenance, *Cell metabolism* 18(6) (2013) 844-59.
- [175] J. Gobel, E. Motori, M. Bergami, Spatiotemporal control of mitochondrial network dynamics in astroglial cells, *Biochem Biophys Res Commun* 500(1) (2018) 17-25.
- [176] Y. Zhang, K. Chen, S.A. Sloan, M.L. Bennett, A.R. Scholze, S. O'Keefe, H.P. Phatnani, P. Guarnieri, C. Caneda, N. Ruderisch, S. Deng, S.A. Liddelow, C. Zhang, R. Daneman, T. Maniatis, B.A. Barres, J.Q. Wu, An RNA-sequencing transcriptome and splicing database of

glia, neurons, and vascular cells of the cerebral cortex, *The Journal of neuroscience : the official journal of the Society for Neuroscience* 34(36) (2014) 11929-47.

[177] N.D. Halim, T. McFate, A. Mohyeldin, P. Okagaki, L.G. Korotchkina, M.S. Patel, N.H. Jeoung, R.A. Harris, M.J. Schell, A. Verma, Phosphorylation status of pyruvate dehydrogenase distinguishes metabolic phenotypes of cultured rat brain astrocytes and neurons, *Glia* 58(10) (2010) 1168-76.

[178] J.G. Jackson, M.B. Robinson, Reciprocal Regulation of Mitochondrial Dynamics and Calcium Signaling in Astrocyte Processes, *The Journal of neuroscience : the official journal of the Society for Neuroscience* 35(45) (2015) 15199-213.

[179] J.C. O'Donnell, J.G. Jackson, M.B. Robinson, Transient Oxygen/Glucose Deprivation Causes a Delayed Loss of Mitochondria and Increases Spontaneous Calcium Signaling in Astrocytic Processes, *The Journal of neuroscience : the official journal of the Society for Neuroscience* 36(27) (2016) 7109-27.

[180] I. Llorente-Folch, C.B. Rueda, B. Pardo, G. Szabadkai, M.R. Duchen, J. Satrustegui, The regulation of neuronal mitochondrial metabolism by calcium, *J Physiol* 593(16) (2015) 3447-62.

[181] J.G. Jackson, J.C. O'Donnell, H. Takano, D.A. Coulter, M.B. Robinson, Neuronal Activity and Glutamate Uptake Decrease Mitochondrial Mobility in Astrocytes and Position Mitochondria Near Glutamate Transporters, *The Journal of Neuroscience* 34(5) (2014) 1613-1624.

[182] S.M. O'Donovan, C.R. Sullivan, R.E. McCullumsmith, The role of glutamate transporters in the pathophysiology of neuropsychiatric disorders, *npj Schizophrenia* 3(1) (2017) 32.

[183] M.C. McKenna, Glutamate Pays Its Own Way in Astrocytes, *Frontiers in Endocrinology* 4 (2013) 191.

[184] E.N. Genda, J.G. Jackson, A.L. Sheldon, S.F. Locke, T.M. Greco, J.C. O'Donnell, L.A. Spruce, R. Xiao, W. Guo, M. Putt, S. Seeholzer, H. Ischiropoulos, M.B. Robinson, Co-

- Compartmentalization of the Astroglial Glutamate Transporter, GLT-1, with Glycolytic Enzymes and Mitochondria, *The Journal of Neuroscience* 31(50) (2011) 18275-18288.
- [185] T.-L. Stephen, N.F. Higgs, D.F. Sheehan, S. Al Awabdh, G. López-Doménech, I.L. Arancibia-Carcamo, J.T. Kittler, Miro1 Regulates Activity-Driven Positioning of Mitochondria within Astrocytic Processes Apposed to Synapses to Regulate Intracellular Calcium Signaling, *The Journal of Neuroscience* 35(48) (2015) 15996-16011.
- [186] A. Agarwal, P.H. Wu, E.G. Hughes, M. Fukaya, M.A. Tischfield, A.J. Langseth, D. Wirtz, D.E. Bergles, Transient Opening of the Mitochondrial Permeability Transition Pore Induces Microdomain Calcium Transients in Astrocyte Processes, *Neuron* 93(3) (2017) 587-605.e7.
- [187] O. Ignatenko, D. Chilov, I. Paetau, E. de Miguel, C.B. Jackson, G. Capin, A. Paetau, M. Terzioglu, L. Euro, A. Suomalainen, Loss of mtDNA activates astrocytes and leads to spongiotic encephalopathy, *Nature Communications* 9(1) (2018) 70.
- [188] J.A. Korhonen, X.H. Pham, M. Pellegrini, M. Falkenberg, Reconstitution of a minimal mtDNA replisome in vitro, *The EMBO journal* 23(12) (2004) 2423-9.
- [189] A. Suomalainen, P. Isohanni, Mitochondrial DNA depletion syndromes – Many genes, common mechanisms, *Neuromuscular Disorders* 20(7) (2010) 429-437.
- [190] P. Martinelli, V. La Mattina, A. Bernacchia, R. Magnoni, F. Cerri, G. Cox, A. Quattrini, G. Casari, E.I. Rugarli, Genetic interaction between the m-AAA protease isoenzymes reveals novel roles in cerebellar degeneration, *Human molecular genetics* 18(11) (2009) 2001-13.
- [191] L.M.L. Chow, J. Zhang, S.J. Baker, Inducible Cre recombinase activity in mouse mature astrocytes and adult neural precursor cells, *Transgenic Research* 17(5) (2008) 919-928.
- [192] F.H. Sterky, S. Lee, R. Wibom, L. Olson, N.-G. Larsson, Impaired mitochondrial transport and Parkin-independent degeneration of respiratory chain-deficient dopamine neurons in vivo, *Proceedings of the National Academy of Sciences of the United States of America* 108(31) (2011) 12937-12942.

-
- [193] S.J. Guyenet, S.A. Furrer, V.M. Damian, T.D. Baughan, A.R. La Spada, G.A. Garden, A simple composite phenotype scoring system for evaluating mouse models of cerebellar ataxia, *Journal of visualized experiments : JoVE* (39) (2010).
- [194] R. Horn, A. Marty, Muscarinic activation of ionic currents measured by a new whole-cell recording method, *The Journal of general physiology* 92(2) (1988) 145-59.
- [195] N. Akaike, N. Harata, Nystatin perforated patch recording and its applications to analyses of intracellular mechanisms, *The Japanese journal of physiology* 44(5) (1994) 433-73.
- [196] R. Kühn, F. Schwenk, Conditional Knockout Mice, in: M.H. Hofker, J. van Deursen (Eds.), *Transgenic Mouse: Methods and Protocols*, Humana Press, Totowa, NJ, 2002, pp. 159-185.
- [197] K. Abremski, R. Hoess, Bacteriophage P1 site-specific recombination. Purification and properties of the Cre recombinase protein, *The Journal of biological chemistry* 259(3) (1984) 1509-14.
- [198] J. Silbereis, E. Cheng, Y.M. Ganat, L.R. Ment, F.M. Vaccarino, Precursors with glial fibrillary acidic protein promoter activity transiently generate GABA interneurons in the postnatal cerebellum, *Stem cells (Dayton, Ohio)* 27(5) (2009) 1152-63.
- [199] T.C. Bellamy, Interactions between Purkinje neurones and Bergmann glia, *Cerebellum (London, England)* 5(2) (2006) 116-26.
- [200] E.R. Whitney, T.L. Kemper, D.L. Rosene, M.L. Bauman, G.J. Blatt, Calbindin-D28k is a more reliable marker of human Purkinje cells than standard Nissl stains: a stereological experiment, *Journal of neuroscience methods* 168(1) (2008) 42-7.
- [201] R. Juliana, K. Kevin, H. Kelly, R. Claire, S. Neil, W. Alastair, Purkinje Cell Pathology and Loss in Multiple Sclerosis Cerebellum, *Brain Pathology* 25(6) (2015) 692-700.
- [202] C.F. Landry, G.O. Ivy, R.J. Dunn, A. Marks, I.R. Brown, Expression of the gene encoding the beta-subunit of S-100 protein in the developing rat brain analyzed by in situ hybridization, *Brain research. Molecular brain research* 6(4) (1989) 251-62.

-
- [203] N. Patro, M. Shrivastava, S. Tripathi, I.K. Patro, S100beta upregulation: a possible mechanism of deltamethrin toxicity and motor coordination deficits, *Neurotoxicology and teratology* 31(3) (2009) 169-76.
- [204] S.E. Lutz, Y. Zhao, M. Gulinello, S.C. Lee, C.S. Raine, C.F. Brosnan, Deletion of astrocyte connexins 43 and 30 leads to a dysmyelinating phenotype and hippocampal CA1 vacuolation, *The Journal of neuroscience : the official journal of the Society for Neuroscience* 29(24) (2009) 7743-52.
- [205] S. Dooves, M. Bugiani, L.E. Wisse, T.E.M. Abbink, M.S. Knaap, V.M. Heine, Bergmann glia translocation: a new disease marker for vanishing white matter identifies therapeutic effects of Guanabenz treatment, *Neuropathology and Applied Neurobiology* 44(4) (2018) 391-403.
- [206] M. Bani-Yaghoub, R.G. Tremblay, J.X. Lei, D. Zhang, B. Zurakowski, J.K. Sandhu, B. Smith, M. Ribocco-Lutkiewicz, J. Kennedy, P.R. Walker, M. Sikorska, Role of Sox2 in the development of the mouse neocortex, *Developmental Biology* 295(1) (2006) 52-66.
- [207] C. Chen, X. Zhong, D.K. Smith, W. Tai, J. Yang, Y. Zou, L.-L. Wang, J. Sun, S. Qin, C.-L. Zhang, Astrocyte-Specific Deletion of Sox2 Promotes Functional Recovery After Traumatic Brain Injury, *Cerebral Cortex* (2017) 1-16.
- [208] J.M. Levine, R. Reynolds, J.W. Fawcett, The oligodendrocyte precursor cell in health and disease, *Trends in neurosciences* 24(1) (2001) 39-47.
- [209] W.B. Stallcup, The NG2 proteoglycan: past insights and future prospects, *Journal of neurocytology* 31(6-7) (2002) 423-35.
- [210] S.H. Chung, F. Guo, P. Jiang, D.E. Pleasure, W. Deng, Olig2/Plp-positive progenitor cells give rise to Bergmann glia in the cerebellum, *Cell death & disease* 4 (2013) e546.
- [211] M. Nolden, S. Ehses, M. Koppen, A. Bernacchia, E.I. Rugarli, T. Langer, The m-AAA protease defective in hereditary spastic paraplegia controls ribosome assembly in mitochondria, *Cell* 123(2) (2005) 277-89.

-
- [212] J.M. Ross, Visualization of mitochondrial respiratory function using cytochrome c oxidase/succinate dehydrogenase (COX/SDH) double-labeling histochemistry, *Journal of visualized experiments : JoVE* (57) (2011) e3266.
- [213] A. Suomalainen, B.J. Battersby, Mitochondrial diseases: the contribution of organelle stress responses to pathology, *Nature reviews. Molecular cell biology* 19(2) (2018) 77-92.
- [214] J. Nikkanen, S. Forsstrom, L. Euro, I. Paetau, R.A. Kohnz, L. Wang, D. Chilov, J. Viinamaki, A. Roivainen, P. Marjamaki, H. Liljenback, S. Ahola, J. Buzkova, M. Terzioglu, N.A. Khan, S. Pirnes-Karhu, A. Paetau, T. Lonqvist, A. Sajantila, P. Isohanni, H. Tyynismaa, D.K. Nomura, B.J. Battersby, V. Velagapudi, C.J. Carroll, A. Suomalainen, Mitochondrial DNA Replication Defects Disturb Cellular dNTP Pools and Remodel One-Carbon Metabolism, *Cell metabolism* 23(4) (2016) 635-48.
- [215] N.A. Khan, J. Nikkanen, S. Yatsuga, C. Jackson, L. Wang, S. Pradhan, R. Kivelä, A. Pessia, V. Velagapudi, A. Suomalainen, mTORC1 Regulates Mitochondrial Integrated Stress Response and Mitochondrial Myopathy Progression, *Cell metabolism* 26(2) (2017) 419-428.e5.
- [216] J.D. Rothstein, L. Martin, A.I. Levey, M. Dykes-Hoberg, L. Jin, D. Wu, N. Nash, R.W. Kuncl, Localization of neuronal and glial glutamate transporters, *Neuron* 13(3) (1994) 713-725.
- [217] J.D. Rothstein, M. Dykes-Hoberg, C.A. Pardo, L.A. Bristol, L. Jin, R.W. Kuncl, Y. Kanai, M.A. Hediger, Y. Wang, J.P. Schielke, D.F. Welty, Knockout of glutamate transporters reveals a major role for astroglial transport in excitotoxicity and clearance of glutamate, *Neuron* 16(3) (1996) 675-86.
- [218] L.K. Bak, A. Schousboe, H.S. Waagepetersen, The glutamate/GABA-glutamine cycle: aspects of transport, neurotransmitter homeostasis and ammonia transfer, *J Neurochem* 98(3) (2006) 641-53.
- [219] M.C. McKenna, The glutamate-glutamine cycle is not stoichiometric: fates of glutamate in brain, *J Neurosci Res* 85(15) (2007) 3347-58.

- [220] M.D. Norenberg, A. Martinez-Hernandez, Fine structural localization of glutamine synthetase in astrocytes of rat brain, *Brain research* 161(2) (1979) 303-10.
- [221] S.A. Lewis, J.M. Balcarek, V. Krek, M. Shelanski, N.J. Cowan, Sequence of a cDNA clone encoding mouse glial fibrillary acidic protein: structural conservation of intermediate filaments, *Proceedings of the National Academy of Sciences* 81(9) (1984) 2743-2746.
- [222] W.M. Carroll, A.R. Jennings, F.L. Mastaglia, Reactive glial cells in CNS demyelination contain both GC and GFAP, *Brain research* 411(2) (1987) 364-369.
- [223] T.G. Bush, N. Puvanachandra, C.H. Horner, A. Polito, T. Ostenfeld, C.N. Svendsen, L. Mucke, M.H. Johnson, M.V. Sofroniew, Leukocyte infiltration, neuronal degeneration, and neurite outgrowth after ablation of scar-forming, reactive astrocytes in adult transgenic mice, *Neuron* 23(2) (1999) 297-308.
- [224] K. Ohsawa, Y. Imai, Y. Sasaki, S. Kohsaka, Microglia/macrophage-specific protein Iba1 binds to fimbrin and enhances its actin-bundling activity, *J Neurochem* 88(4) (2004) 844-56.
- [225] F. Lopez-Redondo, K. Nakajima, S. Honda, S. Kohsaka, Glutamate transporter GLT-1 is highly expressed in activated microglia following facial nerve axotomy, *Brain research. Molecular brain research* 76(2) (2000) 429-35.
- [226] M. Persson, L. Ronnback, Microglial self-defence mediated through GLT-1 and glutathione, *Amino acids* 42(1) (2012) 207-19.
- [227] A. Latham, D.H. Paul, Spontaneous activity of cerebellar Purkinje cells and their responses to impulses in climbing fibres, *The Journal of Physiology* 213(1) (1971) 135-156.
- [228] M. Kessler, B. Kiliman, C. Humes, A.C. Arai, Spontaneous activity in Purkinje cells: Multi-electrode recording from organotypic cerebellar slice cultures, *Brain research* 1218 (2008) 54-69.
- [229] E. Lorenzetto, L. Caselli, G. Feng, W. Yuan, J.M. Nerbonne, J.R. Sanes, M. Buffelli, Genetic perturbation of postsynaptic activity regulates synapse elimination in developing cerebellum, *Proceedings of the National Academy of Sciences* 106(38) (2009) 16475-16480.

- [230] R. Krencik, J.V. van Asperen, E.M. Ullian, Human astrocytes are distinct contributors to the complexity of synaptic function, *Brain Research Bulletin*.
- [231] E.M. Ullian, S.K. Sapperstein, K.S. Christopherson, B.A. Barres, Control of Synapse Number by Glia, *Science (New York, N.Y.)* 291(5504) (2001) 657-661.
- [232] C. Di Malta, J.D. Fryer, C. Settembre, A. Ballabio, Astrocyte dysfunction triggers neurodegeneration in a lysosomal storage disorder, *Proceedings of the National Academy of Sciences* 109(35) (2012) E2334-E2342.
- [233] K. Kuter, Ł. Olech, U. Głowacka, Prolonged Dysfunction of Astrocytes and Activation of Microglia Accelerate Degeneration of Dopaminergic Neurons in the Rat Substantia Nigra and Block Compensation of Early Motor Dysfunction Induced by 6-OHDA, *Molecular Neurobiology* 55(4) (2018) 3049-3066.
- [234] B.B. Wolf, M. Schuler, F. Echeverri, D.R. Green, Caspase-3 is the primary activator of apoptotic DNA fragmentation via DNA fragmentation factor-45/inhibitor of caspase-activated DNase inactivation, *The Journal of biological chemistry* 274(43) (1999) 30651-6.
- [235] B. Dejanovic, T. Djemie, N. Grunewald, A. Suls, V. Kress, F. Hetsch, D. Craiu, M. Zemel, P. Gormley, D. Lal, C.T. Myers, H.C. Mefford, A. Palotie, I. Helbig, J.C. Meier, P. De Jonghe, S. Weckhuysen, G. Schwarz, Simultaneous impairment of neuronal and metabolic function of mutated gephyrin in a patient with epileptic encephalopathy, *EMBO molecular medicine* 7(12) (2015) 1580-94.
- [236] T.P. Morais, D. Coelho, S.H. Vaz, A.M. Sebastiao, C.A. Valente, Glycine Receptor Activation Impairs ATP-Induced Calcium Transients in Cultured Cortical Astrocytes, *Frontiers in molecular neuroscience* 10 (2017) 444.
- [237] C. Cheng, M. Sourial, L.C. Doering, Astrocytes and Developmental Plasticity in Fragile X, *Neural Plasticity* 2012 (2012) 12.
- [238] E.W. Lee, J. Seo, M. Jeong, S. Lee, J. Song, The roles of FADD in extrinsic apoptosis and necroptosis, *BMB reports* 45(9) (2012) 496-508.

-
- [239] K. Newton, RIPK1 and RIPK3: critical regulators of inflammation and cell death, *Trends in cell biology* 25(6) (2015) 347-353.
- [240] S. Yoon, A. Kovalenko, K. Bogdanov, D. Wallach, MLKL, the Protein that Mediates Necroptosis, Also Regulates Endosomal Trafficking and Extracellular Vesicle Generation, *Immunity* 47(1) (2017) 51-65.e7.
- [241] K. Newton, K.E. Wickliffe, A. Maltzman, D.L. Dugger, A. Strasser, V.C. Pham, J.R. Lill, M. Roose-Girma, S. Warming, M. Solon, H. Ngu, J.D. Webster, V.M. Dixit, RIPK1 inhibits ZBP1-driven necroptosis during development, *Nature* 540 (2016) 129.
- [242] D. Westphal, G. Dewson, P.E. Czabotar, R.M. Kluck, Molecular biology of Bax and Bak activation and action, *Biochimica et Biophysica Acta (BBA) - Molecular Cell Research* 1813(4) (2011) 521-531.
- [243] K. Nakano, K.H. Vousden, PUMA, a novel proapoptotic gene, is induced by p53, *Mol Cell* 7(3) (2001) 683-94.
- [244] L.W. Thomas, C. Lam, S.W. Edwards, Mcl-1; the molecular regulation of protein function, *FEBS Letters* 584(14) (2010) 2981-2989.
- [245] D. Chen, J. Tong, L. Yang, L. Wei, D.B. Stolz, J. Yu, J. Zhang, L. Zhang, PUMA amplifies necroptosis signaling by activating cytosolic DNA sensors, *Proceedings of the National Academy of Sciences* 115(15) (2018) 3930-3935.
- [246] H. Fan, K. Zhang, L. Shan, F. Kuang, K. Chen, K. Zhu, H. Ma, G. Ju, Y.-Z. Wang, Reactive astrocytes undergo M1 microglia/macrophages-induced necroptosis in spinal cord injury, *Molecular Neurodegeneration* 11(1) (2016) 14.
- [247] Z. Huang, T. Zhou, X. Sun, Y. Zheng, B. Cheng, M. Li, X. Liu, C. He, Necroptosis in microglia contributes to neuroinflammation and retinal degeneration through TLR4 activation, *Cell Death And Differentiation* 25 (2017) 180.
- [248] H.D.E. Booth, W.D. Hirst, R. Wade-Martins, The Role of Astrocyte Dysfunction in Parkinson's Disease Pathogenesis, *Trends in neurosciences* 40(6) (2017) 358-370.

-
- [249] S. Jayadev, T.D. Bird, Hereditary ataxias: overview, *Genetics in medicine : official journal of the American College of Medical Genetics* 15(9) (2013) 673-83.
- [250] S. Arnold, G.W. de Araujo, C. Beyer, Gender-specific regulation of mitochondrial fusion and fission gene transcription and viability of cortical astrocytes by steroid hormones, *Journal of molecular endocrinology* 41(5) (2008) 289-300.
- [251] L.L. Falke, R. Broekhuizen, A. Huitema, E. Maarseveen, T.Q. Nguyen, R. Goldschmeding, Tamoxifen for induction of Cre-recombination may confound fibrosis studies in female mice, *Journal of Cell Communication and Signaling* 11(2) (2017) 205-211.
- [252] H.M. Jahn, C.V. Kasakow, A. Helfer, J. Michely, A. Verkhatsky, H.H. Maurer, A. Scheller, F. Kirchhoff, Refined protocols of tamoxifen injection for inducible DNA recombination in mouse astroglia, *Scientific Reports* 8(1) (2018) 5913.
- [253] C. Arias, A. Zepeda, K. Hernandez-Ortega, P. Leal-Galicia, C. Lojero, I. Camacho-Arroyo, Sex and estrous cycle-dependent differences in glial fibrillary acidic protein immunoreactivity in the adult rat hippocampus, *Hormones and behavior* 55(1) (2009) 257-63.
- [254] M. Santos-Galindo, E. Acaz-Fonseca, M.J. Bellini, L.M. Garcia-Segura, Sex differences in the inflammatory response of primary astrocytes to lipopolysaccharide, *Biology of Sex Differences* 2 (2011) 7-7.
- [255] N. Ishihara, Y. Fujita, T. Oka, K. Mihara, Regulation of mitochondrial morphology through proteolytic cleavage of OPA1, *The EMBO journal* 25(13) (2006) 2966-2977.
- [256] A. Olichon, L. Baricault, N. Gas, E. Guillou, A. Valette, P. Belenguer, G. Lenaers, Loss of OPA1 perturbs the mitochondrial inner membrane structure and integrity, leading to cytochrome c release and apoptosis, *The Journal of biological chemistry* 278(10) (2003) 7743-6.
- [257] G. Civiletto, T. Varanita, R. Cerutti, T. Gorletta, S. Barbaro, S. Marchet, C. Lamperti, C. Viscomi, L. Scorrano, M. Zeviani, Opa1 overexpression ameliorates the phenotype of two mitochondrial disease mouse models, *Cell metabolism* 21(6) (2015) 845-54.

- [258] T. Varanita, M.E. Soriano, V. Romanello, T. Zaglia, R. Quintana-Cabrera, M. Semenzato, R. Menabo, V. Costa, G. Civiletto, P. Pesce, C. Viscomi, M. Zeviani, F. Di Lisa, M. Mongillo, M. Sandri, L. Scorrano, The opa1-dependent mitochondrial cristae remodeling pathway controls atrophic, apoptotic, and ischemic tissue damage, *Cell metabolism* 21(6) (2015) 834-44.
- [259] K. Newton, X. Sun, V.M. Dixit, Kinase RIP3 Is Dispensable for Normal NF- κ Bs, Signaling by the B-Cell and T-Cell Receptors, Tumor Necrosis Factor Receptor 1, and Toll-Like Receptors 2 and 4, *Molecular and cellular biology* 24(4) (2004) 1464-1469.
- [260] S.K. Custer, G.A. Garden, N. Gill, U. Rueb, R.T. Libby, C. Schultz, S.J. Guyenet, T. Deller, L.E. Westrum, B.L. Sopher, A.R. La Spada, Bergmann glia expression of polyglutamine-expanded ataxin-7 produces neurodegeneration by impairing glutamate transport, *Nature neuroscience* 9(10) (2006) 1302-11.
- [261] G. Sicot, L. Servais, D.M. Dinca, A. Leroy, C. Prigogine, F. Medja, S.O. Braz, A. Huguet-Lachon, C. Chhuon, A. Nicole, N. Gueriba, R. Oliveira, B. Dan, D. Furling, M.S. Swanson, I.C. Guerrera, G. Cheron, G. Gourdon, M. Gomes-Pereira, Downregulation of the Glial GLT1 Glutamate Transporter and Purkinje Cell Dysfunction in a Mouse Model of Myotonic Dystrophy, *Cell reports* 19(13) (2017) 2718-2729.

8 APPENDIX

Supplementary figures.

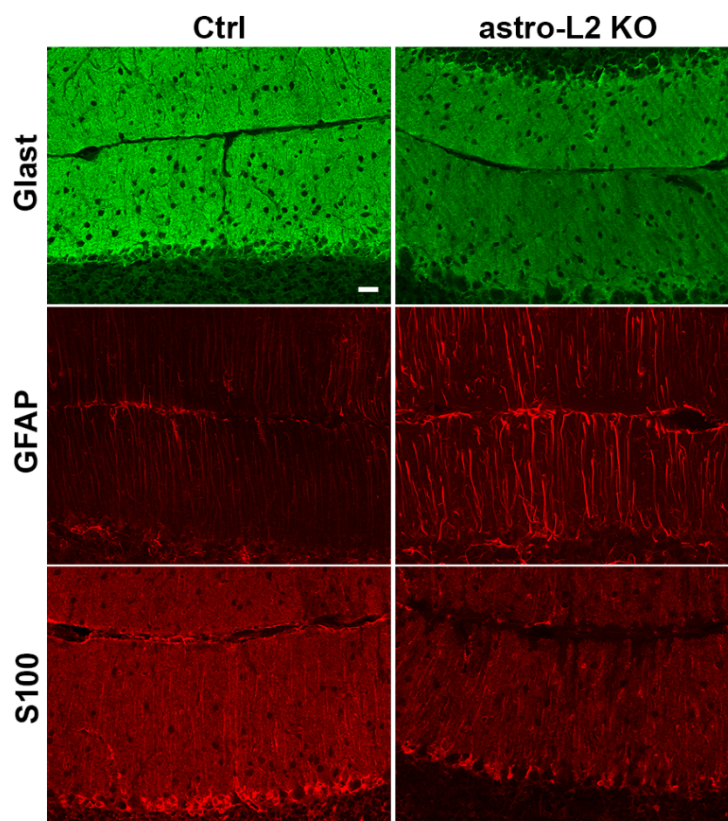


Figure S1: astro-L2 KO females show delayed cerebellar morphological changes. Mild reactive astrogliosis and BG displacement occurs at 62 weeks in females, a later stage compared to male counterparts. $n=3$ for each group of female mice. Scale bar= 20 μm .

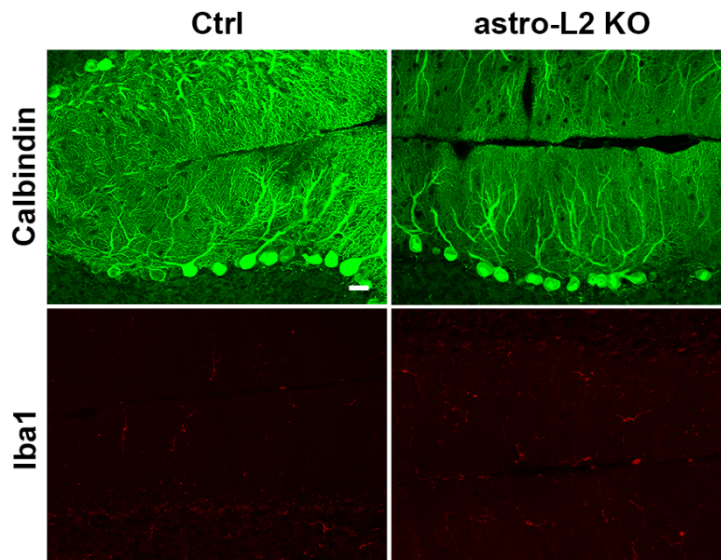


Figure S2: astro-L2 KO females show PCs aggregation at 62 weeks. PCs cell bodies appear clustered, there is no sign of inflammation.=3 for each group of female mice. Scale bar= 20 μ m.

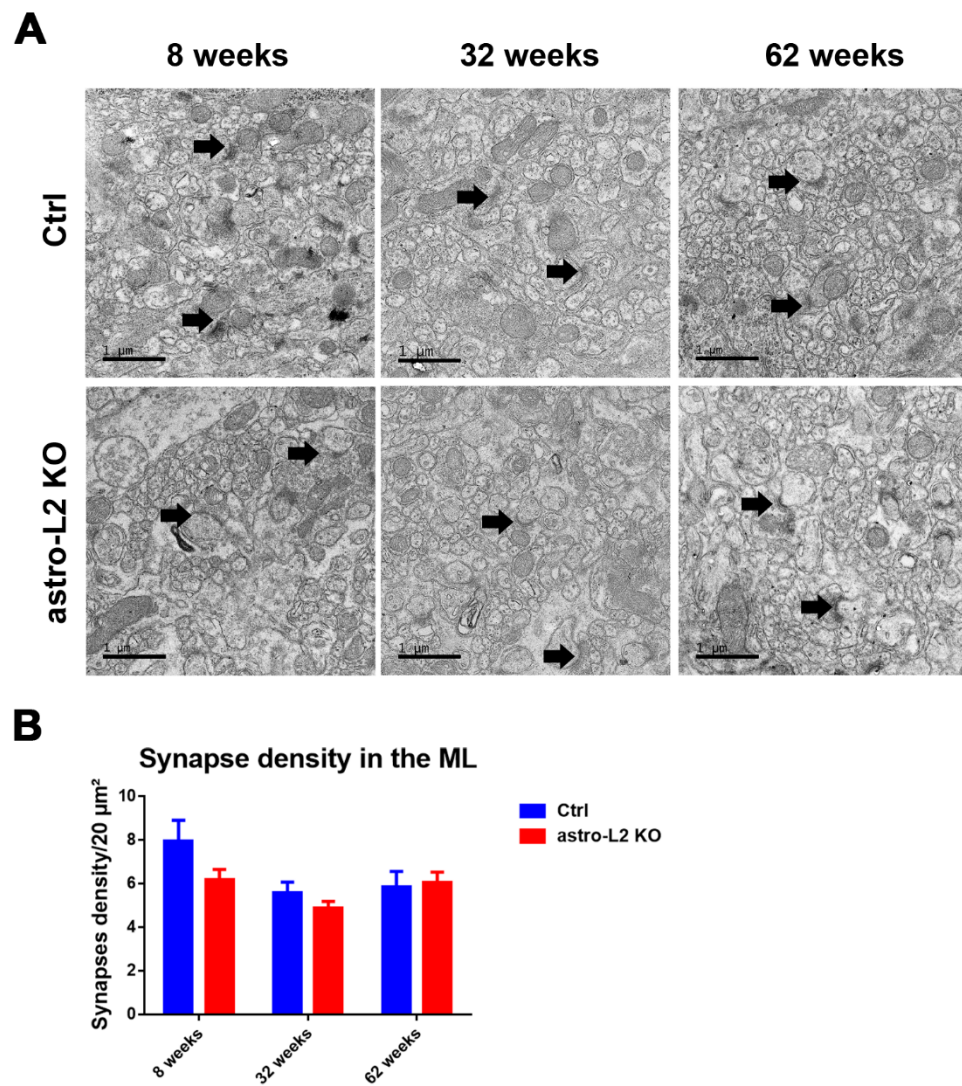


Figure S3: astro-L2 KO mice do not have a decreased synaptic number in the ML. (A) Electron microscopy pictures of the cerebellar ML of astro-L2 KO mice and relative controls. Black arrows indicate some of the synapses on the pictures. Scale bar = 1 μm (B) Quantification of the synapses, normalized to 20 μm^2 , $n \geq 3$ for each group at each time point. Data represent mean \pm SEM, Student's *t* test $p \leq 0.05$.

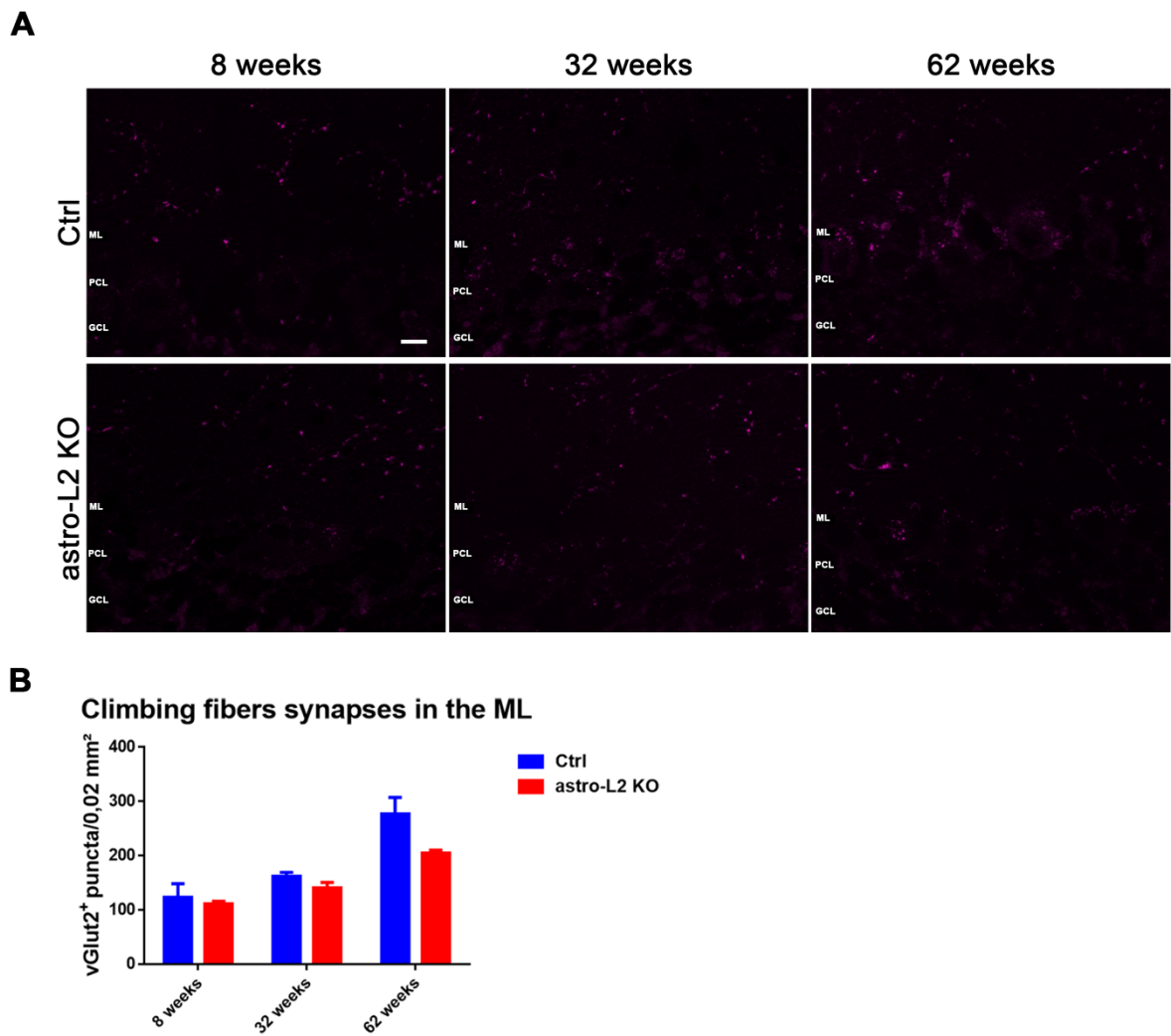


Figure S4:astro-L2 KOs do not show any alteration in the number of climbing fibers synapses. (A) Immunofluorescence staining for vGlut2, a marker for climbing fibers synapses. n=3 for each group at each time point. Scale bar= 10 μ m (B) Quantification of the vGlut2 fluorescent signal, normalized to 0.02 mm². (C) Quantification of the synapses, normalized to 20 μ m² Data represent mean \pm SEM, Student's t test $p \leq 0.05$.

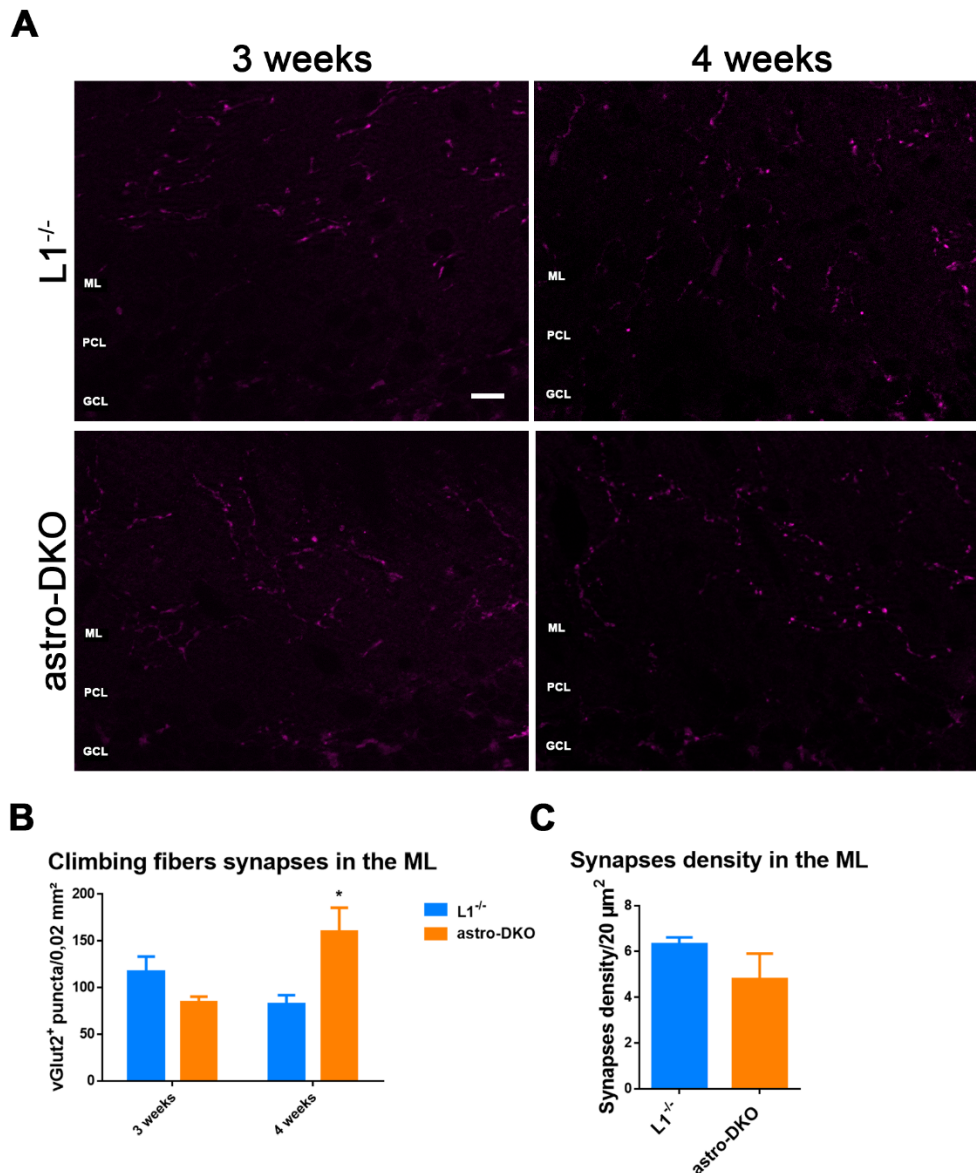


Figure S5:astroDKOs show increased climbing fibers synapses density, but overall unchanged number in total synapses. (A) Immunofluorescence staining for vGlut2, a marker for climbing fibers synapses. n=3 for each group at each time point. Scale bar= 10 μm (B) Quantification of the vGlut2 fluorescent signal, normalized to 0.02 mm². (C) Quantification of the synapses, normalized to 20 μm². Data represent mean±SEM, Student's t test $p \leq 0.05$.

9 ACKNOWLEDGEMENTS

My way to the PhD was really intense and full of challenging experiences. Nevertheless, a growing experience. I had the pleasure to meet incredibly talented scientists, friendly and supportive colleagues, “humane” university staff.

First I would like to thank my supervisor, Prof. Elena Rugarli, for the challenging project, for the motivation, for helping me growing as a human and as a scientist. We went through the challenge together. You did not forget me when I thought you did, and you helped me to get away of a difficult situation when I felt helpless. I will never forget it, and I hope I made you proud. Thank you for everything.

I am deeply thankful to all the lab colleagues I had the honor to work with. Shuaiyu, thanks for introducing me to the world of the *m*-AAA protease, and for being such a lovely person. Desy and Nimesha, you are amazing girls, helpful lab mates, a reference point in the lab, thanks for helping me every time I needed. Marie, our dark side and love for the sea led us to weird conversations and topics..I enjoyed it very much..not sure about the others.. Lennart and Simon, I had so much fun mocking you and being mocked by you. BABIDIBUBIDI! And panzerotti are not a type of pasta! David, my Mediterranean companion during this time, I enjoyed our chats, but I still think that Italian olive oil is better than the Spanish one! Marta, with you I finally had someone to talk to in Italian, about Italian stuff and science, about astrocytes and cerebellum! I felt like I was not alone with my project anymore, thank you. Mujeeb, every conversation we had was very interesting, I really enjoy your attempts to talk in Italian. Matteo, our new entry, we did not spend a lot of time together, but I hope I was somehow helpful for you. My dear Esther, I loved our coffee-time together, chats about GOT and more. You are always ready to help! Also when I made certain stupid mistakes..such as trashing the DNA of my 80+ ear punches..Thanks for the great job! And for sure, we will discuss more about GOT!!

I would also like to thank my thesis advisory committee, Prof. Dr Matteo Bergami and Prof. Dr Brunhilde Wirth, together with Prof Kloppmburg, Dr Simon Hess and Dr Susanne Brodesser. If this thesis is finished, it is also because of you, of your input, because of your help. A group work. Thank you all.

My deepest gratitude goes to the amazing people of the RTG-NCA. From students to PIs, you are a great community. I cannot express how helpful our chats were, not only scientific talks, but also everyday struggle talks. I loved our retreats and every time we were together I felt a little more like at home. Ansgar, every time I had a talk, you were so encouraging, thanks a lot for the great job with the RTG-NCA. Katerina, Isabell e Kathy. For you guys, I have no words. You are the best. Always there if I needed, so caring, so lovely, sooooo helpful. Always. Just a big thank you for everything, from the bottom of my heart. I think that the RTG-NCA is great also because of you.

Ora, non so nemmeno da dove iniziare. Mami e Pitto. Spero di avervi resi orgogliosi. Come faccio a ringraziarvi? Da cosa dovrei partire? Siete una roccia. Siete un'ispirazione per me. Con tutto quello che avete passato, siete andati avanti, contro tutto e tutti, per quello in cui credete. Nonostante le delusioni, non avete mai mollato. E in questi anni mi sono resa conto di quanto vi somiglio, e di quanto sono felice di somigliarvi. Spirito di sacrificio, impegno, determinazione, pazienza, amore per il prossimo, voglia di realizzarsi, uno spirito guerriero inarrestabile. Grazie per avermi ispirata, per avermi sorretta, per avermi incoraggiata, per aver creduto in me quando io non riuscivo a farlo. Vi voglio un mondo di bene. Questa piccola vittoria è anche vostra.

Miiiiii Allllll, Shubllllll e Looooo!!!!!! Voi siete stati il mio primo amore, i miei primi compagni di vita. Le nostre chiacchierate mi hanno sempre riportata a casa, mi hanno sempre ricordato che

c'è qualcuno da cui tornare, qualcuno che mi aspetta sulla soglia. Spero che siate orgogliosi di me, come io lo sono di voi. Vi voglio tanto bene che non si può nemmeno descrivere.

The Mamelis', la mia seconda famiglia. Anche per voi, le parole sono difficili da trovare. Non avrei potuto chiedere di meglio. Mi avete fatta sentire una figlia, avete ascoltato le mie disavventure e abbiamo riso a crepapelle per quel famoso pacco che i miei genitori dovevano mandarmi.. e non solo! Il vostro affetto mi ha sempre supportata, e pure i vostri pacchi devo dire! Grazie mille per tutto, soprattutto per Giacomo :D

Lally, la mia dolcissima amica equilibrata. Ma quanto ti ho tormentata con le mie disavventure? Con i miei audio da 20 minuti? Come avrei fatto senza di te? La tua calma, e il tuo equilibrio mi hanno aiutata a superare piccole e grandi montagne di problemi, solo parlandotene. Sei un' amica speciale. Grazie mille per tutto! E ovviamente #mainagioia! E #iltèverdetifadimagrireslsevaiaprenderloincina!#ossagrosse

Franci, ci siamo conosciute in un modo assurdo, e non ci siamo più lasciate. Le tue disavventure mi hanno fatta ridere, arrabbiare, preoccupare. Mi hai sempre ricordato di quanto, in fin dei conti, la mia vita sia lineare. Mi hai sempre riportata con i piedi per terra. La tua ammirazione nei miei confronti mi ha spinto a lavorare su me stessa per migliorarmi. Tu non lo sai, ma sei un pezzo importante della mia vita, la sorella che non ho avuto. Ti voglio bene tesi. Le risate che ci siamo fatte hanno illuminato le mie giornate più buie!

A tutti gli altri amici, a tutte le altre persone che mi hanno incoraggiata, sostenuta, aiutata. Grazie di cuore.

E poi ci sei tu, Nenno. E anche qui, le parole non possono esprimere quanto io mi senta fortunata ad averti al mio fianco. Tu mi hai cambiato la vita in un modo che non ritenevo possibile. Il tuo sostegno e il tuo amore sono stati la mia ancora di salvezza. Sempre lì pronto a sgridarmi o

incoraggiarmi in base al momento. Siamo cresciuti tanto insieme, questa è la nostra piccola vittoria. Senza di te non ce l'avrei fatta. Mi hai accompagnata in questo percorso lasciandoti dietro tutto, la terra che ami, il mare che ti scorre nelle vene, il sole che ti scalda il cuore e la famiglia che è la tua essenza. Hai lasciato tutto per me. E sei venuto qui in terra straniera, e ti sei rimboccato le maniche, fino ad arrivare dove sei ora. Grazie per aver ascoltato tutte le mie lamentele, le mie paranoie, le mie insicurezze, e per averle distrutte una ad una, facendomi diventare più forte. La strada non è ancora finita Nenno, chissà dove ci porta, ma se il viaggio lo faccio con te, mano nella mano, non mi fa paura!

10 EIDESSTATTLICHE ERKLÄRUNG

Ich versichere, dass ich die von mir vorgelegte Dissertation selbständig angefertigt, die benutzten Quellen und Hilfsmittel vollständig angegeben und die Stellen der Arbeit – einschließlich Tabellen, Karten und Abbildungen –, die anderen Werken im Wortlaut oder dem Sinn nach entnommen sind, in jedem Einzelfall als Entlehnung kenntlich gemacht habe; dass diese Dissertation noch keiner anderen Fakultät oder Universität zur Prüfung vorgelegen hat; dass sie – abgesehen von unten angegebenen Teilpublikationen – noch nicht veröffentlicht worden ist sowie, dass ich eine solche Veröffentlichung vor Abschluss des Promotionsverfahrens nicht vornehmen werde. Die Bestimmungen der Promotionsordnung sind mir bekannt. Die von mir vorgelegte Dissertation ist von Prof. Dr. Elena I. Rugarli betreut worden.

Köln, den

Sara Murru

11 CURRICULUM VITAE

Personal Information

Name	Sara Murru
Date and place of birth	June 8 th , 1987, Carbonia, Italy
Address:	Hospeltstraße 15, 50825, Köln, Germany
Phone number	+49 1736823352
Email address	saramurru@outlook.it
Linkedin	www.linkedin.com/in/sara-murru1987

Educational background

January 2015—Present	<p>Ph.D., University of Cologne, Cologne, Germany</p> <p>I am currently working on elucidating the effect of astrocytes-specific dysfunction in the development of neurological phenotypes associated with the <i>m</i>-AAA protease dysfunction.</p>
February 2013-July 2014	<p>Ph.D. candidate, University of Haifa, Haifa, Israel</p> <p>I worked on the role of the ubiquitin-proteasome system in memory consolidation and long-term maintenance.</p>
October 2010-September 2012	<p>M.Sc. in Neuropsychobiology, University of Cagliari, Cagliari, Italy</p> <p>The aim of my Master thesis work was to elucidate the effect of social enrichment in neuronal plasticity of chronically stressed animals.</p>
October 2006-July 2010	<p>B.Sc. in Experimental Biology, University of Cagliari, Cagliari, Italy</p> <p>During my Bachelor thesis, I investigated the effect of a novel polyanionic compound called ATA in blocking the HIV2 reverse transcriptase.</p>

Publications

The Mitochondrial m-AAA Protease Prevents Demyelination and Hair Greying

Wang S, Jacquemyn J, [Murru S](#), Martinelli P, Barth E, et al. (2016) The Mitochondrial *m*-AAA Protease Prevents Demyelination and Hair Greying. *PLOS Genetics* 12(12): e1006463. doi: 10.1371/journal.pgen.1006463

Language skills

Mother tongue language	Italian
Other languages	English (proficient)
	German (basic)
	Russian (basic)